

FINAL VERSION

Chapter for *ADVANCES IN PROTEIN CHEMISTRY* volume entitled “Linkage Thermodynamics of Macromolecular Interactions” dedicated to J. Wyman

**ALLOSTERIC TRANSITIONS OF THE
ACETYLCHOLINE RECEPTOR**

STUART J. EDELSTEIN^{*,†} and JEAN-PIERRE CHANGEUX^{*}

^{*}Neurobiologie Moléculaire, Institut Pasteur, 75734 Paris Cedex 15, France, and
[†]Département de Biochimie, Université de Genève, CH-1211 Genève 4, Switzerland,

23,433 WORDS, INCLUDING REFERENCES AND FIGURE LEGENDS

I. Introduction

A. The acetylcholine receptor: similarities and differences with respect to other allosteric proteins

B. Consequences of pseudo-symmetric oligomeric structure

C. Role of mutational studies

II. Mechanistic models

A. The MWC-type model

B. Linear free energy relations

C. Alternative models

III. Recovery from desensitization

IV. Kinetic basis of dose-response curves

A. Dependence on desensitization rate

B. Desensitization by low-concentration pre-pulses

V. Multiple phenotypes

A. Generalized allosteric network

B. The K phenotype

C. The L phenotype

D. The γ phenotype

E. Limiting properties at extremes of L

VI. Deductions from single channel measurements

A. Separation of single ionic and single ligand-binding events

B. Consequences of non-equivalent sites

C. Convergence of mechanistic models at high agonist concentrations

D. Kinetic consequences of mutant phenotypes

VII. Allosteric effectors and coincidence detection

VIII. General Considerations

A. Evaluation of mechanistic models

B. Implications for synaptic plasticity

C. Diseases and nicotine dependency

References

I. INTRODUCTION

A. The acetylcholine receptor: similarities and differences with respect to other allosteric proteins

The nicotinic acetylcholine receptor (nAChR) and other members of the super-family of ligand-gated channels are responsible for rapid chemo-electrical transduction in the nervous system. The chemical relay between electric impulses at the synapses of neuromuscular junctions or between neurons occurs via the quantal release into the synaptic cleft of neurotransmitter molecules in "pulses" of mM concentration and ms duration (Kuffler and Yoshikami, 1975; Clements *et al.*, 1992). The post-synaptic membrane contains a high density of these ionotropic receptors, present mainly in closed states prior to neurotransmitter release, but capable of interconverting rapidly upon binding of neurotransmitter to an open state with a permeable ion channel. However, the open state is transient and closure occurs either by returning to the initial state (following a brief pulse of neurotransmitter, as commonly occurs under physiological conditions) or by converting to desensitized states (when neurotransmitters or other modulators are present for longer times). Presynaptic effects of nAChR may also contribute to synaptic function by potentiating the response of other ligand gated channels (Brussard *et al.*, 1995; Gray *et al.*, 1996; Role and Berg, 1996; Wonnacott, 1997; Léna and Changeux, 1997).

Mechanistic models capable of representing these various properties include principles of the Monod-Wyman-Changeux theory of concerted transitions between conformational states (Monod *et al.*, 1965). This theory was initially developed to account for the kinetic properties of bacterial and mammalian regulatory enzymes on the basis of symmetry features of their quaternary structures. It had its origins in Wyman's pioneering developments of linkage relationships for hemoglobin (Wyman, 1948; Wyman, 1964) and has been applied to various

aspects of ligand-gating (Changeux *et al.*, 1967; Karlin, 1967; Edelstein, 1972; Colquhoun, 1973; Heidmann and Changeux, 1979; Changeux *et al.*, 1984; Changeux, 1990; Jackson, 1989; Galzi *et al.*, 1996b), including an extended form that generates values for all of the relevant kinetic constants through the application of linear free energy relations (Edelstein *et al.*, 1996). More restricted schemes have also been considered in which the conformational transition to the open state is limited to receptors fully saturated with agonist (Colquhoun and Sakmann, 1985).

The nAChR and other ionotropic receptors constitute a special class of allosteric proteins (Galzi and Changeux, 1995). They possess a number of features in common with allosteric enzymes and hemoglobin (Monod *et al.*, 1965; Edelstein, 1975; Perutz, 1989), including: (1) an oligomeric structure; (2) topologically distinct sites responsible for homotropic and heterotropic interactions that can be related to the interaction of pharmacological agonists, antagonists, and effectors; and (3) concerted transitions between discrete conformational states as revealed by all-or-nothing opening of the ion channel. In addition, the nAChR possesses distinct features (Galzi and Changeux, 1995; Galzi *et al.*, 1996b), including: (1) pseudo-symmetry among the subunits related by a five-fold rotational axis perpendicular to the plane of the membrane; (2) homotropic interactions between partially equivalent sites; (3) a set of conformational states (activatable, active and desensitized) with interaction times that operate in ranges varying from milliseconds to minutes; and (4) pleiotropic phenotypes in which point mutations result in concomitant modifications of apparent agonist affinity, channel conductance, and agonist-versus-antagonist specificity.

The nAChR also possess properties permitting observation of single ion channels (Sakmann *et al.*, 1980), a powerful experimental approach for the determination of kinetic properties and conductance levels of the channel. In this respect, conformational changes

dependent on the concentration of ligand are more readily measured than direct binding interactions. In contrast, for many other allosteric proteins ligand binding is more readily monitored than independent indices of conformational change (Edelstein and Changeux, 1996). Hence, for certain approaches, particularly analysis of stochastic processes, the nAChR appears in advance of other allosteric proteins and may lead to novel experimental approaches that could be applied to other allosteric systems. In addition, the possible monitoring of single ligand-binding events (Edelstein *et al.*, 1997b) may be possible with anticipated technical advances in fluorescence correlation spectroscopy (Eigen and Rigler, 1994; Schwille *et al.*, 1997).

B. Consequences of pseudo-symmetric oligomeric structure

Historically, concepts concerning the nAChR were developed initially from studies on receptors from fish electric organs and vertebrate muscle (Changeux, 1990). Biochemical analysis, cloning, and sequencing of these receptors' subunits established their heteropentameric [$2\alpha:1\beta:1\gamma/\varepsilon:1\delta$] structure and led to the identification of related neuronal forms (see Fig. 1), as well to more distant invertebrate forms (Le Novère and Changeux, 1995). The neuronal subunits $\alpha 2$ - $\alpha 5$ require interactions with β subunits in order to form functional receptors, with a putative [$2\alpha_i:3\beta_j$] stoichiometry (Cooper *et al.*, 1991; Lindstrom, 1996) or more complicated combinations in certain cases (Conroy *et al.*, 1992; Vernallis *et al.*, 1993; Ramirez-Latorre *et al.*, 1996; Le Novère *et al.*, 1996), whereas $\alpha 7$ - $\alpha 9$ subunits may form functional homopentamers (Couturier *et al.*, 1990; Sargent, 1993; Elgoyhen *et al.*, 1994; Palma *et al.*, 1996). Several experimental approaches have lead to the identification of functional domains, particularly chemical labeling and site-directed mutagenesis . In this respect, studies on $\alpha 7$ using site-directed mutagenesis have been particularly fruitful (Bertrand

and Changeux, 1995). These investigations have led to the current structural model (Devillers-Thiéry et al., 1993; Unwin, 1993a; Galzi and Changeux, 1994; Bertrand and Changeux, 1995; Karlin and Akabas, 1995), with the agonist binding site in the N-terminal domain (Karlin and Akabas, 1995; Galzi and Changeux, 1994) and the ion channel constituted by residues of the M2 transmembrane domain (Giraudat et al., 1986; Hucho et al., 1986; Imoto et al., 1988; Devillers-Thiéry *et al.*, 1993), as presented in Fig. 2 a. However, other transmembrane regions may also contribute directly or indirectly to channel properties (Lo *et al.*, 1991; Li *et al.*, 1994; Akabas and Karlin, 1995). Features of the three-dimensional structure of the *Torpedo* nAChR have been obtained by electron microscopic studies of ordered arrays at 9 Å resolution (Unwin, 1993b; Unwin, 1996), as represented in outline in Fig. 2 b.

Numerous studies indicate that the binding sites for nicotinic ligands are located at the α/γ and α/δ interfaces, or at equivalent positions for non-muscle receptors (Oswald and Changeux, 1982; Pedersen and Cohen, 1990; Chatrenet *et al.*, 1990; Galzi *et al.*, 1991b; Czajkowski *et al.*, 1993; Fu and Sine, 1994; Corringer *et al.*, 1995), with the subunits arranged as shown in Fig. 2 c (Machold *et al.*, 1995). However, alternative interpretations have been presented which place the nicotinic binding sites closer to the center of each α subunit and the β subunit between the two α subunits (Unwin, 1996). For nicotinic agonists, it has been suggested that higher affinity binding takes place at the α/δ interface and that lower affinity binding occurs at the α/γ interface (Blount and Merlie, 1989; Sine and Claudio, 1991; Prince and Sine, 1996). In contrast, higher affinity has been assigned to the α/γ site for the competitive antagonist *d*-tubocurarine (Pedersen and Cohen, 1990). Hence, the site that binds more strongly may vary for different agonists or antagonists and for a particular ligand, the degree of non-equivalence may vary from one conformational state to another.

C. Role of mutational studies

In this chapter, the generalized MWC-type model (Edelstein *et al.*, 1996) will be described and contrasted with the sequential model (Colquhoun and Sakmann, 1985) that has also been used to analyze the kinetic properties of the nAChR. Applications of the models to experimental data, particularly for several mutant forms, will be evaluated for dose-response experiments and kinetic experiments (including single channel recordings). The analysis of both site-directed and spontaneous mutations has been critical to the current understanding of the functional mechanism. For example, the channel mutant L247T, first studied by site-directed mutagenesis in $\alpha 7$ (Revah *et al.*, 1991; Bertrand *et al.*, 1992), was subsequently incorporated into muscle nAChR (Filatov and White, 1995; Labarca *et al.*, 1995) and recently identified in a congenital myasthenic syndrome (Gomez *et al.*, 1996). Neighboring sites have also been implicated in receptor function, by site-directed mutagenesis in $\alpha 7$ (Devillers-Thiéry *et al.*, 1992; Galzi *et al.*, 1992), or as naturally occurring myasthenic mutants (Vincent *et al.*, 1997). The data published for the myasthenic mutant ϵ T264P (Ohno *et al.*, 1995) are particularly valuable for the discrimination between functional models and are described more fully in section VI.

II. MECHANISTIC MODELS

A. The MWC-type model

In order to account for *in vitro* fast kinetic observations on ligand binding and ion channel opening with *Torpedo* receptors four conformational states, B, A, I, and D, were postulated (Heidmann and Changeux, 1980; Neubig and Cohen, 1980; Changeux, 1990), where B is the basal (resting) activatable state, A is the active (open) state, I is the initial desensitized state, and D is the final desensitized state. The four states are in equilibrium, with an interconversion pattern that corresponds to the vertices of a tetrahedron (Fig. 3 a), and three

degrees of ligation ($i = 0, 1, \text{ or } 2$) are possible for each state. The affinity of each state for agonist increases in the order B-A-I-D. The B state was originally designated as “R”, but “B” (for “basal”) was proposed (Edelstein *et al.*, 1996) to replace “R” in order to avoid confusions with the high affinity state in the original MWC formulation (Monod *et al.*, 1965). According to the scheme in Fig. 3 a, all interaction pathways are in principle possible. Hence with 6 pairs of interactions and three degrees of ligation, a total of 36 conformational interconversion rates would be required to fully characterized the system (in addition to the ligand on and off rates for each state).

The 36 interconversion rates are clearly too numerous to be evaluated, but their number could be limited by structural or kinetic constraints of the receptor that render obligatory a certain order of passage between states. Indeed, the different time regimes observed for the various transitions (\sim msec for B \rightarrow A; \sim 100 msec for A \rightarrow I; \sim 10 sec for I \rightarrow D) lead to selection of a predominant kinetic pathway, as indicated in Fig. 3 b, that corresponds to the passage between states over the lowest transition state barriers. Since the secondary pathways (indicated by dotted arrows) can be assumed to contribute to less than 1% (Edelstein *et al.*, 1996), the tetrahedral arrangement reduces to the linear cascade: $B_i \rightleftharpoons A_i \rightleftharpoons I_i \rightleftharpoons D_i$.

The linear progression permits the full description of all ligand-binding and conformational transition rates in the two-dimensional kinetic network depicted in Fig. 4, with ligand (agonist) reactions represented vertically and conformational interconversion reactions represented horizontally. The ratios of the various ligand binding and interconversion rate constants define the equilibrium parameters with respect to the key affinity ratio, c , as summarized in Fig. 5 for the B-A pair of states. The linear progression reduces the number of independent interconversion rate constants that must be evaluated to describe the system from 36 to 18. Nevertheless, 18 interconversion rate constants remain too large a number of

independent parameters to be determined, but a substantial additional reduction can be achieved through the application of linear free energy relations.

B. Linear free energy relations

Linear free-energy relationships have been widely used to relate the kinetic features of related reactions to properties of their respective transition states. (Leffler, 1953; Szabo, 1978; Jencks, 1985; Fersht *et al.*, 1986). They have been particularly successful in describing the variations as a function of ligand binding for the interconversion rate constants of the two principal conformational states of hemoglobin over a wide range of rates (Sawicki and Gibson, 1976; Eaton *et al.*, 1991). Similar principles have been assumed to apply to the conformational interconversions of the nAChR and have been used to characterize the transition state for the interconversion between each pair of conformations in terms of its position on a hypothetical linear reaction coordinate (Edelstein *et al.*, 1996). The position determines the effect of ligand binding on the interconversion rates, thereby limiting the degrees of freedom in the assignment of values to the rate constants.

Specifically, the application of linear free energy relations is based on the difference in affinity for agonists between the partners of each pair of states, as indicated by the affinity ratio $^{BAc} = K_A/K_B$ defined in Fig. 5 (or the equivalent ratios for AIc and IDc for the A-I and I-D pairs of states, respectively). The dependence of conformational interconversion rates on ligand binding is assumed to follow from the stabilization of the transition state for each interconversion by the ligand. The extent of this stabilization is assumed to be intermediate with respect to the effects of ligand binding on each on the two participating allosteric states and weighted toward the properties of the allosteric state that the transition state more closely resembles. This assumption may be expressed quantitatively in terms of the position of the

transition state on a hypothetical reaction coordinate. In this case, for each pair of states a positional parameter is defined (^{BA}p , ^{A}p , or ^{ID}p), as presented in Fig. 6 for ^{BA}p , such that this parameter characterizes the transition state on a linear scale between 0 and 1 with respect to its proximity to the lower affinity state of the pair.

On the basis of these relations the full series of rate constants for the $B_i \rightleftharpoons A_i$ interconversions can be generated from the ligand binding parameters (^{BA}c) with three additional values: ^{BA}p , one $B \rightarrow A$ rate constant, and one $A \rightarrow B$ rate constant (see legend to Fig. 6). In this way the 6 rate constants for each pair of states in the linear scheme are reduced to 2 rate constants and 1 positional parameter. With homopentameric receptors, the same number of parameters provides estimates for all 12 interconversion rates for each pair of states (Edelstein and Changeux, 1996). For detailed kinetic studies on muscle nAChR, because of the distinct time ranges over which the three pairs of states interconvert, sufficient data are available to permit reasonable estimates for all values (Edelstein *et al.*, 1996), as listed in Table 1. The value of $^{BA}p = 0.2$ indicates that with each ligand binding step the increase in the $B \rightarrow A$ rate is larger than the decrease in the $A \rightarrow B$ rate.

C. Alternative models

For many of the experimental measurements on nAChR reported in the literature (for reviews see Lingle *et al.*, 1992 ; Edmonds *et al.*, 1995), the data for activation has been interpreted in terms of a “sequential” model, in which channel opening for muscle type receptors occurs only upon binding of the second molecule of agonist (represented in Fig. 7 by the step $B_2 \rightleftharpoons A_2$), as formulated by Colquhoun and Sakmann (1985). In this case, channel opening and closing are characterized by only two rate constants, β and α , respectively. We refer to this description as the C&S-type model. The reasons for having invoked this model

include the difficulties of implementing a full MWC-type model prior to the introduction of the linear free energy relations (Edelstein *et al.*, 1996) and the fact that under certain experimental conditions (such as relatively high agonist concentrations), the assumption that channel opening occurs only for bi-liganded molecules provides an adequate description of the system. However, in a number of cases the C&S-type model is not adequate and such cases are considered in Sections V and VI.

Additional aspects concern desensitization (as represented in Fig. 7 by the step $A_2 \rightleftharpoons D_2$) and recovery. Ever since the benchmark studies of Katz and Thesleff (1957) it has been generally noted that following desensitization, recovery occurs spontaneously upon removal of the agonist, but “silently”, i.e., with no channel opening during the recovery period. Since return to the resting state via A_2 would imply channel opening events, it has been argued that a distinct “recovery” pathway must exist, as represented in Fig. 7 by the series $D_2 \rightarrow D_1 \rightarrow D_0 \rightarrow B_0$. The overall model presented in Fig. 7, with activation restricted to bi-liganded molecules and a distinct recovery sequence, represents the “cyclic” scheme that has been used to interpret experimental data (Franke *et al.*, 1993). However, an explanation of how silent recovery can also be accommodated by an MWC-type model is presented in the following section.

III. RECOVERY FROM DESENSITIZATION

When the various relationships linking ligand binding, allosteric equilibria, and transition state barriers were evaluated for all three pairs of states for muscle receptors studied by single channel measurements or rapid agonist application (Colquhoun and Sakmann, 1985; Franke *et al.*, 1993), the values for the various parameters presented in Table 1 were deduced (Edelstein *et al.*, 1996). The overall properties of the system may then be represented by the free energy

profile presented in Fig. 8. The vertical ladders for each state and the intervening transition states correspond to the change in free energy for each molecule of agonist bound. Hence the step sizes for the B, A, I and D states increase with affinity according to the series of dissociation constants $K_B > K_A > K_I > K_D$. The vertical alignment of the ladder for each state is set by the values assigned to the relative concentrations of B_0 , A_0 , I_0 , and D_0 . The transition state heights are determined by the positional parameters (see Fig. 6).

The progression of doubly-liganded states $B_2 \rightarrow A_2 \rightarrow I_2 \rightarrow D_2$ represents the allosteric cascade for the conformational changes elicited by application of a strong and prolonged pulse of agonist, with the time of passage through A_2 corresponding to the average open time in single channel measurements. The kinetic properties of the system can be represented in simulations, as shown in Fig. 9 a & b, with the time axis presented on a logarithmic scale to permit visualization over several time regimes (Edelstein *et al.*, 1996). Since the concentration of agonist is high, this simulation follows the path $B_0 \rightarrow B_1 \rightarrow B_2 \rightarrow A_2 \rightarrow I_2 \rightarrow D_2$. At early times in Fig. 9 b the progression from unliganded to liganded forms is apparent for B, followed by interconversion of biliganded B to biliganded A and I. Transient channel opening corresponds to the appearance and disappearance of A. The population of biliganded D increases only at longer times via conversion from biliganded I due to the slow rate of the $I_2 \rightarrow D_2$ interconversion.

Following termination of the pulse, agonist dissociation drives the system to the unliganded states and the initial distribution is reestablished relatively rapidly, particularly from I_2 along the pathway; $I_2 \rightarrow I_1 \rightarrow I_0 \rightarrow A_0 \rightarrow B_0$ (Fig. 8). These features can be visualized in the kinetic simulation of recovery presented in Fig. 9 c. With ${}^{AB}k_0 \gg {}^{IA}k_0$, recovery along the pathway: $I_0 \rightarrow A_0 \rightarrow B_0$ occurs with so rapid a passage through the A_0 state that channel opening is negligible (Edelstein *et al.*, 1996). Following agonist removal, the I_2 state loses agonist

molecules and is transformed to B_0 in less than 1 s. The D_2 state loses agonist molecules to form D_0 within 10 s, but requires longer times (10^3 - 10^4 s) to re-equilibrate with B_0 and to return to the initial low levels. Such long recovery times could account for certain slow physiological responses, possibly related to nicotine pharmacology (see Section VIII). It is clear from this simulation that the four-state model predicts virtually negligible channel opening during the recovery period, but without the necessity of imposing a separate recovery pathway from I (or D) to B that arbitrarily disallows passage through A, as required in the “cyclic” model (Franke *et al.*, 1993).

IV. KINETIC BASIS OF DOSE-RESPONSE CURVES

A. Dependence on desensitization rate

The dose-response analysis has been widely used for characterization of the cooperativity and affinity (EC_{50}) of ligand-gated channels, but it is important to ascertain under what conditions such an equilibrium-based analysis is appropriate for a transient phenomenon. Therefore, simulations were performed with the complete four-state model to test this issue (Edelstein *et al.*, 1996). The relative rate of the initial phase of desensitization, $A_2 \rightarrow I_2$, can result in systematic errors in the apparent values of the Hill coefficient, n , and EC_{50} , as described in Fig. 10. The errors are relatively minor for the value of $^{AI}k_2 = 20 \text{ s}^{-1}$ (Table 1) but for higher values of $^{AI}k_2$, significant distortions in the simulated dose-response curves were predicted. For example, the apparent values of the Hill coefficient and affinity at $^{AI}k_2 = 20 \text{ s}^{-1}$, $n = 1.6$ and $EC_{50} = 10 \text{ }\mu\text{M}$, differ only slightly from the values observed with a desensitization sufficiently low ($^{AI}k_2 = 2 \text{ s}^{-1}$) to avoid any distortions: $n = 1.7$ and $EC_{50} = 9 \text{ }\mu\text{M}$. Hence, for both the n and EC_{50} values, the apparent rate constants for the AChR (Table 1) are such that errors are limited to $\sim 10\%$ (Fig. 10 b). However, were the $^{AI}k_2$ value 10-fold faster ($^{AI}k_2 = 200$

s⁻¹), the relevant values would be $n = 1.3$ and $EC_{50} = 20 \mu\text{M}$ (Edelstein *et al.*, 1996), with major discrepancies between the apparent and true (desensitization-free) properties. Therefore, as long as desensitization is sufficiently slow so as not to introduce significant errors, dose-response analysis for the nAChR can provide a useful experimental protocol and a number of investigations relying principally on such measurements have led to important observations concerning pleiotropic mutant phenotypes, as described in Section V.

B. Desensitization by low-concentration pre-pulses

A prominent feature of ligand-gated channels is the desensitization by low “pre-pulse” concentrations of agonist that are insufficient to provoke significant channel opening, but elicit desensitization when followed by a stronger test pulse (Katz and Thesleff, 1957; Rang and Ritter, 1970). By studying a range of pre-pulse concentrations and plotting the fraction of residual activity observed with the strong pulse, desensitization curves are obtained with the mid-point defining an apparent inactivation constant, IC_{50} . Typically, the pre-pulse is applied for a duration of $\sim 10\text{s}$ (Franke *et al.*, 1993). If equilibrium conditions prevailed, the IC_{50} value obtained would be related to the dissociation constant for the high-affinity of the desensitized state (Heidmann and Changeux, 1978). Therefore, to test whether the equilibrium assumption is reasonable for such an analysis, simulations were performed at very low pre-pulse concentrations of ligand. As presented in Figure 11 a, kinetic simulations reveal that for a low concentration such as $0.4 \mu\text{M}$, progression through the B-A-I-D states is relatively slow and for a 10 s pre-pulse some I state appears, but only a small fraction of the D state that would be produced by a pulse sufficiently long ($\sim 1000\text{ s}$) to reach the final equilibrium value.

When a series of simulations at different concentrations are performed, the degree of desensitization after 10 s can be measured and compared to the equilibrium value of

desensitization. In this way a hypothetical curve for the determination of IC_{50} is produced for the equilibrium properties and compared to the simulated values with 10 s pre-pulses. These data, presented in Fig. 11 b, show the systematic divergence of the two curves. The points obtained from the simulations for 10 s pre-pulses are considerably to the right of the equilibrium curve, and imply an apparent affinity for the D state (using IC_{50} values) that is significantly weaker than the true equilibrium value (Edelstein *et al.*, 1996).

V. MULTIPLE PHENOTYPES

A. Generalized allosteric network

Point mutations within receptor subunit genes often result in "complex" and extremely pleiotropic phenotypes with, for instance, concomitant modifications of the apparent affinity for agonist, channel properties, and agonist versus antagonist specificity (Revah *et al.*, 1991; Bertrand *et al.*, 1992; Devillers-Thiéry *et al.*, 1992; Yakel *et al.*, 1993; Langosh *et al.*, 1994; Rajendra *et al.*, 1994; Labarca *et al.*, 1995). Following the discovery of these mutations, the interpretation of their complex phenotype in molecular terms became a challenging issue. For example, a single mutation in the MII channel domain of the $\alpha 7$ nAChR, Leu 247 to Thr (Revah *et al.*, 1991; Bertrand *et al.*, 1992; Devillers-Thiéry *et al.*, 1992), yields a receptor which is insensitive to the channel blocker QX222, has lost desensitization, and displays an apparent affinity for acetylcholine (ACh) up to 200-fold higher than for wild type. In addition, the mutant receptor exhibits two conducting states activated by high (the 40 pS state) versus low (the 80 pS state) concentrations of ACh. Moreover, a competitive antagonist of the wild-type receptor, dihydro- β -erythroidine (DH β E), behaves on this mutant as a full agonist (with 10-fold higher apparent affinity than ACh) and exclusively activates the high conductance state.

In order to interpret such complex properties it is necessary to take into account the fact that mutations at several different positions along the primary sequence of receptor subunits may produce similar, although not identical, phenotypes. For instance, shifts in the neurotransmitter dose-response curve are obtained by mutating amino acids contributing to either the ligand binding domain (Schmieden *et al.*, 1992; Galzi *et al.*, 1991a; Tomaselli *et al.*, 1991; O'Leary and White, 1992; Aylwin and White, 1994) or to the ion channel domain (Revah *et al.*, 1991; Bertrand *et al.*, 1992; Devillers-Thiéry *et al.*, 1992; Yakel *et al.*, 1993; Langosh *et al.*, 1994; Rajendra *et al.*, 1994; Labarca *et al.*, 1995), even though they are located 20-40Å away from each other in nicotinic receptors (Herz *et al.*, 1989). Moreover, mutations may alter the number and distribution of the multiple conducting states, as noted for the L247T mutation of the $\alpha 7$ nAChR, as well as for the hyperekplexia mutations of the glycine receptor (Langosh *et al.*, 1994; Rajendra *et al.*, 1995).

A context for these phenomena has been provided (Galzi *et al.*, 1996b) by noting that the four-state allosteric model can be extended to a generalized allosteric network, as summarized in Fig. 12. Receptor molecules are assumed to exist in several (at least three) discrete conformations, S_i , which correspond to thermodynamically stable states with defined tertiary and quaternary structures. These conformations are qualitatively described by a structural parameter Σ_i , and functionally defined as closed (but activatable), active (channel open), and desensitized (closed but refractory states). Each state is characterized by its affinity for the agonist (K_i) or other ligands, and its conductance (γ_i , in pS).

The interconversion between any two conformational states S_i and S_j occurs freely with an allosteric equilibrium constant $i \rightleftharpoons j L = [S_j] / [S_i]$, and ligands stabilize the conformations to which they bind with higher affinity. One receptor oligomer, with a given subunit composition, has access to a unique set of conformational states, possibly including more than one conducting

(Revah *et al.*, 1991; Bormann *et al.*, 1993) or desensitized (Heidmann and Changeux, 1980; Sakmann *et al.*, 1980) state. Substituting one subunit for another, or mutating amino acids in one or more subunits, may alter the pattern of the conformational network by: i) changing the intrinsic binding properties (K phenotype) or the conductance (γ phenotype) of one or more conformations; or ii) changing the equilibrium constants between conformational states (L phenotype). In addition, the number of conformational states may vary, i.e. certain conformations may become virtually inaccessible, or conversely, stable.

For the sake of simplicity, in all cases considered both the wild-type and mutant receptors were assumed to interconvert to the same finite number of identical quaternary structures (Σ). Also, as kinetics of receptor activation and desensitization take place over significantly different time scales (desensitization is generally slow compared to activation, as discussed above in relation to Fig. 10), the conformational scheme used to describe receptor activation was, in a first approximation, reduced to only those interconverting states involved in the activation process (resting and active states). Taking into account the intrinsic properties of individual conformational states and their possibilities to isomerize to other conformational states (Fig 12), three main classes of effects may be expected in such an allosteric system with increasing numbers of interconverting states (Galzi *et al.*, 1996b): (1) the binding or “K” phenotype; (2); the conformational interconversion or “L” phenotype; and (3) the conductance or “ γ ” phenotype.

B. The K phenotype

The K phenotype is assumed to result from mutations which selectively alter the intrinsic binding affinities of individual conformational states. In this context two possibilities may be envisioned. First, the affinity of each conformation changes but the affinity ratio ($i_j c = K_i / K_j$) between conformations remains constant. The apparent affinity (EC_{50}) for response activation

would then change with neither modifications of cooperativity (Hill coefficient) nor response amplitude. In other words, the wild-type and mutant dose-response curves are parallel. Second, the mutation selectively alters the affinity of certain states only, leading to changes in the affinity ratios (i_j/c). In this case, not only would the apparent affinity be affected, but also cooperativity and possibly response amplitude. Furthermore, as c increases, agonists may progressively become partial agonists or even competitive antagonists. Finally, for none of the K phenotypes would the spontaneous equilibrium between any states S_i and S_j be altered in the absence of ligand.

A possible example of this phenotype may be considered on the basis of the amino acids Tyr-93, Trp-148, Tyr-190 and Tyr-198 identified by affinity and photoaffinity labeling of the ACh binding site from electric organ nicotinic receptor (Devillers-Thiéry *et al.*, 1993). Substitution of their homologs to phenylalanine on the corresponding chick neuronal $\alpha 7$ residues Tyr-92, Trp-148 and Tyr-187 (Galzi *et al.*, 1991a) or on mouse muscle $\alpha 1$ subunits (Tomaselli *et al.*, 1991; Aylwin and White, 1994) yields functional receptors, with reduced sensitivity to ACh, but unchanged Hill coefficients and maximal current amplitudes. These alterations may be interpreted in terms of a "K" phenotype, with the intrinsic affinity of the activatable and active conformations being affected to the same extent. As recently reported (Galzi *et al.*, 1996b) simulation of $\alpha 7$ nicotinic receptor dose-response curves with changes in solely the K values for Y92F, W148F and Y187F mutant receptors fits the experimental data points (Galzi *et al.*, 1991a) and yield EC_{50} values and Hill coefficients consistent with the experimentally determined values.

Mutations in other parts of the extracellular domain of ligand-gated ion channels alter the pharmacological specificity in a different way. Mutation of Asp-200 in muscle $\alpha 1$ (O'Leary and White, 1992) or Gln-198 in neuronal nicotinic $\alpha 3$ (Galzi *et al.*, 1992), as well as Ile-111 and

Ala-212 in $\alpha 1$ glycine receptor subunits (Schmieden *et al.*, 1992), affect the relative affinity and efficacy of distinct agonists. Mutation of Asp-200 to Asn, in particular, converts the partial agonists TMA and PTMA into competitive antagonists (O'Leary and White, 1992), as expected for changes of intrinsic binding properties of only certain states within the network: i.e. altered c values in a K phenotype (Galzi *et al.*, 1996b). Yet, uncertainties persist about this interpretation since the properties of these mutants may also be accounted for by an L phenotype. Additional experimental data are required to reach definitive conclusions.

C. The L phenotype

The L phenotype is assumed to result from mutations which selectively alter the equilibrium constant between two given interconvertible conformations. The intrinsic properties of each conformation, i.e. the microscopic binding constants and the state of channel activity, are further assumed to remain unchanged. Considering the two states comprising an inactive (channel closed) B and an active (channel open) A state, the fraction of receptor molecules spontaneously existing in the active state is described by ${}^{BA}L=[B]/[A]$. Furthermore, regulation of channel opening by an agonist depends on its affinity for the active state, as compared to its affinity for the inactive state (${}^{BA}c = K_A/K_B$). Agonists are characterized by a small value of ${}^{BA}c$, partial agonists by a larger ${}^{BA}c$ value and competitive antagonists by an even larger one. For an "L phenotype", as ${}^{BA}L$ increases, agonists may progressively become partial agonists and competitive antagonists, as shown in Fig. 13. For decreasing ${}^{BA}L$ values, the reciprocal progression takes place, and, in addition, competitive antagonists, may become partial agonists (intermediate ${}^{BA}c$ values) or remain competitive antagonists (large ${}^{BA}c$ values). Also, in equilibrium binding experiments, apparent affinities will be displaced more for ligands with small ${}^{BA}c$ values than for ligands with large ${}^{BA}c$ values. Furthermore, the model predicts that for

very low values of ^{BA}L , spontaneous stabilization in the active state may occur, yielding constitutively active mutants (spontaneous channel opening), a phenomenon that cannot be accounted for by the C&S-type model. In addition, at low ^{BA}L positive allosteric effectors of the wild-type, which behave as very weak agonists, may become partial agonists of the mutant. Finally, changes in the ^{BA}L value will generally be accompanied by changes in cooperativity and maximal response amplitude.

A possible example of this phenotype may be considered on the basis of chemical labeling of *Torpedo* nicotinic receptor with noncompetitive blockers which led to the identification of amino acid rings from the M2 segment of all five subunits that contribute to the channel domain and are conserved in the family of nicotinic receptors (Devillers-Thiéry *et al.*, 1992; Karlin, 1993). In the case of the $\alpha 7$ nicotinic receptor, the available data on the alterations of receptor properties which take place upon substitution of the ring of Val-251 to Thr or of Thr-244 to Gln, can be interpreted in terms of "L" phenotypes. Indeed, ACh dose-response curves can be simulated for wild-type and mutant receptors (Galzi *et al.*, 1996b), with the single assumption that L values are high for the wild-type ($^{BA}L = 8 \times 10^5$) and low for the mutants ($^{BA}L = 20$), corresponding to within the limits of precision of the experimental data to the simulated curves presented in Fig. 13. Such simulations also account for the higher maximal amplitudes of the ionic response observed for these mutants (Devillers-Thiéry *et al.*, 1992; Luetje *et al.*, 1993). Furthermore, the competitive antagonist of the wild-type receptor, DH β E, with its specific binding K and ^{BA}c values (see details in legend to Fig. 13), behaves as a competitive antagonist when the ^{BA}L value corresponds to the wild-type receptor, and as a partial agonist when the ^{BA}L value corresponds to the V251T or T244Q mutant receptor.

An interesting comparison with the L phenotype for the nAChR is afforded by certain mutations in the channel domain of glycine receptors. Two mutations identified in M2 from the

glycine receptor at position R271 (mutations R271L and R271Q) cause the neurological disorder hyperekplexia (Shiang *et al.*, 1993) by drastically reducing the apparent affinity of the receptor for the agonist glycine (Langosh *et al.*, 1994; Rajendra *et al.*, 1994; Rajendra *et al.*, 1995). These mutations, in addition, decrease the maximal amplitude of agonist-evoked currents, reduce the number of conducting states when present in the homooligomeric $\alpha 1$ receptors from 5 (wild-type) to 3 (R271L) or 1 (R271Q), and convert the partial agonists β -alanine and taurine into competitive antagonists. Accordingly, their phenotype appears as a "mirror image" of the phenotypic changes observed in the nicotinic $\alpha 7$ receptor L247T or V251T: the glycine receptor mutants would then resemble nAChR wild-type (Galzi *et al.*, 1996b).

D. The γ phenotype

The γ phenotype is assumed to result from changes of the state of activity of the ion channel (e.g. nonconducting to conducting) in one (or possibly more) conformation, with no alterations of the intrinsic binding parameters of each state (i.e. its pharmacological specificity) nor of the equilibria (and kinetics) of interconversions. For example, it may be assumed that one desensitized conformation, which exhibits high affinity for agonists but has a closed channel, becomes conducting after a mutation. In such a three state model (one activatable and two conducting states), the expected changes of the physiological response properties are four-fold, as compared to wild-type: i) desensitization of the response to agonists is reduced, since isomerization to a desensitized conformation is no longer accompanied by a closing of the ion channel; ii) the apparent affinity for activation is higher for agonists, since desensitized conformations exhibit higher affinity for agonists; iii) a new conducting state, in addition to the wild-type conducting state, may be observed and; iv) the pharmacological drug profile of the two conducting states differ. Agonists cause the opening of one conducting state at low

concentration (the high affinity desensitized but conducting state) and of two conducting states at high concentration, while competitive antagonists, if stabilizing the desensitized conformation, will activate only the new conducting state at any concentration used.

Analogies exist between the phenotypes of the M2 mutants L247T, and T244Q or V251T. Yet, if the L247T mutant receptor were to correspond to an "L phenotype", a single change in L value would not fully account for the experimentally determined ACh and DH β E dose-response curves (Revah *et al.*, 1991; Bertrand *et al.*, 1992; Devillers-Thiéry *et al.*, 1992). Indeed, with the L value yielding an appropriate EC₅₀ for ACh, DH β E will not behave as a full agonist, but rather as a partial agonist as on the T244Q or V251T mutants; moreover, under no circumstances will the apparent affinity for DH β E be, as observed, higher than for ACh. Rather, the occurrence, in addition, in L247T of two conducting states with distinct pharmacological profiles (Revah *et al.*, 1991; Bertrand *et al.*, 1992; Devillers-Thiéry *et al.*, 1992), favors an interpretation in terms of the " γ phenotype" scheme. In such a case, simulated dose-response curves satisfactorily fit the experimental data, as shown in Fig. 14 for both ACh (ligand 2) and DH β E (ligand 1), assuming that one of the conducting states is identical to the wild-type conducting states (not stabilized by DH β E), while the other (assumed to correspond to a desensitized conformation of the wild-type) binds DH β E with affinity higher than for ACh (Galzi *et al.*, 1996b).

E. Limiting properties at extremes of L

The range of properties resulting from the L phenotype arises from differences in the binding (\bar{Y}) and ionic response (\bar{A}) functions. As pointed out some thirty years ago (Rubin and Changeux, 1966; Changeux and Rubin, 1968), where it is possible to monitor \bar{Y} and \bar{A} separately, distinctive differences in the two functions may be observed, thereby constituting a

diagnostic test of the two-state model. For very low values of L , a significant fraction of molecules is in the A state in the absence of ligand: the system may be qualified as *hyper-responsive* (Edelstein and Changeux, 1996). Upon addition of ligand, the curve for \bar{A} remains above the curve for \bar{Y} as a function of ligand binding, with the curve for \bar{A} approaching saturation at ligand concentrations that give incomplete binding. For very high L values, the curve for \bar{A} remains below the curve for \bar{Y} , with a maximal value of $\bar{A} < 1$, even when all binding sites are saturated: the system is *hypo-responsive*. At intermediate values of L , differences between \bar{Y} and \bar{A} may also occur, but they involve more subtle distinctions in the shape of curves.

The full extent of possible differences between \bar{Y} and \bar{A} as a function of the L value are presented in Fig. 15 for a protein with 5 sites (Edelstein and Changeux, 1996), such as the $\alpha 7$ nAChR (Palma *et al.*, 1996). For ligand binding, \bar{Y} always varies from 0-1 and occurs, for a protein with A and B states, within the affinity limits of Y_A and Y_B that define the “ligand binding range”. In contrast, for the state function, at the extremes of L , \bar{A} does not vary between 0 and 1 with increasing ligand binding, but has a limited allosteric range, Q (Rubin and Changeux, 1966), as summarized in the lower portion of Fig. 16. Moreover, as noted in Fig. 15, the “ligand response range” \bar{A} can extend significantly beyond the limits of K_A and K_B . For a protein with 5 sites, the apparent affinity, EC_{50} (as reflected by $[X]_{50}$, the concentration of ligand at the midpoint of the \bar{A} curve) may be as much as 6.7 times lower than K_A (the extreme hyper-responsive pattern) or 6.7 times higher than K_B (the extreme hypo-responsive pattern). This distinction is relevant for $\alpha 7$ receptors, since for the wild-type, according to the simulations described in Fig. 13, the EC_{50} value is ~ 5 times higher than the value of K_B and thus close to the theoretical limit of 6.7 for a pentamer.

Differences in the cooperativity of the binding and state functions also occur, as measured for example by the Hill coefficients, n_{50} at $\bar{Y} = 0.5$ and n'_{50} at $\bar{A}' = 0.5$ (Fig. 16), where \bar{A}' is the normalized form of the response (Changeux and Rubin, 1968). The maximum value for n'_{50} is higher than for n_{50} and at the extremes of L the value of n_{50} falls to the limit of 1.0 (Rubin and Changeux, 1966), but the lower limit of \bar{A}' for a homopentamer (for $^{BA}c = 0.1$) is $n'_{50} = 1.27$ (Edelstein and Bardsley, 1997). This value >1 arises from the contributions of higher order reactions to the formation of molecules in the A state, as summarized in Fig. 17. In this context, the cooperativity of the dose-response curves of the $\alpha 7$ nAChR predicted by a two-state model, $n'_{50} = 1.27$ (Fig. 13) and the value observed experimentally, $n = 1.4$ (Revah *et al.*, 1991) imply that the system is near the lower theoretical limit for a pentamer.

VI. DEDUCTIONS FROM SINGLE CHANNEL MEASUREMENTS

A. Separation of single ionic and single ligand-binding events

Single channel measurements on muscle nAChR have made a profound contribution to the understanding of these receptors, since they provide high temporal resolution and the advantage of observations at the level of individual molecules (Neher and Sakmann, 1976; Sakmann *et al.*, 1980; Colquhoun and Sakmann, 1985; Jackson, 1988; Sine *et al.*, 1990). However, up to the present time, the linked events of ligand binding have only been inferred, *indirectly*, from single channel recordings, since parallel observations on binding steps have not been possible. Yet, developments in the field of fluorescence correlation spectroscopy (Eigen and Rigler, 1994; Rauer *et al.*, 1996; Edman *et al.*, 1996; Schwille *et al.*, 1997) now place such measurements in the realm of possibilities for the near future. Therefore, we have undertaken simulations in order to study what additional insights would be available with measurements that follow simultaneously both single ionic and binding events (Edelstein *et*

al., 1997b). In this respect, theory precedes experiment, but should provide a stimulus for the necessary technical advances. In addition, the simulations include the A state at all degrees of ligand binding (Fig. 4), thereby permitting comparisons with the C&S model which incorporates formation of the A state only for bi-liganded receptors (Fig. 7).

Stochastic simulations anticipating both single binding events and single ionic events are illustrated in Fig. 18 for muscle-type nAChR. The simulations generate a train of molecular species that vary with respect to conformational state and/or the degree of binding site occupancy, as illustrated in Fig. 18 a. On the basis of such simulations, single binding events and single ionic events can be separated. Binding events are registered, as depicted in Fig. 18 b, when passage from one molecular species to the next involves a change in the number of ligands bound. Ionic events are registered, as depicted in Fig. 18 c, for each transition to an A-state molecular species, with termination of the event occurring with the transition to a B-state or I-state molecular species. No transitions to the D state occurred in the course of this simulation. It may be noted that opening events are on average longer for A_2 than for A_1 events. Opening events for A_0 events are on average even shorter, although none appeared in the simulation presented here. Overall, far fewer ionic events are predicted than binding events with the parameters used for this simulation. Most of the ligand binding events, involving the B state, are of short duration, but longer ligand binding events coincide with passage to the A state. In the simulation shown, the longest binding event occurs with passage to I_2 . For the simulations summarized in Figures 19 and 21-23, only the binding events and ionic events are presented, since on the basis of this information the sequence of molecular species can be deduced.

When simulations of the stochastic properties of wild-type AChR based on the MWC-type model are generated for a low ligand concentration (3×10^{-7} M) and compared to the behavior

predicted for the same concentration by the C&S-model, marked differences appear, as presented in Fig. 19. Portions of the stochastic simulations obtained with the MWC-type model are presented for binding events (in Fig. 19 a) and for ionic events (in Fig. 19 b), along with the complete descriptions of both based on dwell time profiles. In order to permit direct comparisons, points (+) are included on the dwell time profiles representing predictions with the C&S-type model. At the low concentration of the simulation, ionic events are predicted to be rare, $\sim 1/s$ (corresponding to a probability of channel opening of $P_{open} = 0.002$), whereas binding events are predicted to be ~ 20 -fold more abundant (corresponding to a probability of ligand binding of $P_{occ} = 0.04$). The ionic events are predicted to occur mainly for A_1 , with fewer events for A_2 and A_0 (Fig. 19 b). Since the C&S-type model incorporates ionic events only for A_2 , less than half as many events and events with an average dwell time about 4 times longer are predicted, as shown in Fig. 19 b (+). Therefore, the quantitative differences between the frequency of durations of opening events predicted by the two models are readily measurable and represent a testable criterion to distinguish between models in suitably designed experiments.

B. Consequences of non-equivalent sites

Two equivalent sites were used in the C&S-type scheme to model single channel measurements (for reviews see Lingle *et al.*, 1992; Edmonds *et al.*, 1995). However, in a number of other studies with muscle nAChR, marked apparent differences (up to two orders of magnitude) in the affinities of the two ligand-binding sites, as may result from specific differences for binding sites at the α - γ and α - δ interfaces (see Section I. B), have been used to develop alternative interpretations of experimental data (Jackson, 1988; Sine *et al.*, 1990; Chen *et al.*, 1995; Zhang *et al.*, 1995; Sine *et al.*, 1995; Akk *et al.*, 1996; Ohno *et al.*, 1996).

Moreover, a wide range of magnitudes for the differences in the kinetic parameters of the two sites for wild-type receptors have been assigned in these reports. Species differences and dependence on expression systems may in part explain such variability in the non-equivalence of the two binding sites (Edmonds *et al.*, 1995), but uncertainties remain concerning the intrinsic functional properties of the two sites. Therefore, simulations were also undertaken to explore whether measurements of both single ionic and single binding events could provide additional criteria concerning the extent of non-equivalence of the binding sites. The MWC-model was modified to incorporate non-equivalent sites as described in Fig. 20.

Simulations that separate binding events and ionic events for wild-type muscle receptors at low ligand concentration using parameters based on data interpreted with non-equivalent sites are presented in Fig. 21. In this case, for a ligand concentration (1.7×10^{-6} M) that yields the same opening probability ($P_{open} = 0.002$) examined for equivalent sites in Fig. 19, the ionic events (Fig. 21 b) show relatively minor differences with respect to the ionic events simulated with equivalent sites (Fig. 19 b). The shoulder at longer times ($\sim 10^{-2}$ s) on the overall profile is slightly more pronounced and at all concentrations fewer events are predicted with the parameters based on non-equivalent sites, due to a lower estimate for the value of ${}^{AB}k_2$. Overall, differences in the predictions of the MWC-type model (thick line) and the C&S model (+) for dwell-times of ionic events are similar to the differences predicted with equivalent sites (Fig. 19). It can therefore be concluded that a compensation in the values of the key parameters leads to similar simulated properties in the two cases. This compensation may explain why experimental data has been satisfactorily interpreted with equivalent sites in some cases and with non-equivalent sites in other cases.

In contrast to the similarity of ionic events, larger differences in the simulated binding events are predicted when equivalent sites (Fig. 19 a) and non-equivalent sites (Fig. 21 a) are

compared. The data interpreted with non-equivalent sites indicate a 700-fold difference in the affinities of the binding sites of the B state (Jackson, 1988). As a result, binding of the first ligand to a receptor is predicted to occur almost exclusively at the higher affinity site to generate $B_{1(H)}$ (Fig. 21 b). Since this site is characterized by a 16-fold lower ligand dissociation rate than in the case of equivalent sites (Table 1), the peak in the dwell time profile for binding at low concentrations is predicted to lie at longer times: 2×10^{-3} s for non-equivalent sites (Fig. 21 a) compared to 1.2×10^{-4} s for equivalent sites (Fig. 19 a). Hence, if single ligand-binding events were to be measured experimentally, their dwell time profiles could provide a direct test of the extent of binding site non-equivalence.

In comparison to these deduction for muscle-type nAChR, the situation for neuronal nAChR is more complicated because of the variety of neuronal forms and the differences for homopentameric and heteropentameric assemblies. For homopentameric neuronal nAChR composed of $\alpha 7$, $\alpha 8$, or $\alpha 9$, the identical subunits presumably impose an equivalence of sites at each interface, with each subunit contributing a *principal component* at one interface and a *complementary component*, at the other interface (Corringer *et al.*, 1995). Other neuronal receptors with the heteropentameric composition $\alpha 4\beta 2$ or $\alpha 3\beta 4$ would presumably possess functionally equivalent ligand binding sites at identical $\alpha 4/\beta 2$ or $\alpha 3/\beta 4$ interfaces, with the complementary component provided in these cases by the β -type subunit. More complicated combinations may be expected for receptors with subunit compositions $\alpha 3\alpha 5\beta 4$ (Vernallis *et al.*, 1993), $\alpha 4\alpha 5\beta 2$ (Conroy *et al.*, 1992; Ramirez-Latorre *et al.*, 1996), or $\alpha 6\beta 2\beta 3$ (Le Novère *et al.*, 1996). For these receptors, it has been suggested that $\alpha 5$ and $\beta 3$ could exert a γ -like role (Le Novère and Changeux, 1995). However, these systems have not as yet been analyzed in sufficient detail to draw conclusions concerning the degree of functional non-equivalence of the ligand-binding sites.

C. Convergence of mechanistic models at high agonist concentrations

For receptors modeled at high ligand concentration (corresponding to a probability of channel opening of $P_{open} = 0.5$) with equivalent sites, the simulated ligand-binding and ionic events are presented in Figure 22. In this case, ionic events (Fig. 22 b) are almost as abundant as binding events (Fig. 22 a), and most ionic events arise from transitions to A_2 . As a result, the points (+) on the dwell time profile corresponding to the C&S model effectively coincide with the profile based on the events predicted with the MWC model (thick line). In addition, for simulations incorporating marked non-equivalence of the binding sites, virtually identical results are also predicted by the two models (Edelstein *et al.*, 1997b), since in this case as well the ionic events are dominated by transitions involving A_2 . With respect to the simulations of binding events at high ligand concentrations, similar properties are also predicted for both equivalent and non-equivalent sites. The contributions of the individual molecular species differ, with B_1 dominating with equivalent sites and B_2 dominating for non-equivalent sites (Edelstein *et al.*, 1997b). However, these distinctions would not necessarily be available from experimental data that recorded overall binding events, and information on site non-equivalence would not therefore be readily provided from measurements at high ligand concentration.

D. Kinetic consequences of mutant phenotypes

Several classes of congenital myasthenic syndromes have been described involving specific components of the neuromuscular junction, including a number of point mutations in the nAChR (see reviews by Engel, 1993; Vincent *et al.*, 1997). Site-directed mutations of the $\alpha 7$ neuronal nAChR had previously permitted identification of residues in the M2 transmembrane

segment where substitution of the wild-type residue produces dramatic increases in the sensitivity to ACh (Revah et al., 1991; Galzi *et al.*, 1992; Devillers-Thiéry *et al.*, 1992) sometimes referred to as “gain of function” (Treinin and Chalfie, 1995). A similar mutation in a human muscle nAChR, ϵ T264P (Ohno *et al.*, 1995) is of particular interest, since it displays high affinity that could contribute to excess calcium uptake, with pathological consequences. The markedly altered channel opening properties of this mutant also provide a unique opportunity to test alternative models. Therefore, simulations based on the data reported with ϵ T264P were carried out for an ACh concentration of 3×10^{-7} M, as presented in Fig. 23. This simulation contrasts markedly with the pattern of binding and opening events predicted for wild-type receptors at the same ACh concentrations (Fig. 19).

Although a complete kinetic analysis was not included in the initial description of the ϵ T264P receptors, the simulation presented in Fig. 23 corresponds approximately to the properties described for an ACh concentration of $0.3 \mu\text{M}$ by using wild-type parameters for muscle nAChR (based on equivalent sites) for all ligand binding events. An adequate fit of the mutant data was achieved by modifying the interconversion rate, i.e., lowering the value of ${}^{\text{BA}}L_0$ 100-fold, which facilitates the B \rightarrow A transitions (Edelstein *et al.*, 1997a). The result is a substantial increase in the sensitivity to ligand, such that at 3×10^{-7} M ACh the probability of opening increases to $P_{\text{open}} = 0.37$ for the ϵ T264P mutant (Fig. 23), compared to the wild-type value of $P_{\text{open}} = 0.002$ at the same concentrations (Fig. 19). Moreover, in contrast to the wild-type pattern, at this concentration of ligand the simulation predicts more ionic events than binding events for the ϵ T264P receptors, in particular because a significant number of ionic events can occur in the absence of ligand binding (Fig. 23). These simulations were performed with equivalent sites, since no indications concerning non-equivalence of the sites at the α - ϵ and α - δ boundaries were reported for this mutant.

For ϵ T264P receptors, the assumption of a diminished value of ${}^{BA}L_0$, but normal ligand-binding constants, leads to the prediction of three distinct peaks in the dwell time profiles of opening events (Fig. 23 b). This pattern is compared to the three peaks reported for recombinant ϵ T264P receptors (Ohno *et al.*, 1995) and represented in Fig. 23 b by the individual points (o) calculated by summing the three experimentally observed phases and scaling the total number of events to minimize amplitude differences with the dwell time peaks predicted by the MWC-type model. Compared to the experimental data, the MWC model over-estimates the height of the intermediate (A_1) peak (and places it at slightly longer times) and under-estimates the heights of the A_0 and A_2 peaks. Nevertheless, this initial fitting gives a reasonably satisfactory agreement between theory and experiment, considering the difficulties in extracting the parameters from the three overlapping experimental curves and the relatively limited quantity of data reported (Ohno *et al.*, 1995). Because the change in ${}^{BA}L_0$ results in a low value of the ${}^{AB}k_2$ rate constant, only slightly greater than the value of ${}^A k_{\text{off}}$ (see legend to Fig. 23), about half of the opening events involving A_2 terminate by dissociation of a ligand to yield A_1 . The sum of events terminating by both $A_2 \rightarrow B_2$ and $A_2 \rightarrow A_1 \rightarrow B_1$ are indicated by the peak labeled ΣA_2 (Fig. 23 b). This figure also presents predictions of the C&S-type model (+). In this case, the restriction of channel opening to doubly-liganded receptors leads to the prediction of a reduced number of ionic events in the region of the A_2 peak. Moreover, since ligand dissociation from the A state is not explicitly introduced in the C&S-type model (Fig. 7), ligand dissociation does not contribute to shortening the dwell time of ionic events and the peak of the dwell time profile for ionic events occurs at longer times ($t > 0.1$ s).

While certain quantitative aspects thus remain to be clarified, the simulations and comparison to experimental data illustrate the key role predicted for the value of ${}^{BA}L_0$ in

determining the relation between binding and ionic events. On the basis of the available data, it may therefore be tentatively concluded that the altered properties of ϵ T264P receptors represent an “L phenotype”(see Section V). Although the properties of ϵ T264P receptors are readily represented by mainly changing ${}^{BA}L_0$, it is appropriate to examine what other changes in the values of the parameters might also adequately represent the data. Changes in ligand-binding properties corresponding to higher affinity could be introduced that would predict openings of A_1 and A_2 molecules at low concentration, but the openings associated with a significant fraction of A_0 in the molecular population can only be explained by a substantial lower value of ${}^{BA}L_0$. Therefore, changes in parameters other than ${}^{BA}L_0$ may contribute to the phenotype, but satisfactory fitting cannot be achieved without a large decrease in ${}^{BA}L_0$. It should be possible to obtain additional information to permit a more complete estimation of all parameters by extending the analysis to a full characterization of open and closed dwell times.

Altered desensitized states may also contribute significantly to mutant phenotypes, as deduced for the myasthenic mutant identified in the region of the agonist binding site, α G153S (Sine *et al.*, 1995). This position occurs in the loop B that has been found to play a critical role in the ligand-binding properties of the desensitized states, while the loop C region participates in agonist selectivity (Corringer *et al.*, 1997), where A, B and C refer to the three regions identified in specific labeling experiments (Devillers-Thiéry *et al.*, 1992). The distinctions in the fine-structure of the agonist-binding sites concerning desensitization and agonist selectivity were deduced by comparing the $\alpha 7$ homooligomer and the $\alpha 4\beta 2$ heterooligomer which display striking differences in their apparent affinities for acetylcholine and in their pharmacological specificity for acetylcholine versus nicotine. Sets of residues from the regions initially identified within the agonist binding site of the $\alpha 4$ subunit were

introduced into the homooligomeric $\alpha 7$ -V201-5HT₃ chimera which carries the intact $\alpha 7$ agonist binding site (Eiselé *et al.*, 1993). Introduction of the $\alpha 4$ residues 151-155 of loop B produced an approximately 100-fold increase in the apparent affinity for both acetylcholine and nicotine in equilibrium binding measurements, whereas electrophysiological recordings revealed a much smaller increase (3 to 4-fold) in the apparent affinity for activation. These observations are consistent with the notion that the residues mutated alter the transition to the desensitized state. In contrast, introduction of the $\alpha 4$ residues 183-191 (from loop C) into $\alpha 7$ selectively increased the apparent affinities for binding and activation by acetylcholine, resulting in a receptor that no longer displays differences in the responses to acetylcholine and nicotine, demonstrating the importance of the C loop in agonist selectivity (Corringer *et al.*, 1997).

VII. ALLOSTERIC EFFECTORS AND COINCIDENCE DETECTION

Various modifications of the functional properties of AChR are produced by non-covalent interactions with pharmacological agents and other modulators (Léna and Changeux, 1993; Changeux, 1996) and covalently by phosphorylation (Huganir and Greengard, 1990; Levitan, 1994). In general, when differences in current are observed in the presence and absence of a potential allosteric effector, it has not generally been determined whether affinity changes and/or specific conductance changes are responsible for the differences. In this respect the study by Mulle *et al.* (1992) is of particular interest, since potentiation by calcium was shown to result from an increase (~3 fold) in the frequency of channel opening. A modeling of these data presented in Fig. 24 indicates that the potentiation by calcium can be represented simply in terms of a 2.3-fold reduction in the allosteric constant, ${}^{\text{BA}}L_0$, with all other parameters remaining unchanged from the values in Table 1. The lower value of ${}^{\text{BA}}L_0$ is sufficient to

account for the shift of the curve to the left and the augmented increased response (Fig. 24 a). The effect of calcium is thus a true allosteric modulation, since the change in frequency of openings indicates an altered value of the rate constant $^{BA}k_2$ that corresponds closely to the change estimated for $^{BAL}_0$, since $^{BAL}_0 \text{ }^{BA}c^2 = ^{AB}k_2 / ^{BA}k_2$. Calcium modulation of the L value for activation has also been observed for the nAChR-5HT₃R chimera (Galzi *et al.*, 1996a) and more general implications of calcium as an intracellular signal may be related to the fact that neuronal nicotinic acetylcholine receptors as a class have a high relative permeability to calcium (Rathouz *et al.*, 1996; Vernino *et al.*, 1992).

Allosteric effects of the type observed for potentiation by calcium have a number of implications for regulation of activity in the nervous system. At synapses, allosteric modulators could provide coincidence detection (Heidmann and Changeux, 1982; Changeux and Heidmann, 1987). Such an effect for ACh and calcium may be visualized in Fig. 24 b, assuming a constant threshold that is attained only in the presence of both ACh and calcium (on the left), but not with ACh alone (on the right). Since calcium may enter neurons via the open ligand-gated cation channel of various neuronal AChR or voltage-gated channels, regulatory effects may also be produced related to intracellular accumulation (such as phosphorylation) or extracellular depletion (such as habituation resulting from repeated stimulation by ACh). In addition to its role in regulating synaptic efficiency, diminished extracellular calcium concentrations could also participate in retrograde signaling. In general, calcium or other allosteric effectors could provide an alternative to the NMDA $\text{Ca}^{2+}/\text{Mg}^{2+}$ coincidence detection system (Wigstrom and Gustafsson, 1985), as discussed more fully in Section VIII. B.

Similar effects that could play a role in coincidence detection by shifting the dose-response curve with a change in maximal response amplitude are observed for modulators

such as steroids (Valera *et al.*, 1992; Buisson and Bertrand, 1997). Allosteric effects may also involve modulation of desensitized states, as for example is observed with substance P (Valenta *et al.*, 1993) or following phosphorylation with cAMP-dependent protein kinase (Huganir *et al.*, 1986). Overall, any substance that alters the pre-existing equilibria between states can exert an effect on synaptic efficiency or coincidence detection (see Changeux, 1990; Changeux, 1996). More complex effects involving a sliding threshold (Bienenstock *et al.*, 1982) may also be formulated (Fig. 24 c) and the general implications for sliding thresholds are presented in Section VIII. B.

VIII. GENERAL CONSIDERATIONS

A. Evaluation of mechanistic models

The simulations presented were used to determine conditions that could lead to experimentally testable differences in the predictions of the MWC-type and C&S-type models. In addition, the simulations explored what additional distinctions could be furnished by measurements of single ligand-binding events, particularly when the binding sites are non-equivalence. The analysis of single binding events remains hypothetical for the time being compared to the single channel measurements that have been extensively developed since the early applications of this technique (Neher and Sakmann, 1976; Sakmann *et al.*, 1980). While a single channel event can be recorded because of the amplification derived from the flux of thousands of ions, no such amplification is produced by a single binding event. However, recording of single binding events are in principle feasible with fluorescence correlation spectroscopy (Elson and Magde, 1974; Magde *et al.*, 1974; Ehrenberg and Rigler, 1974), in the light of recent advances (Eigen and Rigler, 1994; Rauer *et al.*, 1996; Edman *et al.*, 1996; Schwille *et al.*, 1997). As indicated by the simulations described here, such measurements

could be utilized to critically evaluate the degree of non-equivalence of the ligand-binding sites. While single-channel data has been interpreted both in terms of equivalent and non-equivalent sites, as recently reviewed (Edmonds *et al.*, 1995), compensating effects in the values of the parameters result in similar predictions in the two cases (see Figs. 19 b and 21 b). However, larger differences are predicted for the dwell time profiles of the binding events at low agonist concentration (Fig. 19 a versus Fig. 21 a) that could readily distinguish between the equivalent and non-equivalent schemes, if the appropriate experiments could be conducted.

With respect to the MWC-type and C&S-type functional models, simulations demonstrate that for wild-type muscle receptors significant differences are predicted for single channel measurements, but only at low ligand concentrations (Fig. 19). In this case, the MWC-model predicts appreciable contributions to channel opening from unliganded and mono-liganded receptors, compared to the C&S-type model which incorporates channel opening only for bi-liganded receptors (see Fig. 7). At higher agonist concentrations in the range of the EC_{50} (Fig. 22), functional properties are dominated by bi-liganded molecules and the predictions of the two models converge. Under these conditions, the C&S model can thus describe the relevant properties with fewer parameters than the MWC model. Considering only activation (with equivalent sites), the C&S model requires the four rates that define K_B and K_{open} (${}^Bk_{on}$, ${}^Bk_{off}$, α , and β), whereas the MWC model requires the six rates that define K_B , K_A , and ${}^{BA}L_0$ (${}^Bk_{on}$, ${}^Bk_{off}$, ${}^Ak_{on}$, ${}^Ak_{off}$, ${}^{BA}k_0$, and ${}^{AB}k_0$), plus the transition state positional parameter ${}^{BA}p$ (Fig. 6). Nevertheless, with the C&S model physical interpretations are limited by the fact that changes in K_{open} are ascribed to "gating," whereas with the MWC model distinctions in the equivalent terms ($K_{open} = {}^{BA}L_0 [K_A/K_B]^2$) can be related to isomerization or binding (Edelstein *et al.*, 1997b). It should also be noted that indications of ionic events for

mono-liganded molecules were reported by Colquhoun and Sakmann (1985) on the basis of brief openings. Although the data did not follow the expected concentration dependence, estimates of β_1 and α_1 (the opening and closing rates of mono-liganded receptors, respectively) were made (Colquhoun and Sakmann, 1985) and these values were incorporated in the MWC-type model with equivalent sites (Edelstein *et al.*, 1996), leading to the values utilized in the simulations reported here (Table 1). Future experimental tests on wild-type receptors at low concentrations or more complete examination of mutants such as ϵ T264P should establish more precise limits on the functional properties of un- and mono-liganded receptors.

Concerning the extent of non-equivalence of the binding sites, an MWC-type model with substantial non-equivalence was proposed to account for the data of wild-type muscle receptors by Jackson (1988). The extent of non-equivalence of the ligand-binding sites for the B state was evaluated entirely on the basis of kinetic measurements derived from single channel recordings. Other measurements, particularly the degree of cooperativity in dose-response curves, can also provide relevant information, where a Hill coefficient (n_H) > 1 indicates positive cooperativity. For wild-type receptors, with the parameters deduced by Jackson (1989) for non-equivalent sites, and at ligand concentrations near the EC_{50} virtually all of the openings accompany binding of the second ligand molecule to the low-affinity site. As a result, the predicted dose-response curve is non-cooperative ($n \cong 1.0$). In contrast, for wild-type receptors with equivalent sites (described by the parameters in Table 1) the predicted dose-response curve is strongly cooperative : $n = 1.7$ (Edelstein *et al.*, 1996). Similarly, for the ϵ T264P mutant receptors, the relevant parameters (Fig. 23) also predict highly cooperative dose-response curves, with $n = 1.8$. Hence, there is a discrepancy only between the non-cooperative dose response curve predicted for wild-type receptors with

strongly non-equivalent sites and the widely observed cooperativity characterized by $n > 1.5$ (Changeux and Edelstein, 1994).

One possible explanation for this discrepancy in the predicted and observed Hill coefficients is the presence of a channel block that modifies the response in such a way as to generate an “apparent” cooperativity (Sine *et al.*, 1990; Forman and Miller, 1988). Adding an ACh channel block with a dissociation constant of 1.3 mM (Colquhoun and Ogden, 1988) reduces the maximal amplitude of the response to about 50%. However, if the maximum ligand concentration examined for the dose-response curve is limited to ~ 1 mM, the reduced amplitude could be considered as a full response and scaled to 100%. In this case, the vertical “stretching” of the dose-response curve would result in an increase in the Hill coefficient to 1.5. Since the dose-response measurement is generally evaluated between arbitrary end-points assumed to correspond to 0 and 100%, the presence of channel block could explain the degree of cooperativity generally observed, even if there is strong non-equivalence of the binding sites. Rapid desensitization that also impinges on the maximal amplitude of the response could in principle exert a similar effect (see Fig. 10), but measured desensitization rates are too slow to cause a significant attenuation of the amplitude (Franke *et al.*, 1993).

While the degree of cooperativity can provide a useful index with respect to mechanisms, in general the amplitudes of dose-response curves are much less sensitive than single channel measurements for discriminating between different mechanistic models. Although indistinguishable current levels would be predicted by MWC-type and C&S-type models at agonist concentrations near the EC_{50} (see Fig. 22), it should be noted that even for low agonist concentrations where marked differences occur in the number of openings predicted by the MWC-type and C&S-type models, the differences in currents are minor. For example, in the simulation at low agonist concentration presented in Fig. 19, the number of single channel

events predicted by the MWC-type model is about 2-fold higher compared to the C&S-type model, but the same data predict a difference of only about 30% in current (Edelstein *et al.*, 1997b). Since precision is low in this amplitude range ($P_{open} = 0.002$) reliable conclusions could not be readily drawn. The greater differences predicted for single channel measurements than for current measurements results from the fact that the channel opening events of unliganded and mono-liganded receptors (Fig. 19) are briefer than the opening events of bi-liganded receptors (4-fold and 15-fold, respectively). Hence, there are many such events, but their predicted contributions to the overall current are small compared to the longer events produced by bi-liganded receptors.

B. Implications for synaptic plasticity

The allosteric model with pre-existing equilibria between a minimum of four conformation states, B, A, I, and D, satisfactorily accounts for the kinetic properties of the AChR *in vivo* and *in vitro*. Application of the model to single channel events by conversion of kinetic constants into probabilities of microscopic events clarifies the effects of ligand binding on the patterns of interconversions between the various states. The formulation of the model in terms of single-channel events also opens the possibility for simulations at the level of a synapse, with a finite number ($\sim 10^3$) of receptors. While many issues remain to be clarified in order to model a synapse more accurately, particularly with respect to quantal analysis (Bekkers, 1994), simulations with a full functional model of the type presented here could provide new insights, since previous efforts have not included desensitization (Bartol *et al.*, 1991; Faber *et al.*, 1992).

With respect to artificial neural networks, an understanding of these aspects should lead to more realistic modeling. While synaptogenesis has also been considered and incorporated in

some models (Adelsberger-Mangan and Levy, 1994; Foldiak, 1990), detailed schema based upon experimental observation have been proposed mainly for the neuromuscular junctions (Changeux *et al.*, 1973; Changeux and Danchin, 1976; Gouzé *et al.*, 1983). Other important features for the development of more biologically-realistic modeling concern delays and oscillatory behavior (Herz *et al.*, 1989; Kerszberg and Zippelius, 1990; Buonomano and Merzenich, 1995; Hopfield, 1995; Hangartner and Cull, 1996; Kerszberg and Masson, 1995), but these aspects have not as yet been brought to the molecular level with respect to ligand-gated ion channels and metabotropic receptors.

In contrast, for the basic concept of synaptic plasticity (Hebb, 1949), as applied in numerous models (Bienenstock *et al.*, 1982; Amit, 1989; Churchland and Sejnowski, 1992; Edelman *et al.*, 1992; Montague and Sejnowski, 1994), plausible mechanisms based upon allosteric regulation of ligand-gated channels have been formulated, particularly in relation to synaptic triads (Heidmann and Changeux, 1982; Dehaene *et al.*, 1987; Changeux and Dehaene, 1989; Dehaene and Changeux, 1989; Dehaene and Changeux, 1991; Changeux, 1993). In this approach, signals produced by a synaptic terminal C acting on neuron B are assumed to regulate the efficacy of the postsynaptic synapse of A→B with an allosteric switch of postsynaptic receptors from neuron B. The regulatory effects could intervene to stabilize one of the allosteric conformations and as a consequence alter the corresponding rates of interconversion. Networks based on such triads can learn and produce temporal sequences (Dehaene *et al.*, 1987) and have been used to formalize neural networks able to perform a number of complex temporal processes, such as delayed-response tasks (Dehaene and Changeux, 1989) or the Wisconsin card sorting test (Dehaene and Changeux, 1991).

The role of these synaptic triads in recognizing and producing temporal sequences is related to their capacity to function as coincidence detectors (Dehaene *et al.*, 1987). Where the

A→B post-synaptic receptor can undergo transitions to short-lived (I) and long-lived (D) desensitized states, systems composed of such triads are capable of both short-term detection and long-term storage and retrieval. We assume that the multiple conformational states of the nAChR, as well as other ligand-gated receptors, could fulfill such functions. Such coincidence detection based on changes in receptor conformation may be contrasted with the conventional view (Montague and Sejnowski, 1994) in which the NMDA receptor is responsible on the basis of its voltage dependent Mg^{2+} channel block (Wigstrom and Gustafsson, 1985). While such a mechanism can play a physiological important role, it can only be short-term in its direct effects and limited to the specific features of the NMDA channel; any subsequent learning processes must be dependent on other cellular components capable of long-term storage (see “LTP” below). Hence, coincidence detection based on conformational transitions would have the advantage of being applicable to virtually all members of the super-family of ligand-gated channels and capable of participating, in principle, in both short-term discrimination and long-term storage.

In a specific example of possible coincidence detection, we have suggested that allosteric effectors of the neuronal nAChR operating at sites distinct from the channel can provide a suitable mechanism (see Fig. 24 b). This hypothesis assumes a direct effect of calcium on receptor properties. Indirect effects could also occur, as postulated in the model assigning a role to calcium in the modulation of intracellular phosphorylation responsible for the forms of hippocampal synaptic plasticity known as long-term potentiation (LTP) or long-term depression (LTD). This model proposes that LTD results from activation of phosphatases at low calcium influxes, whereas LTP results from activation of kinases at higher calcium influxes (Lisman, 1989; Lisman, 1994). This biphasic pattern has been interpreted in terms of the sliding threshold model (Bienenstock *et al.*, 1982) first developed to account for aspects of

visual cortical development and subsequently observed in other neurological systems (Bear, 1995).

The role of CaM kinase II in this form of plasticity has been addressed by the production of genetically modified mice. Mice with a targeted disruption of the CaM kinase α subunit lack LTD (Silva *et al.*, 1992; Stevens *et al.*, 1997). A specific application of the sliding threshold model has been reported for mice with a site-directed mutation (T286D) in CaM kinase II that possesses high constitutive activity in the absence of activation by calcium (Mayford *et al.*, 1995). Compared to wild-type mice, the threshold for the transition from LTD to LTP in the CA1 region of the hippocampus appears to move to higher frequencies in the transgenic mice with the T286D mutation of CaM Kinase II (Mayford *et al.*, 1995). While evidence for a role of phosphorylation is accumulating, the targets of the phosphorylation effects are not yet fully established. Although receptor phosphorylation may be involved, particularly AMPA-type glutamate receptors (Raymond *et al.*, 1993), pre-synaptic processes, possibly triggered by retrograde signals, have also been implicated, as demonstrated in mice with reduced synthesis of NO leading to reduced LTP in the same region of the hippocampus (Son *et al.*, 1996).

While the exact role of phosphorylation in LTD and LTP remains unclear, it is of interest to note that phosphorylation-dependent changes in the equilibria between allosteric states for a ligand-gated receptor can readily lead to biphasic responses and sliding thresholds, as illustrated in Fig. 24 c. If phosphorylation activates the receptor, the requirement is simply that the appropriate phosphatase is activated at low calcium concentrations, but with low cooperativity with respect to calcium, while the relevant kinase is activated at higher concentrations, but with a more cooperative response to calcium. In this case, the phosphatase will dominate at low calcium (corresponding to low stimulation frequencies) to produce LTD, but the kinase will gradually become dominant as the calcium concentration rises

(corresponding to higher frequencies), producing LTD. Such biphasic behavior can also be generated if phosphorylation inhibits the receptor, but in this case the kinase must be activated at lower calcium concentrations with low cooperativity and the phosphatase activated at higher calcium concentrations with high cooperativity.

In the simulation presented in Fig. 24 c, the threshold is displaced to higher frequencies by increased phosphorylation. This behavior is achieved by assuming that phosphorylation shifts the equilibria between the B and A states in favor of B, or in an equivalent manner by favoring one of the desensitized states (Huganir *et al.*, 1986). It is further assumed that in the presence of a mutated kinase phosphorylation is enhanced, resulting in increased LTD and displacement of the threshold to the right. This simulation is based on the parameters of the nAChR, but the curves resemble the data presented for wild type and mutant CaM-kinase (Mayford *et al.*, 1995). Thus a sliding threshold based on the allosteric transitions of a ligand-gated channel could be responsible for the biphasic behavior reported, but considerable additional data will be required to establish the detailed molecular basis for such a mechanism in hippocampal LTD-LTP.

C. Diseases and dependency

While additional insights should be obtainable in future studies of wild-type receptors under conditions where alternative models differ in their predictions, more critical experiments may be achieved with receptors resulting from mutations that produce strong perturbations. Site-directed mutations can play an important role in this respect (see below), but spontaneous mutations responsible for myasthenic syndromes have also provided new insights into the mechanism of muscle nAChR and clarified the pathology of these clinical

syndromes (Ohno *et al.*, 1995; Sine *et al.*, 1995; Gomez and Gammack, 1995; Ohno *et al.*, 1996; Gomez *et al.*, 1996; Vincent *et al.*, 1997). Opening frequencies superior to the wild-type levels appear to cause cellular damage, probably due to an excessive influx of electrolytes, particularly calcium (Engel, 1993). Among the mutations responsible for the various myasthenic syndromes, the high-affinity ϵ T264P mutant receptors examined here illustrate the physiological consequences resulting from facilitation of the transition to the open state.

The results reported for ϵ T264P mutant receptors (Ohno *et al.*, 1995) are particularly striking, since the profile of open channel dwell times displays three peaks, compared to the single peak for wild-type receptors. Assuming that the energy required for the B \rightarrow A transition is reduced, as represented by a value of ${}^{\text{B}}L_0 = 200$ for ϵ T264P (Fig. 23), significant channel opening is predicted for receptors with no ligands or one molecule of ligand bound. In this case, in contrast to wild-type receptors (Fig. 19), more ionic events than binding events are predicted (Fig. 23). The three peaks for the mutant receptors may then be readily interpreted with the MWC-type model (L phenotype) as reflecting un-, mono-, and bi-liganded receptors, with reasonable agreement obtained between theory and experiment (Fig. 23 c). The failure of the C&S-type model to accommodate these data stems principally from the absence of un- or mono-liganded open states and secondarily from the fact that dissociation of ligand from the active state is not explicitly introduced in the model (Fig. 7).

The ϵ T264P mutation represents a class of high-affinity mutants lying in the channel, as first discovered for the L247T mutation of neuronal $\alpha 7$ AChR (Revah *et al.*, 1991) and subsequently confirmed with muscle nAChR (Labarca *et al.*, 1995; Filatov and White, 1995), as well as with 5-HT₃ receptors (Yakel *et al.*, 1993) and GABA_A receptors (Chang *et al.*, 1996). A Leu \rightarrow Met mutation at the position in the β subunit of human muscle AChR corresponding to L247 in $\alpha 7$ is responsible for a severe slow-channel myasthenic syndrome

(Gomez *et al.*, 1996). The $\alpha 7$ mutations such as L247T dramatically increase the sensitivity to ligand, convert the competitive antagonist dihydro- β -erythroidine to a partial agonist (Bertrand *et al.*, 1992), alter single-channel conductances (Revah *et al.*, 1991), and lead to spontaneous channel opening (Bertrand *et al.*, 1996). These results are most readily interpreted by a normally closed, high-affinity desensitized state that is rendered conducting by the Leu \rightarrow Thr replacement in the channel, thereby constituting a γ phenotype (Galzi *et al.*, 1996b). Related mutations such as V251T, characterized in $\alpha 7$ receptors (Devillers-Thiéry *et al.*, 1992; Galzi *et al.*, 1992) share some features with L247T, but can be interpreted in terms of an L phenotype (Galzi *et al.*, 1996b). The myasthenic mutation ϵ T264P occurs at the residue adjacent to the Val corresponding to the $\alpha 7$ site mutated in V251T. Similarly, an Ile \rightarrow Asn mutation in the deg-3 AChR gene that induces neurotoxicity in *C. elegans* occurs at the site in M2 equivalent to the Val mutated in $\alpha 7$ V251T (Treinin and Chalfie, 1995).

Neuronal nAChRs have also been implicated in inherited forms of epilepsy due to channel mutations in the neuronal AChR $\alpha 4$ subunit (Steinlein *et al.*, 1995; Steinlein *et al.*, 1997). In one case (Steinlein *et al.*, 1995; Weiland *et al.*, 1996), mutation of Ser 248 to Phe at the homologous site of the chlorpromazine-labeled Ser in *Torpedo* receptor M2 (Giraudat *et al.*, 1986; Hucho *et al.*, 1986) causes a significant enhancement of desensitization and a reduction of maximal response at saturating ACh concentrations. In the other case, insertion of an additional Leu at the C-terminal end of M2 causes an increase of affinity associated with a lower calcium permeability (Steinlein *et al.*, 1997). With respect to other neurological disorders, indirect evidence has linked $\alpha 7$ to an inherited form of schizophrenia (Freedman *et al.*, 1997).

Finally, studies on the molecular properties of nAChR should clarify the molecular basis of nicotine addiction via smoking. Some insights may already be available from desensitization

experiments. The utilization of the low-concentration pre-pulse method to evaluate desensitization is shown to produce measurements of IC_{50} that introduce systematic distortions, since the system is far from equilibrium unless pre-pulse duration times approach tens of minutes (Fig. 11). Because of these latter limitations for obtaining equilibrium IC_{50} values, considerable additional data will be required with long pre-pulse times in order to define the parameters of the D state more fully. Recovery times from the D state can be extremely long (hours), since they will be limited by $^{DI}k_0$, which may be as low $\sim 10^{-4} \text{ s}^{-1}$ (Table 1; see also Fig. 9 c). It is interesting to note that slow structural changes have been reported (Chang and Bock, 1977). Response times in this range could contribute to upregulation, downregulation, and other pharmacological effects associated with both chronic and acute nicotine administration (Ochoa *et al.*, 1990; Lukas and Bencherif, 1992; Peng *et al.*, 1994; Dani and Heinemann, 1996). Heavy and light smoking regimes may be related to maintaining the D state by the former, and permitting stimulatory effects via action on the A state by the latter (Wonnacott, 1990). Nevertheless, a great deal of additional information will be required to establish the exact sites where nicotine exerts its pharmacological effect and which forms of the neuronal nAChR participate. Although $\alpha 4\beta 2$ has been suggested as a likely target (Peng *et al.*, 1994), a prime role for $\alpha 6$ has recently been proposed (Le Novère *et al.*, 1996). The studies using transgenic mice are also providing a powerful tool for the elucidation of specific effects of neuronal nAChR subunits (Picciotto *et al.*, 1995). Ultimately, the allosteric scheme may contribute insights into diseases related to altered transitions between conformational states and aid in the understanding of drug addiction.

ACKNOWLEDGEMENTS

The research described here from our own laboratories was supported by the Swiss National Science Foundation, the Association Française Contre Les Myopathies, the Collège

de France, the Centre National de la Recherche Scientifique, the Institut National de la Santé et de la Recherche Médicale, the Direction des Recherches Etudes et Techniques, Human Frontiers, EEC Biotech and Biomed, and the Council for Tobacco Research .

REFERENCES

- Adelsberger-Mangan, D.M. and Levy, W.B. (1994). The influence of limited presynaptic growth and synapse removal on adaptive synaptogenesis. *Biol. Cybern.* **71**, 461-468.
- Akabas, M.H. and Karlin, A. (1995). Identification of acetylcholine receptor channel-lining residues in the M1 segment of the α subunit. *Biochemistry* **34**, 12496-12500.
- Akk, G., Sine, S., and Auerbach, A. (1996). Binding sites contribute unequally to the gating of mouse nicotinic α D200N acetylcholine receptors. *J. Physiol.* **496**, 185-196.
- Amit, D.J. (1989). Modeling brain functions (Cambridge: Cambridge University Press).
- Aylwin, M.L. and White, M.M. (1994). Gating properties of mutant acetylcholine receptors. *Molec. Pharmacol.* **46**, 1149-1155.
- Bartol, T.M., Land, B.R., Salpeter, E.E., and Salpeter, M.M. (1991). Monte Carlo simulation of miniature endplate current generation in the vertebrate neuromuscular junction. *Biophys. J.* **59**, 1290-1307.
- Bear, M.F. (1995). Mechanism for a sliding synaptic modification threshold. *Neuron* **15**, 1-4.
- Bekkers, J.M. (1994). Quantal analysis of synaptic transmission in the central nervous system. *Curr. Opin. in Neurobiol.* **4**, 360-365.
- Bertrand, D., Devillers-Thiéry, A., Revah, F., Galzi, J.-L., Hussy, N., Mulle, C., Bertrand, S., Ballivet, M., and Changeux, J.-P. (1992). Unconventional pharmacology of a neural nicotinic receptor mutated in the channel domain. *Proc. Natl. Acad. Sci. USA* **89**, 1261-1265.
- Bertrand, D. and Changeux, J.-P. (1995). Nicotinic receptor: an allosteric protein specialized for intracellular communication. *Seminars in the Neurosciences* **7**, 75-90.
- Bertrand, S., Palma, E., Corringer, P.J., Edelstein, S.J., Changeux, J.-P., and Bertrand, D. (1996). Methylcaconitine a competitive inhibitor of the α 7 desensitized open mutant L247T. Soc. Neurosci. Abstr. 22, 1522

- Bienenstock, E.L., Cooper, L.N., and Munro, P.W. (1982). Theory for the development of neuron selectivity: orientation specificity and binocular interaction in visual cortex. *J. Neurosci.* **2**, 32-48.
- Blount, P. and Merlie, J.P. (1989). Molecular basis of the two nonequivalent ligand binding sites of the muscle nicotinic acetylcholine receptor. *Neuron* **3**, 349-357.
- Bormann, J., Rundström, N., Betz, H., and Langosh, D. (1993). Residues within transmembrane segment M2 determine chloride conductance of glycine receptor homo- and hetero-oligomers. *EMBO J.* **12**, 3729-3737.
- Brussard, A.B., Yang, X., Doyle, J.P., Huck, S., and Role, L.W. (1995). Nicotinic enhancement of fast excitatory synaptic transmission in CNS by presynaptic receptors. *Science* **269**, 1692-1696.
- Buisson, B. and Bertrand, D. (1997). Steroid modulation of the nicotinic receptor. *Comp. Endocrinol.* *in press*
- Buonomano, D.V. and Merzenich, M.M. (1995). Temporal information transformed into a spatial code by a neural network with realistic properties. *Science* **267**, 1028-1030.
- Chang, H.W. and Bock, E. (1977). Molecular forms of acetylcholine receptor. Effects of calcium ions and a sulfhydryl reagent on the occurrence of oligomers. *Biochemistry* **16**, 4513-4520.
- Chang, Y., Wang, R., Barot, S., and Weiss, D.S. (1996). Stoichiometry of a recombinant GABA_A receptor. *J. Neurosci.* **16**, 5415-5424.
- Changeux, J.-P., Thiéry, J.-P., Tung, T., and Kittel, C. (1967). On the cooperativity of biological membranes. *Proc. Natl. Acad. Sci. USA* **57**, 335-341.
- Changeux, J.-P., Courrège, P., and Danchin, A. (1973). A theory of the epigenesis of neural networks by selective stabilization of synapses. *Proc. Natl. Acad. Sci. USA* **70**, 2974-2978.
- Changeux, J.-P., Devillers-Thiéry, A., and Chemouilli, P. (1984). Acetylcholine receptor: an allosteric protein. *Science* **225**, 1335-1345.

- Changeux, J.-P. (1990). Functional architecture and dynamics of the nicotinic acetylcholine receptor: an allosteric ligand-gated channel. In Fidia Research Foundation Neurosciences Award Lectures, Vol. 4. J.-P. Changeux, R.R. Llinas, D. Purves, and F.F. Bloom, eds. (New York: Raven Press, Ltd.), pp. 17-168.
- Changeux, J.-P. (1993). A critical view of neuronal models of learning and memory. In *Memory Concepts - 1993. Basic and Clinical Aspects*. P. Anderson, O. Hvalby, O. Paulsen, and B. Hokfelt, eds. (Amsterdam: Elsevier), pp. 413-433.
- Changeux, J.-P. (1996). Neurotransmitter receptors in the changing brain: allosteric transitions, gene expression and pathology at the molecular level. In *The Nobel Symposium 1994: Individual Development over the Lifespan: Biological and Psychosocial Perspectives*. D. Magnusson, ed. (Cambridge: Cambridge University Press), pp. 107-138.
- Changeux, J.-P. and Danchin, A. (1976). Selective stabilization of developing synapses as a mechanism for the specification of neuronal networks. *Nature* **264**, 705-712.
- Changeux, J.-P. and Dehaene, S. (1989). Neuronal models of cognitive functions. *Cognition* **33**, 63-109.
- Changeux, J.-P. and Edelstein, S.J. (1994). On allosteric transitions and acetylcholine receptors. *Trends Biochem. Sci.* **19**, 399-340.
- Changeux, J.-P. and Heidmann, T. (1987). Allosteric receptors and molecular models of learning. In *Synaptic Function*. G. Edelman, W.E. Gall, and W.M. Cowan, eds. (New York: Wiley), pp. 549-601.
- Changeux, J.-P. and Rubin, M.M. (1968). Allosteric interactions in aspartate transcarbamylase. III. Interpretations of experimental data in terms of the model of Monod, Wyman, and Changeux. *Biochemistry* **7**, 553-561.

- Chatrenet, B., Trémeau, O., Bontems, F., Goeldner, M.P., Hirth, C.G., and Ménez, A. (1990).
Topography of toxin-acetylcholine receptor complexes by using photoactivatable toxin derivatives.
Proc. Natl. Acad. Sci. USA **87**, 3378-3382.
- Chen, J., Zhang, H., Akk, G., Sine, S., and Auerbach, A. (1995). Activation kinetics of recombinant
mouse nicotinic acetylcholine receptors: mutations of α -subunit tyrosine 190 affect both binding
and gating. *Biophys. J.* **69**, 849-859.
- Churchland, P.S. and Sejnowski, T.J. (1992). *The Computational Brain* (Cambridge: MIT Press).
- Clements, J.D., Lester, R.A.J., Tong, G., Jahr, C.E., and Westbrook, G.L. (1992). The time course of
glutamate in the synaptic cleft. *Science* **258**, 1498-1501.
- Colquhoun, D. (1973). The relation between classical and cooperative models for drug action. In *Drug
Receptors*. H.P. Rang, ed. (London: Macmillan), pp. 149-182.
- Colquhoun, D. and Ogden, D.C. (1988). Activation of ion channels in the frog end-plate by high
concentrations of acetylcholine. *J. Physiol.* **395**, 131-159.
- Colquhoun, D. and Sakmann, B. (1985). Fast events in single-channel currents activated by
acetylcholine and its analogues at the frog muscle end-plate. *J. Physiol.* **369**, 501-557.
- Conroy, W., Vernallis, A.B., and Berg, D.K. (1992). The $\alpha 5$ gene product assembles with multiple
acetylcholine receptor subunits to form distinctive receptor subtypes in brain. *Neuron* **9**, 1-20.
- Cooper, E., Couturier, S., and Ballivet, M. (1991). Pentameric structure and subunit stoichiometry of
a neuronal nicotinic acetylcholine receptor. *Nature* **350**, 235-238.
- Corringer, P.-J., Bertrand, S., Bohler, S., Edelstein, S.J., Changeux, J.-P., and Bertrand, D. (1997).
Identification of critical elements modulating desensitization of neuronal nicotinic receptors. *To be
completed.*

- Corringer, P.J., Galzi, J.-L., Eiselé, J.-L., Bertrand, S., Changeux, J.-P., and Bertrand, D. (1995). Identification of a new component of the agonist binding site of the nicotinic $\alpha 7$ homooligomeric receptor. *J. Biol. Chem.* **270**, 11749-11752.
- Couturier, S., Bertrand, D., Matter, J.-M., Hernandez, M.-C., Bertrand, S., Millar, N., Valera, S., Barkas, T., and Ballivet, M. (1990). A neuronal nicotinic acetylcholine receptor subunit ($\alpha 7$) is developmentally regulated and forms a homo-oligomeric channel blocked by α -BTX. *Neuron* **5**, 847-856.
- Czajkowski, C., Kaufmann, C., and Karlin, A. (1993). Negatively charged amino acid residues in the nicotinic receptor δ subunit that contribute to the binding of acetylcholine. *Proc. Natl. Acad. Sci. USA* **90**, 6285-6289.
- Dani, J.A. and Heinemann, S. (1996). Molecular and Cellular Aspects of Nicotine Abuse. *Neuron* **16**, 905-908.
- Dehaene, S., Changeux, J.-P., and Nadal, J.-P. (1987). Neural networks that learn temporal sequences by selection. *Proc. Natl. Acad. Sci. USA* **84**, 2727-2731.
- Dehaene, S. and Changeux, J.-P. (1989). A simple model of prefrontal cortex function in delayed-response tasks. *J. Cognitive Neurosci.* **1**, 244-261.
- Dehaene, S. and Changeux, J.-P. (1991). The Wisconsin card sorting test: theoretical analysis and modeling in a neuronal network. *Cerebral Cortex* **1**, 62-79.
- Devillers-Thiéry, A., Galzi, J.-L., Bertrand, S., Changeux, J.-P., and Bertrand, D. (1992). Stratified organization of the nicotinic acetylcholine receptor channel. *Neuroreport* **3**, 1001-1004.
- Devillers-Thiéry, A., Galzi, J.-L., Eiselé, J.-L., Bertrand, S., Bertrand, D., and Changeux, J.-P. (1993). Functional architecture of the nicotinic acetylcholine receptor: a prototype of ligand-gated ion channels. *J. Membrane Biol.* **136**, 97-112.

- Eaton, W.A., Henry, E.R., and Hofrichter, J. (1991). Application of linear free energy relations to protein conformational changes: The quaternary structural change of hemoglobin. *Proc. Natl. Acad. Sci. USA* **88**, 4472-4475.
- Edelman, G.M., Reeke, G.N., Gall, W.E., Tononi, G., Williams, D., and Sporns, O. (1992). Synthetic neural modeling applied to a real-world artifact. *Proc. Natl. Acad. Sci. USA* **89**, 7267-7271.
- Edelstein, S.J. (1972). An allosteric mechanism for the acetylcholine receptor. *Biochem. Biophys. Res. Commun.* **48**, 1160-1165.
- Edelstein, S.J. (1975). Cooperative interactions of hemoglobin. *Annu. Rev. Biochem.* **44**, 209-232.
- Edelstein, S.J., Schaad, O., Henry, E., Bertrand, D., and Changeux, J.-P. (1996). A kinetic mechanism for nicotinic acetylcholine receptors based on multiple allosteric transitions. *Biol. Cybern.* **75**, 361-380.
- Edelstein, S.J., Schaad, O., and Changeux, J.-P. (1997a). A test of the allosteric model using nicotinic receptor mutants. *To be completed*
- Edelstein, S.J., Schaad, O., and Changeux, J.-P. (1997b). Single bindings versus single channel recordings: a new approach to ionotropic receptors. *To be completed*
- Edelstein, S.J. and Bardsley, W.G. (1997). Contributions of individual molecular species to the Hill coefficient for ligand binding by an oligomeric protein. *J. Mol. Biol.* **267**, 10-16.
- Edelstein, S.J. and Changeux, J.-P. (1996). Allosteric proteins after thirty years: the binding and state functions of the neuronal $\alpha 7$ nicotinic acetylcholine receptor. *Experientia* **52**, 1083-1090.
- Edman, L., Mets, U., and Rigler, R. (1996). Conformational transitions monitored by single molecules in solution. *Proc. Natl. Acad. Sci. USA* **93**, 6710-6715.
- Edmonds, B., Gibb, A.J., and Colquhoun, D. (1995). Mechanisms of activation of muscle nicotinic acetylcholine receptors and the time course of endplate currents. *Annu. Rev. Physiol.* **57**, 469-493.

- Ehrenberg, M. and Rigler, R. (1974). Rotational Brownian motion and fluorescence intensity fluctuations. *J. Chem. Phys.* **4**, 390-410.
- Eigen, M. and Rigler, R. (1994). Sorting single molecules: application to diagnostics and evolutionary biotechnology. *Proc. Natl. Acad. Sci. USA* **91**, 5740-5747.
- Eiselé, J.-L., Bertrand, S., Galzi, J.-L., Devillers-Thiéry, A., Changeux, J.-P., and Bertrand, D. (1993). Chimeric nicotinic-serotonergic receptor combines distinct ligand binding and channel specificities. *Nature* **366**, 479-483.
- Elgoyhen, A.B., Johnson, D.S., Boulter, J., Vetter, D.E., and Heinemann, S. (1994). $\alpha 9$: an acetylcholine receptor with novel pharmacological properties expressed in rat cochlear hair cells. *Cell* **79**, 705-715.
- Elson, E. and Magde, D. (1974). Fluorescence correlation spectroscopy I. Conceptual basis and theory. *Biopolymers* **13**, 1-27.
- Engel, A.G. (1993). The investigation of congenital myasthenic syndromes. *Ann. N. Y. Acad. Sci.* **681**, 425-434.
- Faber, D.S., Young, W.S., Legendre, P., and Korn, H. (1992). Intrinsic quantal variability due to stochastic properties of receptor-transmitter interactions. *Science* **258**, 1494-1498.
- Fersht, A.R., Leatherbarrow, R.J., and Wells, T.N.C. (1986). Quantitative analysis of structure-activity relationships in engineering proteins by linear free-energy relationships. *Nature* **322**, 284-286.
- Filatov, G.N. and White, M.M. (1995). The role of conserved leucines in the M2 domain of the acetylcholine receptor in channel gating. *Molec. Pharmacol.* **48**, 379-384.
- Foldiak, P. (1990). Forming sparse representations by local anti-Hebbian learning. *Biol. Cybern.* **64**, 165-170.

- Forman, S.A. and Miller, K.W. (1988). High acetylcholine concentrations cause rapid inactivation before fast desensitization in nicotinic acetylcholine receptors from *Torpedo*. *Biophys. J.* **54**, 149-158.
- Franke, C., Parnas, H., Hovav, G., and Dudel, J. (1993). A molecular scheme for the reaction between acetylcholine and nicotinic channels. *Biophys. J.* **64**, 339-356.
- Freedman, R., Coon, H., Myles-Worsley, M., Orr-Urtreger, A., Olincy, A., Davis, A., Polymeropoulos, M., Holik, J., Hopkins, J., Hoff, M., Rosenthal, J., Waldo, M.C., Reimherr, F., Wender, P., Yaw, J., Young, D.A., Breese, C.R., Adams, C., Patterson, D., Adler, L.E., Kruglyak, L., Leonard, S., and Byerley, W. (1997). Linkage of a neurophysiological deficit in schizophrenia to a chromosome 15 locus. *Proc. Natl. Acad. Sci. USA* **94**, 587-592.
- Fu, D.X. and Sine, S.M. (1994). Competitive antagonists bridge the α - γ subunit interface of the acetylcholine receptor through quaternary ammonium-aromatic interactions. *J. Biol. Chem.* **269**, 26152-26157.
- Galzi, J.-L., Bertrand, D., Devillers-Thiéry, A., Revah, F., Bertrand, S., and Changeux, J.-P. (1991a). Functional significance of aromatic amino acids from three peptide loops of the $\alpha 7$ neuronal nicotinic receptor site investigated by site-directed mutagenesis. *FEBS Lett.* **294**, 198-202.
- Galzi, J.-L., Revah, F., Bouet, F., Ménez, A., Goeldner, M., Hirth, C., and Changeux, J.-P. (1991b). Allosteric transitions of the acetylcholine receptor probed at the amino acid level with a photolabile cholinergic ligand. *Proc. Natl. Acad. Sci. USA* **88**, 5051-5055.
- Galzi, J.-L., Devillers-Thiéry, A., Hussy, N., Bertrand, S., Changeux, J.-P., and Bertrand, D. (1992). Mutations in the channel domain of a neuronal nicotinic receptor convert ion selectivity from cationic to anionic. *Nature* **359**, 500-505.

- Galzi, J.-L., Bertrand, S., Corringer, P.-J., Changeux, J.-P., and Bertrand, D. (1996a). Identification of calcium binding sites that regulate potentiation of a neuronal nicotinic acetylcholine receptor. *EMBO J.* **15**, 5824-5832.
- Galzi, J.-L., Edelstein, S.J., and Changeux, J.-P. (1996b). The multiple phenotypes of allosteric receptor mutants. *Proc. Natl. Acad. Sci. USA* **93**, 1853-1858.
- Galzi, J.-L. and Changeux, J.-P. (1994). Neurotransmitter-gated ion channels as unconventional allosteric proteins. *Curr. Opinion in Structural Biol.* **4**, 554-565.
- Galzi, J.-L. and Changeux, J.-P. (1995). Neuronal nicotinic receptors: molecular organization and regulations. *Neuropharmacology* **34**, 563-582.
- Giraudat, J., Dennis, M., Heidmann, T., Chang, J.Y., and Changeux, J.-P. (1986). Structure of the high affinity site for noncompetitive blockers of the acetylcholine receptor: serine-262 of the delta subunit is labeled by [³H]-chlorpromazine. *Proc. Natl. Acad. Sci. USA* **83**, 2719-2723.
- Gomez, C.M., Maselli, R., Gammack, B.S., Lasalde, J., Tamamizu, S., Cornblath, D.R., Lehar, M., McNamee, M., and Kuncel, R.W. (1996). A β -subunit mutations in the acetylcholine receptor channel gate causes severe slow-channel syndrome. *Ann. Neurol.* **39**, 712-723.
- Gomez, C.M. and Gammack, J.T. (1995). A leucine-to-phenylalanine substitution in the acetylcholine receptor ion channel in a family with the slow-channel syndrome. *Neurology* **45**, 982-985.
- Gouzé, J.-L., Lasry, J.-M., and Changeux, J.-P. (1983). Selective stabilization of muscle innervation during development: a mathematical model. *Biol. Cybern.* **46**, 207-215.
- Gray, R., Rajan, A.S., Radcliffe, K.A., Yakehiro, M., and Dani, J.A. (1996). Hippocampal synaptic transmission enhanced by low concentrations of nicotine. *Nature* **383**, 713-716.
- Hangartner, R.D. and Cull, P. (1996). A ternary logic model for recurrent neuromime networks with delay. *Biol. Cybern.* **73**, 177-188.

- Hebb, D.O. (1949). *The Organization of Behavior* (New York: Wiley).
- Heidmann, T. and Changeux, J.-P. (1978). Structural and functional properties of the acetylcholine receptor protein in its purified and membrane-bound states. *Annu. Rev. Biochem.* **47**, 317-357.
- Heidmann, T. and Changeux, J.-P. (1979). Fast kinetic studies on the interaction of a fluorescent agonist with the membrane-bound acetylcholine receptor from *Torpedo marmorata*. *Eur. J. Biochem.* **94**, 255-279.
- Heidmann, T. and Changeux, J.-P. (1980). Interaction of a fluorescent agonist with the membrane-bound acetylcholine receptor from *Torpedo marmorata* in the millisecond time range: resolution of an "intermediate" conformational transition and evidence for positive cooperative effects. *Biochem. Biophys. Res. Commun.* **97**, 889-896.
- Heidmann, T. and Changeux, J.-P. (1982). Un modèle moléculaire de régulation d'efficacité au niveau postsynaptique d'une synapse chimique. *C. R. Acad. Sci. Paris* **295**, 665-670.
- Herz, A., Sulzer, B., and Kuhn, R. (1989). Hebbian learning reconsidered: representation of static and dynamic objects in associative neural nets. *Biol. Cybern.* **60**, 457-467.
- Herz, J.M., Johnson, D.A., and Taylor, P. (1989). Distance between the agonist and noncompetitive inhibitor sites on the nicotinic acetylcholine receptor. *J. Biol. Chem.* **264**, 12439-12448.
- Hopfield, J.J. (1995). Pattern recognition computation using action potential timing for stimulus representation. *Nature* **376**, 33-36.
- Hucho, F., Oberthur, W., and Lottspeich, F. (1986). The ion channel of the nicotinic acetylcholine receptor is formed by the homologous helices M2 of the receptor subunits. *FEBS Lett.* **205**, 137-142.
- Huganir, R.L., Delcour, A.J., Greengard, P., and Hess, G.P. (1986). Phosphorylation of the nicotinic acetylcholine receptor regulates its rate of desensitization. *Nature* **321**, 774-776.

- Huganir, R.L. and Greengard, P. (1990). Regulation of neurotransmitter receptor desensitization by protein phosphorylation. *Neuron* **5**, 555-567.
- Imoto, K., Busch, C., Sakmann, B., Mishina, M., Konno, T., Nakai, J., Bujo, H., Mori, Y., Fukuda, K., and Numa, S. (1988). Rings of negatively charged amino acids determine the acetylcholine receptor channel conductance. *Nature* **335**, 645-648.
- Jackson, M.B. (1988). Dependence of acetylcholine receptor channel kinetics on agonist concentration in cultured mouse muscle fibers. *J. Physiol.* **397**, 555-583.
- Jackson, M.B. (1989). Perfection of a synaptic receptor: kinetics and energetics of the acetylcholine receptor. *Proc. Natl. Acad. Sci. USA* **86**, 2199-2203.
- Jackson, M.B. (1993). Activation of receptors directly coupled to channels. In *Thermodynamics of membrane receptors and channels*. M.B. Jackson, ed. (Boca Raton: CRC Press), pp. 249-293.
- Jencks, W.P. (1985). A primer for the Bema Hapothle. An empirical approach to the characterization of changing transition-state structures. *Chem. Rev.* **85**, 511-527
- Karlin, A. (1967). On the application of "a plausible model" of allosteric proteins to the receptor of acetylcholine. *J. Theor. Biol.* **16**, 306-320.
- Karlin, A. (1993). Structure of nicotinic acetylcholine receptors. *Curr. Opinion in Neurobiol.* **3**, 299-309.
- Karlin, A. and Akabas, M.H. (1995). Toward a structural basis for the function of nicotinic acetylcholine receptors. *Neuron* **15**, 1231-1244.
- Katz, B. and Thesleff, S. (1957). A study of "desensitization" produced by acetylcholine at the motor end-plate. *J. Physiol.* **138**, 83-80.
- Kerszberg, M. and Masson, C. (1995). Signal-induced selection among spontaneous oscillatory patterns in a model honeybee olfactory glomeruli. *Biol. Cybern.* **72**, 487-495.

- Kerszberg, M. and Zippelius, A. (1990). Synchronization in neural assemblies. *Physica Scripta* **T33**, 54-64.
- Kuffler, S.W. and Yoshikami, D. (1975). The distribution of acetylcholine sensitivity at the post-synaptic membrane of vertebrate skeletal twitch muscles: iontophoretic mapping in the micron range. *J. Physiol.* **244**, 703-730.
- Labarca, C., Nowak, M.W., Zhang, H., Tang, L., Desphande, P., and Lester, H.A. (1995). Channel gating governed symmetrically by conserved leucine residues in the M2 domain of nicotinic receptors. *Nature* **376**, 514-516.
- Langosh, D., Laube, B., Rundström, N., Schmieden, V., Bormann, J., and Betz, H. (1994). Decreased agonist affinity and chloride conductance of mutant glycine receptors associated with human hereditary hyperekplexia. *EMBO J.* **13**, 4223-4228.
- Le Novère, N., Zoli, M., and Changeux, J.-P. (1996). Neuronal nicotinic receptor $\alpha 6$ subunit RNA is selectively concentrated in catecholaminergic nuclei of the rat brain. *Eur. J. Neurosci.* **8**, 2428-2439.
- Le Novère, N. and Changeux, J.-P. (1995). Molecular evolution of the nicotinic acetylcholine receptor: an example of multigene family in excitable cells. *J. Mol. Evol.* **40**, 155-172.
- Leffler, J.E. (1953). Parameters for the description of transition states. *Science* **117**, 340-341.
- Levitan, I.B. (1994). Modulation of ion channels by protein phosphorylation and dephosphorylation. *Ann. Rev. Physiol.* **56**, 193-212.
- Léna, C. and Changeux, J.-P. (1993). Allosteric modulations of the nicotinic acetylcholine receptor. *Trends Neurosci.* **16**, 181-186.
- Léna, C. and Changeux, J.-P. (1997). Role of Ca^{2+} ions in nicotinic facilitation of GABA release in mouse thalamus. *J. Neurosci.* **17**, 576-585.

- Li, Y.H., Li, L., Lasalde, J., Rojas, L., McNamee, M., Ortiz-Miranda, S.I., and Pappone, P. (1994). Mutations in the M4 domain of *Torpedo californica* acetylcholine receptor dramatically alter channel function. *Biophys. J.* **66**, 646-653.
- Lindstrom, J. (1996). Neuronal nicotinic acetylcholine receptors. In *Ion Channels*. T. Narahashi, ed. (New York: Plenum Press), pp. 377-450.
- Lingle, C.J., Maconochie, D., and Steinbach, J.H. (1992). Activation of skeletal muscle nicotinic acetylcholine receptors. *J. Membrane Biol.* **126**, 195-217.
- Lisman, J. (1989). A mechanism for the Hebb and anti-Hebb processes underlying learning and memory. *Proc. Natl. Acad. Sci. USA* **86**, 9574-9578.
- Lisman, J. (1994). The CaM kinase hypothesis for the storage of synaptic memory. *Trends Neurosci.* **17**, 406-412.
- Lo, D.C., Pinkham, J.L., and Stevens, C.F. (1991). Role of a key cysteine residue in the gating of the acetylcholine receptor. *Neuron* **6**, 31-40.
- Luetje, C.W., Piattoni, M., and Patrick, J. (1993). Mapping of ligand binding sites of neuronal nicotinic acetylcholine receptors using chimeric alpha subunits. *Neuron* **44**, 657-666.
- Lukas, R.J. and Bencherif, M. (1992). Heterogeneity and regulation of nicotinic acetylcholine receptors. *Int. Rev. Neurobiol.* **34**, 25-131.
- Machold, J., Weise, C., Utkin, Y., Tsetlin, V., and Hucho, F. (1995). The handedness of the subunit arrangement of the nicotinic acetylcholine receptor from *Torpedo californica*. *Eur. J. Biochem.* **234**, 427-430.
- Magde, D., Elson, E., and Webb, W. (1974). Fluorescence correlation spectroscopy II. An experimental realization. *Biopolymers* **13**, 29-61.

- Mayford, M., Wang, J., Kandel, E.R., and O'Dell, T.J. (1995). CaMKII regulates the frequency-response function of hippocampal synapses for the production of both LTD and LTP. *Cell* **81**, 891-904.
- Monod, J., Wyman, J., and Changeux, J.-P. (1965). On the nature of allosteric transitions: A plausible model. *J. Mol. Biol.* **12**, 88-118.
- Montague, P.R. and Sejnowski, T.J. (1994). The predictive brain: temporal coincidence and temporal order in synaptic learning mechanisms. *Learn. Mem.* **1**, 1-33.
- Mulle, C., Léna, C., and Changeux, J.-P. (1992). Potentiation of nicotinic receptor response by external calcium in rat central neurons. *Neuron* **8**, 937-945.
- Neher, E. and Sakmann, B. (1976). Single channel currents recorded from membrane of denervated frog muscle fibers. *Nature* **260**, 799-802.
- Neubig, R.R. and Cohen, J.B. (1980). Permeability control by cholinergic receptors in *Torpedo* post-synaptic membranes: Agonist dose-response relations measured at second and millisecond times. *Biochemistry* **19**, 2770-2779.
- O'Leary, M.E. and White, M.M. (1992). Mutational analysis of ligand-induced activation of the *Torpedo* acetylcholine receptor. *J. Biol. Chem.* **267**, 8360-8365.
- Ochoa, E.L.M., Li, L., and McNamee, M.G. (1990). Desensitization of central cholinergic mechanisms and neuroadaptation to nicotine. *Molec. Neurobiol.* **4**, 251-287.
- Ohno, K., Hutchison, D.O., Milone, M., Brengman, J.M., Bouzat, C., Sine, S.M., and Engel, A.G. (1995). Congenital myasthenic syndrome caused by prolonged acetylcholine receptor channel openings due to a mutation in the M2 domain of the ϵ subunit. *Proc. Natl. Acad. Sci. USA* **92**, 758-762.

- Ohno, K., Wang, H.-L., Milone, M., Bren, N., Brengman, J.M., Nakano, S., Quiram, P., Pruitt, J.N., Sine, S.M., and Engel, A.G. (1996). Congenital myasthenic syndrome caused by decreased agonist binding affinity due to a mutation in the acetylcholine ϵ subunit. *Neuron* **17**, 157-170.
- Oswald, R.E. and Changeux, J.-P. (1982). Crosslinking of α -bungarotoxin to the acetylcholine receptor from *Torpedo marmorata* by ultraviolet light irradiation. *FEBS Lett.* **139**, 225-229.
- Palma, E., Bertrand, S., Binzoni, T., and Bertrand, D. (1996). Neural nicotinic $\alpha 7$ receptor expressed in *Xenopus* oocytes presents five putative binding sites for methyllycaconitine. *J. Physiol.* **491.1**, 151-161.
- Pedersen, S.E. and Cohen, J.B. (1990). *d*-Tubocurarine binding sites are located at α - γ and α - δ subunit interfaces of the nicotinic acetylcholine receptor. *Proc. Natl. Acad. Sci. USA* **87**, 2785-2789.
- Peng, X., Gerzanich, V., Anand, R., Whiting, P.J., and Lindstrom, J. (1994). Nicotine-induced increase in neuronal nicotine receptors results from a decrease in the rate of receptor turnover. *Molec. Pharmacol.* **46**, 523-530.
- Perutz, M.F. (1989). Mechanisms of cooperativity and allosteric regulation in proteins. *Quart. Rev. Biophys.* **22**, 139-236.
- Picciotto, M.R., Zoli, M., Léna, C., Bessis, A., Lallemand, Y., Le Novère, N., Vincent, P., Merlo Pich, E., Brûlet, P., and Changeux, J.-P. (1995). Abnormal avoidance learning in mice lacking functional high-affinity nicotine receptor in the brain. *Nature* **374**, 65-67.
- Prince, R.J. and Sine, S.M. (1996). Identification of agonist selectivity determinants in the muscle acetylcholine receptor (nAChR). *Biophys. J.* **70**, A251
- Rajendra, S., Lynch, J., Pierce, K.D., French, C.R., Barry, P.H., and Schofield, P.R. (1994). Startle disease mutations reduce the agonist sensitivity of the human inhibitory glycine receptor. *J. Biol. Chem.* **269**, 18739-18742.

- Rajendra, S., Lynch, J., Pierce, K.D., French, C.R., Barry, P.H., and Schofield, P.R. (1995). Mutation of an arginine residue transforms β -alanine and taurine from agonists into competitive antagonists. *Neuron* **14**, 169-175.
- Ramirez-Latorre, J., Yu, C.R., Qu, X., Perin, F., Karlin, A., and Role, L. (1996). Functional contributions of $\alpha 5$ subunit to neuronal acetylcholine receptor channels. *Nature* **380**, 347-351.
- Rang, H.P. and Ritter, J.M. (1970). On the mechanism of desensitization of cholinergic receptors. *Molec. Pharmacol.* **6**, 357-382.
- Rathouz, M.M., Vijayaraghavan, S., and Berg, D.K. (1996). Elevation of intracellular calcium levels in neurons by nicotinic acetylcholine receptors. *Molec. Neurobiol.* **12**, 117-131.
- Rauer, B., Neumann, E., Widengren, J., and Rigler, R. (1996). Fluorescence correlation spectrometry of the interaction kinetics of tetramethylrhodamin α -bungarotoxin with *Torpedo californica* acetylcholine receptor. *Biophys. Chem.* **58**, 3-12.
- Raymond, L.A., Blackstone, C.D., and Huganir, R.L. (1993). Phosphorylation of amino acid neurotransmitter receptors in synaptic plasticity. *Trends Neurosci.* **16**, 147-153.
- Revah, F., Bertrand, D., Galzi, J.-L., Devillers-Thiéry, A., Mulle, C., Hussy, N., Bertrand, S., Ballivet, M., and Changeux, J.-P. (1991). Mutations in the channel domain alter desensitization of a neuronal nicotinic receptor. *Nature* **353**, 846-849.
- Role, L.W. and Berg, D.K. (1996). Nicotinic receptors in the development and modulation of CNS synapses. *Neuron* **16**, 1077-1085.
- Rubin, M.M. and Changeux, J.-P. (1966). On the nature of allosteric transitions: Implications of non-exclusive ligand binding. *J. Mol. Biol.* **21**, 265-274.
- Sakmann, B., Patlak, J., and Neher, E. (1980). Single acetylcholine-activated channels show burst-kinetics in presence of desensitizing concentrations of agonist. *Nature* **286**, 71-73.

- Sargent, P.B. (1993). The diversity of neuronal nicotinic acetylcholine receptors. *Annu. Rev. Neurosci.* **16**, 403-443.
- Sawicki, C.A. and Gibson, Q.H. (1976). Quaternary conformational changes in human hemoglobin studied by laser photolysis of carboxyhemoglobin. *J. Biol. Chem.* **251**, 1533-1542.
- Schmieden, V., Kushe, J., and Betz, H. (1992). Agonist pharmacology of neonatal and adult glycine receptor alpha subunits : identification of amino acid residues involved in taurine activation. *EMBO J.* **11**. 2025-2032.
- Schwille, P., Meyer-Almes, F.-J., and Rigler, R. (1997). Dual-color fluorescence cross-correlation spectroscopy for multicomponent diffusional analysis in solution. *Biophys. J.* **72**, 1878-1886.
- Shiang, R., Ryan, S.G., Zhu, Y.Z., Hahn, A.F., O'Connell, P., and Wasmuth, J.J. (1993). Mutations in the alpha1 subunit of the inhibitory glycine receptor cause the dominant neurologic disorder, hyperekplexia. *Nature Genetics* **5**, 351-358.
- Sigworth, F.J. and Sine, S.M. (1987). Data transformations for improved display and fitting of single-channel dwell time histograms. *Biophys. J.* **52**, 1047-1054.
- Silva, A.J., Stevens, C.F., Tonegawa, S., and Wang, Y. (1992). Deficient hippocampal long-term potentiation in α -calcium-calmodulin kinase II mutant mice. *Science* **257**, 201-206.
- Sine, S.M., Claudio, T., and Sigworth, F.J. (1990). Activation of *Torpedo* acetylcholine receptors expressed in mouse fibroblasts: single channel current kinetics reveal distinct agonist binding affinities. *J. Gen. Physiol.* **96**, 395-437.
- Sine, S.M., Ohno, K., Bouzat, C., Auerbach, A., Milone, M., Pruitt, J.N., and Engel, A.G. (1995). Mutation of the acetylcholine receptor α subunit causes a slow-channel myasthenic syndrome by enhancing agonist binding affinity. *Neuron* **15**, 229-239.
- Sine, S.M. and Claudio, T. (1991). γ - and δ -subunits regulate the affinity and the cooperativity of ligand binding to the acetylcholine receptor. *J. Biol. Chem.* **266**, 19369-19377.

- Son, H., Hawkins, R.D., Martin, K., Kiebler, M., Huang, P.L., Fishman, M.C., and Kandel, E.R. (1996). Long-term potentiation is reduced in mice that are doubly mutant in endothelial and neuronal nitric oxide synthase. *Cell* **87**, 1015-1023.
- Steinfeld, J.I., Francisco, J.S., and Hase, W.L. (1989). *Chemical Kinetics and Dynamics* (Englewood Cliffs: Prentice-Hall).
- Steinlein, O.K., Mulley, J.C., Propping, P., Wallace, R.H., Phillips, H.A., Sutherland, G.R., Scheffer, I.E., and Berkovic, S.F. (1995). A missense mutation in the neuronal nicotinic receptor $\alpha 4$ subunit is associated with autosomal dominant nocturnal frontal lobe epilepsy. *Nature Genetics* **11**, 201-203.
- Steinlein, O.K., Magnusson, A., Stoodl, J., Bertrand, S., Weiland, S., Berkovic, S.F., Nakken, K.O., Propping, P., and Bertrand, D. (1997). An insertion mutation of the CHRNA4 gene in a family with autosomal dominant nocturnal frontal lobe epilepsy. *Hum. Molec. Genet.*, *in press*
- Stevens, C.F., Tonegawa, S., and Wang, Y. (1997). The role of calcium-calmodulin kinase II in three forms of synaptic plasticity. *Curr. Biol.* **4**, 687-693.
- Szabo, A. (1978). Kinetics of hemoglobin and transition state theory. *Proc. Natl. Acad. Sci. USA* **75**, 2108-2111.
- Tomaselli, G.F., McLaughlin, J.T., Jurman, M., Hawrot, E., and Yellen, G. (1991). Mutations affecting agonist sensitivity of the nicotinic acetylcholine receptor. *Biophys. J.* **60**, 721-727.
- Treinin, M. and Chalfie, M. (1995). A mutated acetylcholine receptor subunit causes neuronal degeneration in *C. elegans*. *Neuron* **14**, 871-877.
- Unwin, N. (1993a). Neurotransmitter action: opening of the ligand-gated ion channels. *Neuron* **10**, 31-41.
- Unwin, N. (1993b). The nicotinic acetylcholine receptor at 9 Å resolution. *J. Mol. Biol.* **229**, 1101-1124.

- Unwin, N. (1996). Projection structure of the nicotinic acetylcholine receptor: distinct conformations of the α subunits. *J. Mol. Biol.* **257**, 586-596.
- Valenta, D.C., Downing, J.E.G., and Role, L.W. (1993). Peptide modulation of ACh receptor desensitization controls neurotransmitter release from chicken sympathetic neurons. *J. Neurophysiol.* **69**, 928-942.
- Valera, S., Ballivet, M., and Bertrand, D. (1992). Progesterone modulates a neuronal nicotinic acetylcholine receptor. *Proc. Natl. Acad. Sci. USA* **89**, 9949-9953.
- Vernallis, A.B., Conroy, W.G., and Berg, D.K. (1993). Neurons assemble acetylcholine receptors with as many as three kinds of subunits while maintaining subunit segregation among receptor subtypes. *Neuron* **10**, 451-464.
- Vernino, S., Amador, M., Luetje, C.W., Patrick, J., and Dani, J.A. (1992). Calcium modulation and high calcium permeability of neuronal nicotinic acetylcholine receptors. *Neuron* **8**, 127-134.
- Vincent, A., Newland, C., Croxen, R., and Beeson, D. (1997). Genes at the junction - candidates for congenital myasthenic syndromes. *Trends Neurosci.* **20**, 15-23.
- Weiland, S., Witzemann, V., Villarroel, A., Propping, P., and Steinlein, O. (1996). An amino acid exchange in the second transmembrane segment of a neuronal nicotinic receptor causes partial epilepsy by altering its desensitization kinetics. *FEBS Lett.* **398**, 91-96.
- Wigstrom, H. and Gustafsson, B. (1985). On long-lasting potentiation in the hippocampus: a proposed mechanism for its dependence on coincident pre- and postsynaptic activity. *Acta Physiol. Scand.* **123**, 519-522.
- Wonnacott, S. (1990). The paradox of nicotinic acetylcholine receptor upregulation by nicotine. *Trends Pharmacol. Sci.* **11**, 216-219.
- Wonnacott, S. (1997). Presynaptic nicotinic ACh receptors. *Trends Neurosci.* **20**, 92-98.
- Wyman, J. (1948). Heme proteins. *Adv. Prot. Chem.* **4**, 407-531.

Wyman, J. (1964). Linked functions and reciprocal effects in hemoglobin: A second look. *Adv. Prot. Chem.* **19**, 223-286.

Yakel, J.L., Lagrutta, A., Adelman, J.P., and North, R.A. (1993). Single amino acid substitution affects desensitization of the 5-hydroxytryptamine type 3 receptor expressed in *Xenopus* oocytes. *Proc. Natl. Acad. Sci. USA* **90**, 5030-5033.

Zhang, Y., Chen, J., and Auerbach, A. (1995). Activation of recombinant mouse acetylcholine receptors by acetylcholine, carbamylcholine and tetramethylammonium. *J. Physiol.* **486**, 189-206.

Table 1. Parameter values for the four-state allosteric kinetic mechanism

A. State Parameters:	<u>B state</u>	<u>A state</u>	<u>I state</u>	<u>D state</u>
<u>Independent parameters:</u>				
Ligand on rates ($M^{-1} s^{-1}$):	${}^B k_{on} = 1.5 \times 10^8$	${}^A k_{on} = 1.5 \times 10^8$	${}^I k_{on} = 1.5 \times 10^8$	${}^D k_{on} = 1.5 \times 10^8$
Ligand off rates (s^{-1}):	${}^B k_{off} = 8000$	${}^A k_{off} = 8.64$	${}^I k_{off} = 4.0$	${}^D k_{off} = 4.0$
<u>Deduced parameters:</u>				
Equilibrium constants (M):	$K_B = 5.3 \times 10^{-5}$	$K_A = 5.7 \times 10^{-8}$	$K_I = 2.7 \times 10^{-8}$	$K_D = 2.7 \times 10^{-8}$
Affinity ratios:	${}^{BA}c = 1.08 \times 10^{-3}$	${}^{AI}c = 0.46$	${}^{ID}c = 1.0$	
B. Interconversion parameters:	<u>B\leftrightarrowA</u>	<u>A\leftrightarrowI</u>	<u>I\leftrightarrowD</u>	
<u>Independent parameters:</u>				
TS positional parameter:	${}^{BA}p = 0.2$	${}^{AI}p = 0.99$	${}^{ID}p = 0.99$	
Interconversion rates (s^{-1})	${}^{BA}k_2 = 3.0 \times 10^4$	${}^{AI}k_2 = 20.0$	${}^{ID}k_2 = 5.0 \times 10^{-2}$	
	${}^{AB}k_2 = 7.0 \times 10^2$	${}^{IA}k_2 = 0.81$	${}^{DI}k_2 = 1.2 \times 10^{-3}$	
<u>Deduced parameters:</u>				
Interconversion rates (s^{-1})	${}^{BA}k_0 = 0.54$	${}^{AI}k_0 = 19.7$	${}^{ID}k_0 = 5.0 \times 10^{-2}$	
	${}^{AB}k_0 = 1.08 \times 10^4$	${}^{IA}k_0 = 3.74$	${}^{DI}k_0 = 1.2 \times 10^{-3}$	
	${}^{BA}k_1 = 1.3 \times 10^2$	${}^{AI}k_1 = 19.85$	${}^{ID}k_1 = 5.0 \times 10^{-2}$	
	${}^{AB}k_1 = 2.74 \times 10^3$	${}^{IA}k_1 = 1.74$	${}^{DI}k_1 = 1.2 \times 10^{-3}$	
Allosteric constants:	${}^{BA}L_0 = 2 \times 10^4$	${}^{AI}L_0 = 0.19$	${}^{ID}L_0 = 2.5 \times 10^{-2}$	
	${}^{BA}L_1 = 21.6$	${}^{AI}L_1 = 8.7 \times 10^{-2}$	${}^{ID}L_1 = 2.5 \times 10^{-2}$	
	${}^{BA}L_2 = 2.3 \times 10^{-2}$	${}^{AI}L_2 = 4.0 \times 10^{-2}$	${}^{ID}L_2 = 2.5 \times 10^{-2}$	

For the 14 independent rate constants (4 on and 4 off rates for ligand, 3 forward and 3 back allosteric transition rates for the doubly-liganded forms, and 3 transition state positional parameters) necessary to define the $B_i \rightleftharpoons A_i$, $A_i \rightleftharpoons I_i$, and $I_i \rightleftharpoons D_i$ allosteric transitions with two equivalent agonist binding sites per molecule, parameter values were deduced for the nAChR on the basis of results with rapid agonist application techniques using outside-out

patches containing embryonic-like nAChR from mouse muscle (Franke *et al.*, 1993) and earlier single-channel measurement (Colquhoun and Sakmann, 1985), as reported previously (Edelstein *et al.*, 1996).

Figure legends.

Figure 1. Evolutionary relationships between the subunits of the nAChR based on the analysis of Le Novère and Changeux (1995) updated for sequence information published subsequently, as kindly supplied by N. Le Novère.

Figure 2. Structural models of the nAChR. a. Schematic representation of functional domains. b. Longitudinal outline of a receptor molecule with respect to the cytoplasmic membrane (Unwin, 1996). Putative α -helices lining the ion channel are indicated by the two kinked bars c. Schematic cross-sectional view of the receptor showing binding sites at α/γ and α/δ interfaces with subunits in the arrangement deduced by Machold *et al.* (1995).

Figure 3. The interconversion of conformational states for the nAChR. a. The full set of reactions. b. The linear progression of states imposed by the relative magnitudes of the rate constants (Edelstein *et al.*, 1996).

Figure 4. The complete network of rate constants for conformational interconversions and two agonist binding sites, based on the linear progression of conformational states. Each column corresponds to a series of ligand binding events at two identical sites per receptor, with the rates specified along the vertical arrows by the state-specific intrinsic "on" and "off" constants, with statistical factors included. Each row corresponds to a series of transitions between states governed by rate constants that vary with the number of ligand molecules bound ($i = 0, 1, \text{ or } 2$), with the initial and final states in the superscript and the number of ligands in the subscript (Edelstein *et al.*, 1996).

Figure 5. The reaction cycle for the B and A pair of states as a function of binding one molecule of agonist. Linkage relations require that each step of ligand binding produces a decrease in the allosteric equilibrium constants ${}^{\text{BAL}}L_i$, as follows from ${}^{\text{BA}}c = {}^{\text{BAL}}L_i/{}^{\text{BAL}}L_{i-1}$. Since for each value of i the ${}^{\text{BAL}}L_i$ value is set by the ratio of the appropriate rate constants, ${}^{\text{BAL}}L_i = {}^{\text{AB}}k_i/{}^{\text{BA}}k_i$, the decrease in ${}^{\text{BAL}}L_i$ with each i^{th} ligand binding step must correspond to changes in the interconversion rates such that ${}^{\text{BA}}c = \frac{{}^{\text{AB}}k_i}{{}^{\text{BA}}k_i} \cdot \frac{{}^{\text{BA}}k_{i-1}}{{}^{\text{AB}}k_{i-1}}$. According to this equation, the stabilization of the higher affinity member of each pair of states resulting from the binding of one molecule of agonist must be reflected by a decreasing interconversion rate constant towards the lower affinity state and/or an increasing interconversion rate constant towards the higher affinity state. Thus, for the progression from ${}^{\text{BAL}}L_{i-1}$ to ${}^{\text{BAL}}L_i$, since ${}^{\text{BAL}}L_{i-1} > {}^{\text{BAL}}L_i$, the decrease upon agonist binding must correspond to ${}^{\text{AB}}k_i/{}^{\text{AB}}k_{i-1} < 1$ and/or ${}^{\text{BA}}k_{i-1}/{}^{\text{BA}}k_i < 1$. Hence, ligand binding drives the $B_i \rightleftharpoons A_i$ equilibrium towards A by systematically increasing the $B \rightarrow A$ rates and/or decreasing the $A \rightarrow B$ rates. Equivalent relations apply to the A-I and I-D pairs of states (Edelstein *et al.*, 1996).

Figure 6. Linear free energy relations and the scaling of transition state barriers. For each conformational state (A or B) or the transition states (TS), the energy of stabilization resulting from ligand binding is depicted by a “ladder” of equally spaced steps. The vertical positions of the ladders are set by $\Delta G = 0$ for B_0 and by $\Delta G = -RT \ln {}^{\text{BAL}}L_0$ for A_0 . The transition states are placed according to the free energy of activation ΔG^\ddagger , derived from transition state theory as expressed by the equation: $k = \kappa(k_B T/h)e^{-\Delta G^\ddagger/RT}$, where κ is the transmission constant (which can be assumed to equal 1.0 if there are no barrier recrossings), k_B is Boltzman's constant, h is Planck's constant, R is the gas constant, and T is the absolute temperature

(Steinfeld *et al.*, 1989). For the interconversions between states, the rate constants for the doubly-liganded forms are specified on the basis of the experimental data, as summarized in Table 1. The changes in the rates for the unliganded and singly-liganded forms are determined by the transition state positional parameters, ^{BA}p . For the series of interconversion reactions, the differences in the activation energies for the successive transition states reflect the differences in the energy of stabilization of the B and A states with each successive ligand binding, weighted by the ^{BA}p . In other terms, the successive interconversion rate constants scale with the corresponding affinity ratio, with the positional parameter in the exponent: $\frac{^{AB}k_i}{^{AB}k_{i-1}} = ^{BA}c \exp(^{BA}p)$ and $\frac{^{BA}k_{i-1}}{^{BA}k_i} = ^{BA}c \exp(1 - ^{BA}p)$. Since the product of these two equations is equivalent to $^{BA}c = \frac{^{AB}k_i}{^{BA}k_i} \cdot \frac{^{BA}k_{i-1}}{^{AB}k_{i-1}}$ (see legend to Fig. 5), these relations permit the positional parameter to define the dependence of the interconversion rate constants on ligand binding (Edelstein *et al.*, 1996). For example, with $^{BA}p = 0.2$ (Table 1), it can be seen that the vertical spacing of the transition states for the $B_i \rightleftharpoons A_i$ interconversions at different degrees of ligand binding more closely resembles the spacing between the A_i forms than the spacing between the B_i forms.

Figure 7. The C&S-type model, with ligand binding to the B and D states and formation of the open state (A_2) from B_2 as defined by the constant $K_{\text{open}} = [B_2]/[A_2] = \alpha/\beta$.

Figure 8. Free energy diagram for the four-state allosteric model, including all liganded and unliganded allosteric states, as well as their respective transition states. The B, A, I, and D states are each represented by a free energy ladder with details as described for the B and A states in Fig. 6 and values of the relevant parameters as described in Table 1.

Figure 9. Kinetic simulations presenting activation, progression through the states upon agonist binding, and recovery following agonist removal. The states are labeled, with the number of ligand molecules bound indicated by the line format (0, dotted; 1, dashed; 2, solid). The ligand concentration is 10^{-5} M. Values of the parameters utilized are presented in Table 1.

a. The appearance of the open state (in the form of a current change, $1 - [A \text{ states}]$) on a scale of log time (in seconds), with the inset presenting the same data on a linear scale (vertical bar = 0.1 fractional amplitude change; horizontal bar = 0.5 s).

b. The fractional population represented by each of the four states during an agonist pulse, with time on a logarithmic scale

c. Recovery begins upon removal of free agonist at the point marked by the arrow in b, corresponding to an agonist pulse of 20 s.

Figure 10. Dose-response simulations. a. Kinetic simulations for increasing concentrations of agonist in the concentration range 10^{-6} to 10^{-3} M, with the value of ${}^A k_2 = 20 \text{ s}^{-1}$ (Table 1).

Simulations for each concentration (in increments of $10^{0.2} = 1.58$ times the previous concentration) are presented as “Response” (calculated as $1 - \bar{A}_{\text{norm}}$) versus log time (in seconds) and the minimum of each curve, corresponding to the maximal channel opening at that concentration, is marked by a filled circle. b. Dose-response curves for the simulation in a. The predicted response curve (presented as the continuous dotted line) is described by

\bar{A}_{norm} , the theoretical equilibrium for the normalized fraction of A in a system limited to the B and A states:

$$\bar{A}_{\text{norm}} = \frac{\frac{(1 + \alpha_A)^N}{(1 + \alpha_A)^N + {}^B A L_0 (1 + {}^B A C \alpha_A)^N} - \bar{A}_{\text{min}}}{\bar{A}_{\text{max}} - \bar{A}_{\text{min}}}, \text{ where } \alpha_A \text{ is the concentration of ligand}$$

(X) normalized to the affinity of the A state: $\alpha_A = (X)/K_A$ and the values of the relevant

parameters are from Table 1. The individual points for maximal channel opening at each concentration from a are transferred to give the corresponding filled circles. In addition, the filled squares correspond to simulations carried out with $^A k_2 = 200 \text{ s}^{-1}$ (Edelstein *et al.*, 1996).

Figure 11. Simulations of pre-pulse desensitization with low concentrations of agonist.

Simulation of the populations of states for an agonist concentration of $4 \times 10^{-7} \text{ M}$. a. Data presented as a function of time in seconds for the predominant molecular species, B_0 , I_2 , D_1 , and D_2 . b. Inhibition-response curve to obtain apparent IC_{50} values. Solid line predicted by the allosteric theory for the normalized fraction of molecules in the D state (\bar{D}_{norm}) and presented as $1 - \bar{D}_{\text{norm}}$, where

$$\bar{D}_{\text{norm}} = \frac{(1 + \alpha_D)^N}{(1 + \alpha_D)^N + {}^I D L_0 (1 + {}^I D_C \alpha_D)^N + {}^A D L_0 (1 + {}^A D_C \alpha_D)^N + {}^B D L_0 (1 + {}^B D_C \alpha_D)^N} - \bar{D}_{\text{min}}$$

$$\bar{D}_{\text{norm}} = \frac{\bar{D}_{\text{max}} - \bar{D}_{\text{min}}}{\bar{D}_{\text{max}} - \bar{D}_{\text{min}}}$$

and α_D is the concentration of ligand (X) normalized to the affinity of the D state: $\alpha_D = (X)/K_D$. Using the values in Table 1 leads to an IC_{50} values of $2.66 \times 10^{-7} \text{ M}$. The points in b are from a series of simulations as in a for the fraction of activatable receptors remaining after a 10 s prepulse at different concentrations of ACh. The dashed curve through the points corresponds to an apparent IC_{50} value of $1.2 \times 10^{-6} \text{ M}$ (Edelstein *et al.*, 1996).

Figure 12. The allosteric network of receptor molecules in multiple conformational states. Each conformation S_i corresponds to a unique quaternary structure (Σ_i) with intrinsic binding properties (K_i) and conductance (γ_i). The interconversion between any two conformational states S_i and S_j is described by an allosteric equilibrium constant ${}^{ij}L = [S_j]/[S_i]$ (Galzi *et al.*, 1996b).

Figure 13. The L phenotype as illustrated with curves of \bar{Y} and \bar{A} for four combinations of ^{BA}L and ^{BA}c (Edelstein and Changeux, 1996): a. High ^{BA}L and low ^{BA}c . b. High ^{BA}L and high ^{BA}c . c. Low ^{BA}L and low ^{BA}c . d. Low ^{BA}L and high ^{BA}c . The values of ^{BA}L and ^{BA}c correspond to the data analyzed with a two-state model (Galzi *et al.*, 1996b) for the nAChR $\alpha 7$, wild type ($^{BA}L = 800,000$) and the channel mutant V251T ($^{BA}L = 20$), with respect to the agonist ACh ($^{BA}c = 0.1$) and the partial agonist dihydro- β -erythroidine ($^{BA}c = 0.5$) on the basis of published experimental data (Devillers-Thiéry *et al.*, 1993; Galzi *et al.*, 1992). In addition the absolute values of the binding affinities are fixed by $K_A = 2.5 \times 10^{-6}$ M for ACh, and $K_A = 3.5 \times 10^{-6}$ M for DH β E.

Figure 14. Theoretical dose-response relationships describing the γ phenotype. The curves are generated with a three state model: $B \rightleftharpoons A \rightleftharpoons I$, assuming that either only the A conformation or both the A and I conformations contribute to physiological response, for the curves as indicated. The equation for the case of both A and I as open states is:

$$\bar{A} + \bar{I} = [(1 + \alpha_1)^n + {}^{AI}L(1 + {}^{AI}c \alpha_1)^n] / [(1 + \alpha_1)^n + {}^{AI}L(1 + {}^{AI}c \alpha_1)^n + {}^{AI}L {}^{BA}L(1 + {}^{AI}c {}^{BA}c \alpha_1)^n],$$

where $\alpha = [X] / K_I$. The L values are for the $B \rightleftharpoons A$ transition: $^{BA}L = 8 \times 10^5$, and for the $A \rightleftharpoons I$ transition: ${}^{AI}L = 1.2 \times 10^{-5}$. The affinity values are, for ligand 1: $K_A = 2.5 \times 10^{-6}$, $^{BA}c = 0.1$, $K_I = 10^{-6}$, ${}^{AI}c = 0.4$, and for ligand 2: $K_A = 3.5 \times 10^{-6}$, $^{BA}c = 0.5$, $K_I = 3 \times 10^{-7}$, ${}^{AI}c = 0.0857$. Intrinsic affinities increase from state B to A to I for both ligands. Ligand 1 is a competitive antagonist when the I state corresponds to a closed channel state and becomes an agonist when the I state has an open channel. Ligand 2, which is an agonist in both cases, stabilizes one or two conducting states depending on the biological activity of the I conformation (Galzi *et al.*, 1996b).

Figure 15. The state and binding functions and their cooperativity for a homopentamer with B and A states. The allosteric functions \bar{A} and \bar{Y} are presented as a function $[X]/K_A$ for a series of values of the allosteric parameter, ${}^{BA}L$. All curves are calculated with ${}^{BA}c = 0.1$. \bar{Y} is determined with the equation:

$$\bar{Y} = [\alpha(1 + \alpha)^{N-1} + {}^{BA}L {}^{BA}c\alpha(1 + {}^{BA}c\alpha)^{N-1}] / [(1 + \alpha)^N + {}^{BA}L(1 + {}^{BA}c\alpha)^N]$$
, where N is the number of ligand-binding sites and α is the concentration of ligand normalized to the affinity of the A state: $\alpha = [X]/K_A$. For \bar{Y} the apparent affinity, $[X]_{50}$ (defined as the value of $[X]$ at $\bar{Y} = 0.5$), occurs between the limits K_A and K_B corresponding, respectively, to pure A state (Y_A) at the low ${}^{BA}L$ extreme and pure B state (Y_B) at the high ${}^{BA}L$ extreme. These limits constitute the “ligand binding range”. The equation for \bar{Y} reduces at very low ${}^{BA}L$ to $\bar{Y}_A = 1/(1 + K_A/[X])$ and at very high L to $\bar{Y}_B = 1/(1 + K_B/[X])$. The limits for binding are thus independent of N and reflect only the intrinsic binding constants of the B and A states. For the state function, the curves are described by the equation:

$$\bar{A} = 1 / [1 + {}^{BA}L(1 + {}^{BA}c\alpha)^N / (1 + \alpha)^N]$$
, which predicts variations between \bar{A}_{\min} in the absence ligand and \bar{A}_{\max} at saturating ligand, where: $\bar{A}_{\min} = 1/(1 + {}^{BA}L)$ and $\bar{A}_{\max} = 1 / (1 + {}^{BA}L [{}^{BA}c]^N)$. The low ${}^{BA}L$ and high ${}^{BA}L$ limits of the mid-points of \bar{A} are set, respectively, by $[X]_{50} = K_A (\sqrt[N]{2}) - 1$ and $[X]_{50} = K_B / [(\sqrt[N]{2}) - 1]$, constituting the “ligand response range” that considerably exceeds the “ligand binding range”.

Figure 16. The Hill coefficients (n) and the allosteric range (Q), in the lower panel, are presented as a function of $[X]_{50}/K_A$ for the curves of \bar{A} and \bar{Y} presented in Fig. 15, where n_{50} corresponds to the value for $\bar{Y} = 0.5$ and n'_{50} the value for $\bar{A}' = 0.5$. At low ${}^{BA}L$ and low ligand concentration $\bar{A}_{\min} > 0$ and at high ${}^{BA}L$ and saturating ligand concentration $\bar{A}_{\max} < 1$. The difference, $\bar{A}_{\max} - \bar{A}_{\min}$, defines the allosteric range, Q (Rubin and Changeux, 1966).

Concerning the Hill coefficients, the values of n'_{50} for the state function are presented for \bar{A}' , the normalized value of \bar{A} , as defined in the legend to Fig. 10. The peaks of the curves of n_{50} and n'_{50} versus $\log {}^{BA}L$ occur at ${}^{BA}L = ({}^{BA}c)^{-N/2}$. At this value of ${}^{BA}L$ the curves for \bar{Y} and \bar{A} are symmetric and n_{50} corresponds to the point of maximal cooperativity (n_{max}). At other values of ${}^{BA}L$, for \bar{Y} the values of n_{50} and n_{max} fall off towards 1.0 as the extremes of ${}^{BA}L$ are approached, with $n_{50} < n_{max}$ and the value of \bar{Y} corresponding to n_{max} decreasing progressively towards $\bar{Y} = 1/N$ at low ${}^{BA}L$ and increasing progressively towards $\bar{Y} = (N-1)/N$ at high ${}^{BA}L$. The value of n_{50} for $\bar{Y} = 0.5$ can be calculated directly from a sum of binding fractions each multiplied by its net reaction order (Edelstein and Bardsley, 1997). While n_{max} for \bar{Y} follows a bell-shaped curve as a function of ${}^{BA}L$ (Rubin and Changeux, 1966), n_{max} for \bar{A}' is independent of ${}^{BA}L$ and always equal to the value of n'_{50} at ${}^{BA}L = ({}^{BA}c)^{-N/2}$. However, the value of \bar{A}' corresponding to n_{max} varies widely, approaching 0 at low ${}^{BA}L$ and 1 at high ${}^{BA}L$, with the exact value given by $1/[1 + {}^{BA}L ({}^{BA}c)^{N/2}]$. Variations in n'_{50} also follow a bell-shaped curve as a function of $\log {}^{BA}L$, but with limits of $n > 1$ at the extremes, as described in Fig. 17.

Figure 17. Receptors at various degrees of saturation during ligand binding. At very high values of L , virtually all channel opening coincides with formation of the fully liganded species, S_5 . (For ${}^{BA}L_0 = 800,000$ and ${}^{BA}c = 0.1$, the fraction of S_5 in the A state is given by $1/(1 + {}^{BA}L_0 {}^{BA}c^5) = 0.11$, whereas the fraction of S_4 in the A state is only 0.01). At the point corresponding to $\bar{A}' = 0.5$ (where the dashed horizontal and vertical lines cross) the observed reaction for the formation of receptor species with 5 ligands (S_5) can be represented by the linear sum of the reactions $S_4 \rightarrow S_5$, $S_3 \rightarrow S_5$, $S_2 \rightarrow S_5$, etc., each with increasing reaction order. As a result the overall cooperativity at 50% is given by the equation:

$$n'_{50} = \frac{[-1] S_4 + [-2] S_3 + [-3] S_2 + \dots}{0.5} = 2 \sum_{i=1}^N i S_i, \text{ where the number in the bracket}$$

corresponds to the order of the reaction for formation of S_5 from S_i and S_i is the fraction of molecules with i ligands bound (Edelstein and Bardsley, 1997). In this case, the values of $n'_{50} = 1.27$ arises from $2([-1] 0.37 + [-2] 0.11 + [-3] 0.016)$, where the values after the intergers in brackets correspond to the fractional population of the species S_4 , S_3 , and S_2 at their values along the dashed vertical line. For the case of $^{BA}c \ll 0.1$, the low limit of cooperativity is $n'_{50} = 1.29$.

Figure 18. Stochastic simulations of ligand-binding and conformational transitions for a receptor with B, A and I states. a. Passages among all possible molecular species. b. Passages scored as binding events. c. Passages scored as ionic events. The simulations were conducted for a ligand concentrations of 3×10^{-6} M, with the program STOIC (Simulations of Transient Openings in Ionotropic-receptor Channels) within the MATLAB environment (Edelstein *et al.*, 1996), modified to take into account non-equivalent ligand-binding sites (Edelstein *et al.*, 1997b). This program is available upon request or via Internet (<http://www.unige.ch:80/sciences/biochimie/Edelstein/Edelstein.html>). The simulations were conducted using parameters listed in Table 1.

Figure 19. Stochastic simulations of single binding events and single ionic events, with the corresponding dwell time probability profiles, for wild-type muscle nAChR at low ligand concentration. a. Binding events. b. Ionic events. The values for all relevant parameters are presented in Table 1. The data are based on a ligand concentration of 3×10^{-7} M, corresponding to a value of $P_{\text{open}} = 0.002$ (Edelstein *et al.*, 1997b). The simulations for binding events and ionic events are derived from the same simulation, with ligand events and

ionic events scored separately, as in the example presented in Fig. 18. Each simulation represents a brief stochastic sample of the corresponding dwell time probability profile below. The profiles indicate the distribution of all species (thick line) and the contributions of the individual components (thin lines) calculated with a theory that takes into account all relevant molecular events (Edelstein *et al.*, 1997b). The dwell times for the A state are prolonged by a series of passages to other states with diminishing probabilities and the composite times are indicated by ΣA (see also Figs. 21-23). In addition, for the distributions of ionic events (in b) the profile predicted by the C&S-type model with all opening events involving doubly-liganded molecules is represented by the individual points (+). The dwell time probability profiles are presented as the square root of the number of events versus time on a logarithmic scale (Sigworth and Sine, 1987).

Figure 20. Subunit structure and ligand binding sites at the α/γ and α/δ interfaces within the B state. Receptors with ligand occupying the higher affinity site for agonist (α/δ) are designated by the subscript “H” and with ligand occupying the lower affinity site for agonist (α/γ) by the subscript “L”. In this case, if $K_{B(H)} \ll K_{B(L)}$, then $K_1 = K_{B(H)}$ and $K_2 = K_{B(L)}$. Where differences between $K_{B(H)}$ and $K_{B(L)}$ are smaller, the exact values are $K_1 = K_{B(H)} K_{B(L)} / (K_{B(H)} + K_{B(L)})$ and $K_2 = K_{B(H)} + K_{B(L)}$. For identical sites, where $K_B = K_{B(H)} = K_{B(L)}$, the values of K_1 and K_2 are set by $K_1 = K_B / 2$ and $K_2 = 2 K_B$. The equilibrium constants are defined by the corresponding rates: $K_{B(H)} = {}^B k_H' / {}^B k_H$ and $K_{B(L)} = {}^B k_L' / {}^B k_L$. Similar definitions may be applied to the other states to incorporate nonequivalence of their binding sites.

Figure 21. Stochastic simulations of binding events and ionic events, with the corresponding dwell time probability profiles, for wild-type muscle nAChR at low ligand concentration

based on data interpreted with non-equivalent sites. The simulations are computed for a ligand concentration of 1.6×10^{-6} M, corresponding a value of $P_{\text{open}} = 0.002$ (Edelstein *et al.*, 1997b). Other details as in Fig. 19. Parameters for the case of non-equivalent sites were derived from the data of Jackson (1988), with corrections incorporated (Jackson, 1993), and small adjustments made to permit agreement with the model based on linear transition state theory: $k_{\text{on}} = 1 \times 10^8 \text{ M}^{-1}\text{s}^{-1}$ for all sites except B_L , for which $k_{\text{on}} = 0.05 \times 10^8 \text{ M}^{-1}\text{s}^{-1}$. The off rates (s^{-1}) are ${}^B k_{\text{H}}' = 500$; ${}^B k_{\text{L}}' = 1.8 \times 10^4$; ${}^A k_{\text{H}}' = 2.5$; ${}^A k_{\text{L}}' = 30$; for the I state identical off rates for both sites were set at 4.0. The interconversion rates (s^{-1}) were: ${}^{\text{BA}} k_0 = 0.028$; ${}^{\text{BA}} k_{1(\text{H})} = 1.8$; ${}^{\text{BA}} k_{1(\text{L})} = 44$; ${}^{\text{BA}} k_2 = 2800$; ${}^{\text{AB}} k_0 = 5013$; ${}^{\text{AB}} k_{\text{H}} = 1604$; ${}^{\text{AB}} k_{\text{L}} = 670$; ${}^{\text{AB}} k_2 = 214$; For the $A \rightleftharpoons I$ transition, since no specific data are available on site non-equivalence, the values for equivalent sites (Table 1) were utilized.

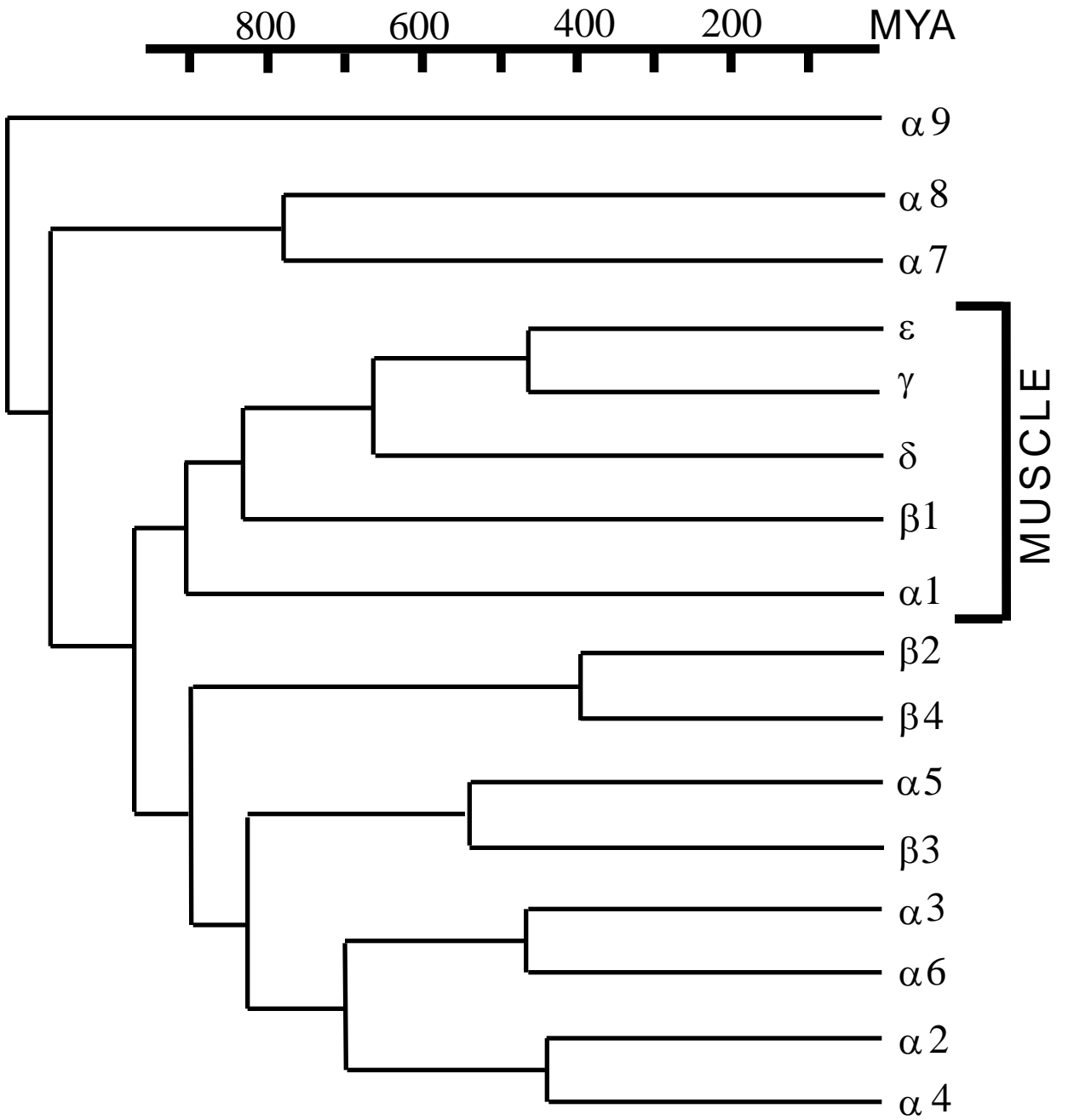
Figure 22. Stochastic simulations of binding events and ionic event, with the corresponding dwell time probability profiles, for wild-type muscle nAChR at high ligand concentration. Details as in Fig. 19, but with ligand concentrations of 0.95×10^{-5} M, corresponding to a value of $P_{\text{open}} = 0.5$.

Figure 23. Stochastic simulations of binding events and ionic event for the myasthenic mutant of human muscle nAChR ϵ T264P (Ohno *et al.*, 1995). Details as in Figure 19, but with values of the parameters for the mutant receptors based on the diminished intrinsic stability of the B state for the ϵ T264P mutant receptors (reflected by the decrease from $L_0 = 2 \times 10^4$ for the wild-type to $L_0 = 200$ for the mutant). The consequences of this change are to modify the values of the following parameters (all units in s^{-1}) compared to the wild-type (Table 1): ${}^A k_{\text{off}} = 4.5$; ${}^{\text{BA}} k_0 = 32.46$; ${}^{\text{BA}} k_1 = 1.65 \times 10^3$; ${}^{\text{BA}} k_2 = 8.4 \times 10^4$; ${}^{\text{AB}} k_0 = 6.58 \times 10^3$; ${}^{\text{AB}} k_1 = 188.3$; ${}^{\text{AB}} k_2$

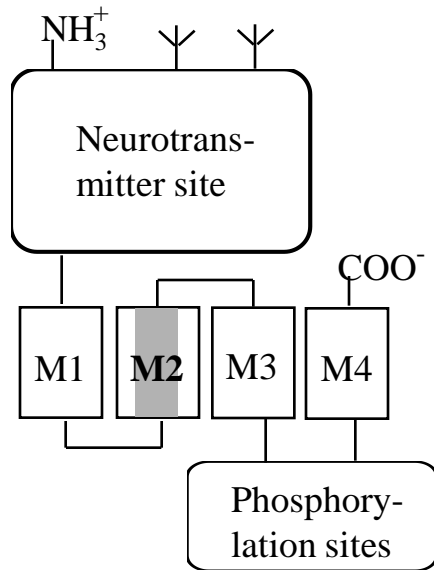
= 5.39 (Edelstein *et al.*, 1997a). For the mutant values of ${}^{AB}k_0$ and ${}^{AB}k_2$ were calculated using the τ_0 and τ_2 values reported for the ACh concentration of 3×10^{-7} M (Ohno *et al.*, 1995). For ${}^{AB}k_1$, the value derived from τ_1 (Ohno *et al.*, 1995) was corrected to 188.3 s^{-1} , since according to linear free energy relations it should be intermediate between ${}^{AB}k_0$ and ${}^{AB}k_2$ on a logarithmic scale (Edelstein *et al.*, 1996). From fitting the dwell time distributions, the value of ${}^{BA}L_0$ was set at 200 and the rates for ${}^{BA}k_0$, ${}^{BA}k_1$, and ${}^{BA}k_2$ were deduced according to linkage relations (Edelstein *et al.*, 1997a). A decrease of about 2-fold in ${}^A k_{\text{off}}$ compared to the wild-type value was also necessary for a satisfactory fit to the data. Desensitized states were not included in these simulations. A ligand concentration of 3×10^{-7} M was employed, corresponding to a value of $P_{\text{open}} = 0.37$. For the ionic events in D, the individual points (o) are presented for the three phases of open dwell times corresponding to the published values for 3×10^{-7} M ACh of $\tau_0 = 150 \text{ }\mu\text{s}$, $a_0 = 0.67$; $\tau_1 = 1.8 \text{ ms}$, $a_1 = 0.16$; and $\tau_2 = 69.5 \text{ ms}$, $a_2 = 0.17$ (Ohno *et al.*, 1995). The distribution predicted by the C&S-type model with all opening from doubly-liganded molecules is indicated by the points (+) in B.

Figure 24. Data and theoretical curves for the potentiation of rat medial habenular neurons by external calcium. a. Dose-response curves for the effect of ACh and currents in the presence of 4 mM calcium (solid squares) and in the absence of added calcium (solid circles) from the report by Mulle *et al.* (1993). The dashed lines are obtained with the four-state allosteric model using the parameters of Table 1, with the exception of the values of ${}^{BAL}_0 = 5.25 \times 10^5$ for the curve that coincides with the squares (corresponding to the presence of 4 mM calcium) and ${}^{BAL}_0 = 1.25 \times 10^6$ for the curve coinciding with the circles (corresponding to no added calcium). b. Illustration of coincidence detection. For kinetic simulations (time in seconds) with an agonist concentration of 2×10^{-4} M, only the response on the left with ${}^{BAL}_0 = 5.25 \times$

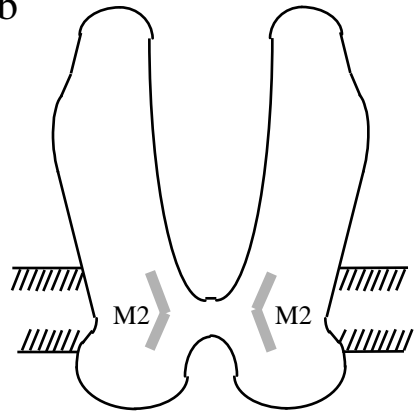
10^5 (corresponding to 4 mM calcium), but not the response on the right with ${}^{BA}L_0 = 1.25 \times 10^6$ (corresponding to no calcium), reaches a hypothetical threshold for neuronal firing (dashed line). c. A sliding threshold model. The normalized response is presented as a function of the stimulation frequency (Hz). For the system at ${}^{BA}L_0 = 5 \times 10^5$ it is assumed that the $B \rightleftharpoons A$ equilibrium may be displaced by phosphorylation away from A and by dephosphorylation towards A. Entry of calcium proportional to the stimulation frequency produces activation of the relevant kinase and phosphate, but with the former more sensitive and the latter more cooperative. In this case \overline{A} is calculated with the standard equation (see legend to Figure 14) for ${}^{BA}L = 5 \times 10^5$ and a ligand concentration (0.17 mM), corresponding to 50% response in the absence of stimulation. The value of ${}^{BA}L$ is assumed to vary with frequency of stimulation and subsequent calcium influx according to the equation ${}^{BA}L' = {}^{BA}L (1 + \phi f^{n\phi}) / (1 + \varphi f^{n\varphi})$, where ϕ and φ are coupling coefficients for the activation of kinase or phosphatase by calcium and $n\phi$ and $n\varphi$ give the apparent Hill coefficients for the interactions. The biphasic depression-potential pattern requires $\phi > \varphi$ and $n\phi < n\varphi$. For the simulation presented here, since phosphorylation leads to inhibition, ϕ corresponds to the kinase and φ corresponds to the phosphatase ($\phi = 1.2$ and $\varphi = 0.6$ in arbitrary units; $n\phi = 1.2$ and $n\varphi = 1.8$). Simulation for the mutant kinase with increased activity is obtained by setting $\phi = 3$. The simulation assumes that the receptor is partially phosphorylated in the absence of stimulation.



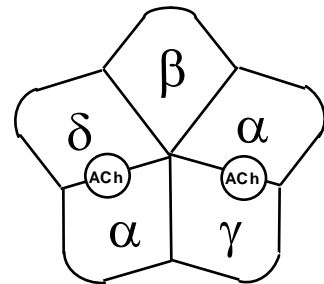
a



b



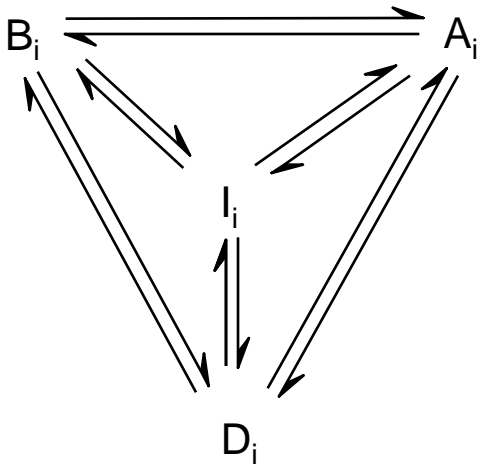
c



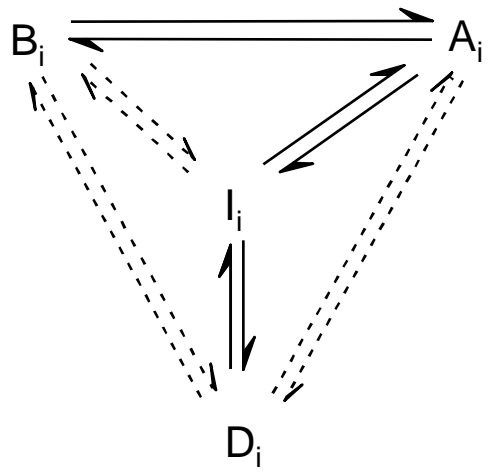
d

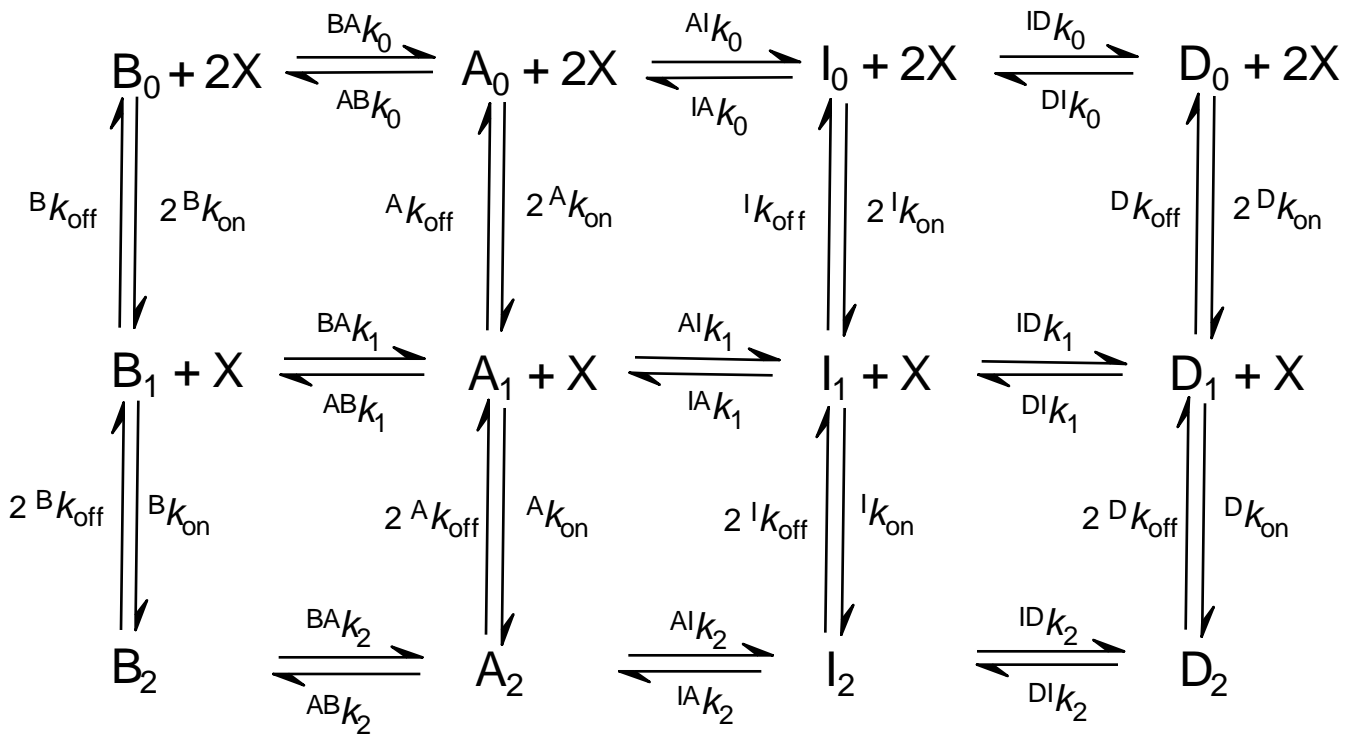
	<u>M2</u>
Chick $\alpha 7$:	I S L G I ^{244Q} T V L ^{247T} L S L T ^{251T} V F M L L V A
Human GlyR $\alpha 1$:	V G L G I T T V L T M T T Q S S G S ^{271L} R
Human AChR $\alpha 1$:	M T L S I S ^{249F} V L L S L ^{254I} T V F L L V I V
Human AChR $\beta 1$:	M G L S I F A L ^{262M} L T L T ^{266M} V F L L L L I
Human AChR ϵ :	C T V S I N V L L A Q ^{264P} T V F L F L I A ^{269F}
Human AChR $\alpha 4$:	I T L C I ^{248F} S V L L S L T V F L ^L L L I T

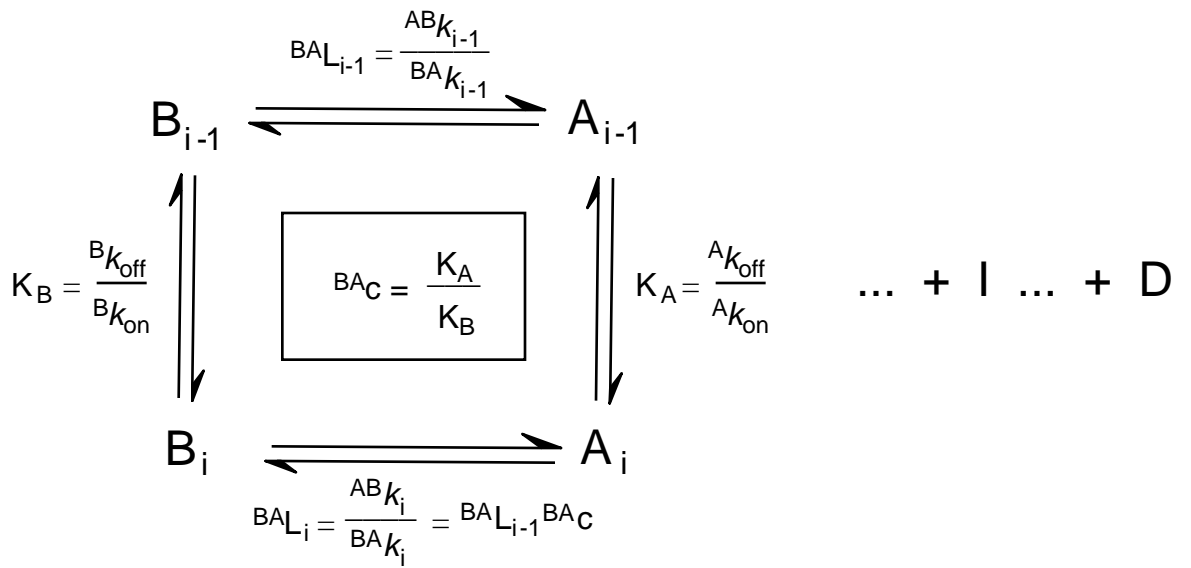
a

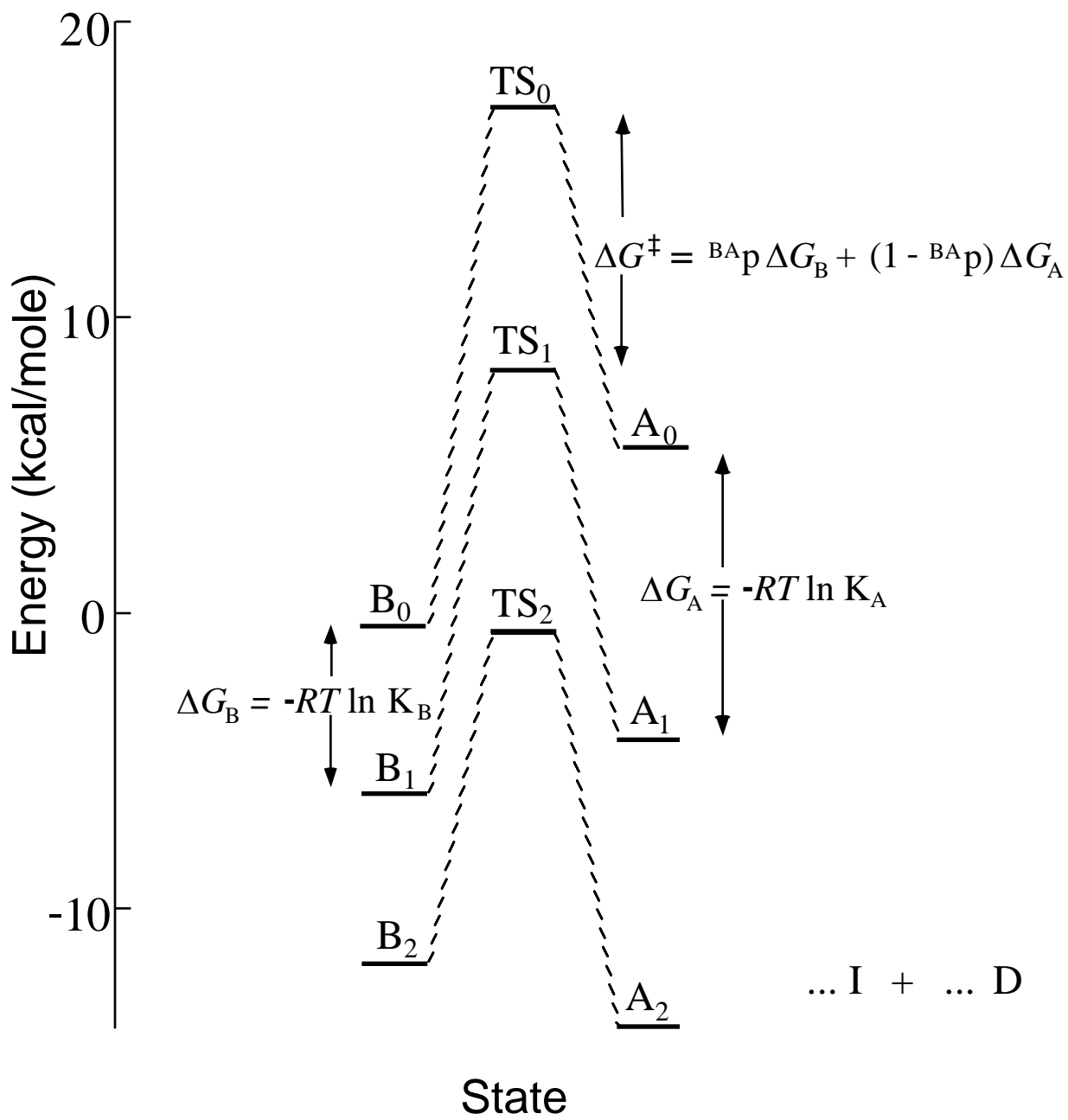
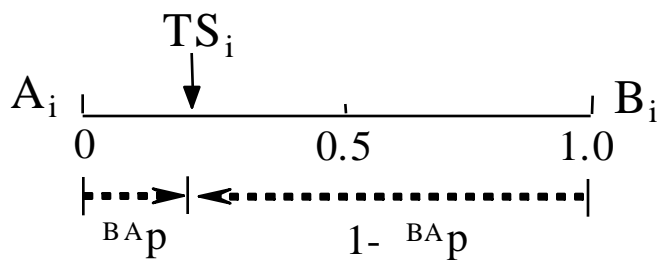


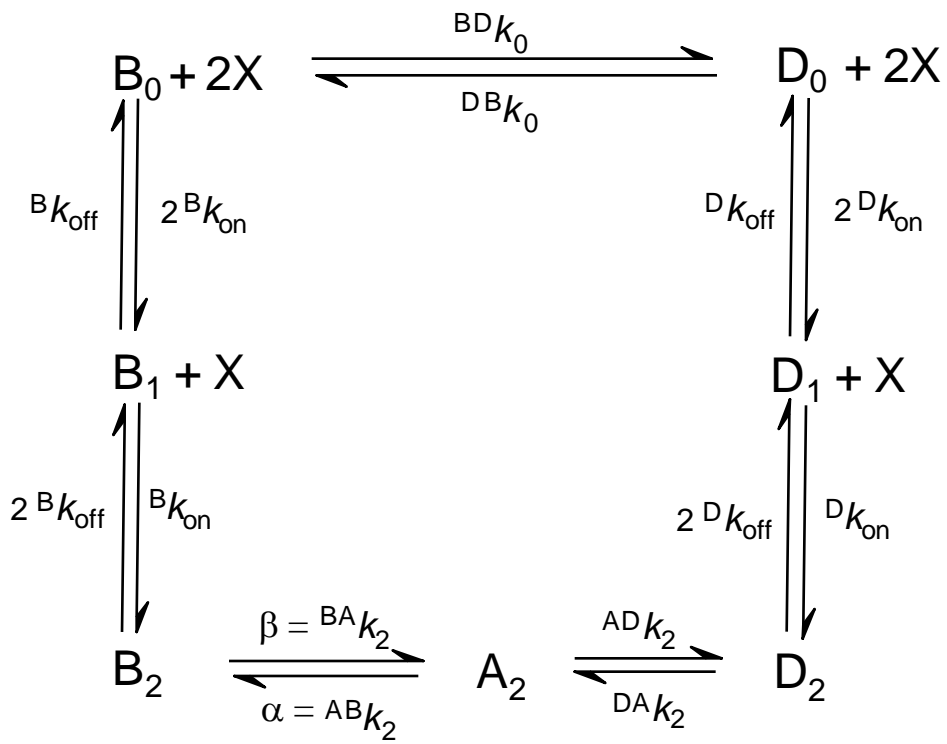
b

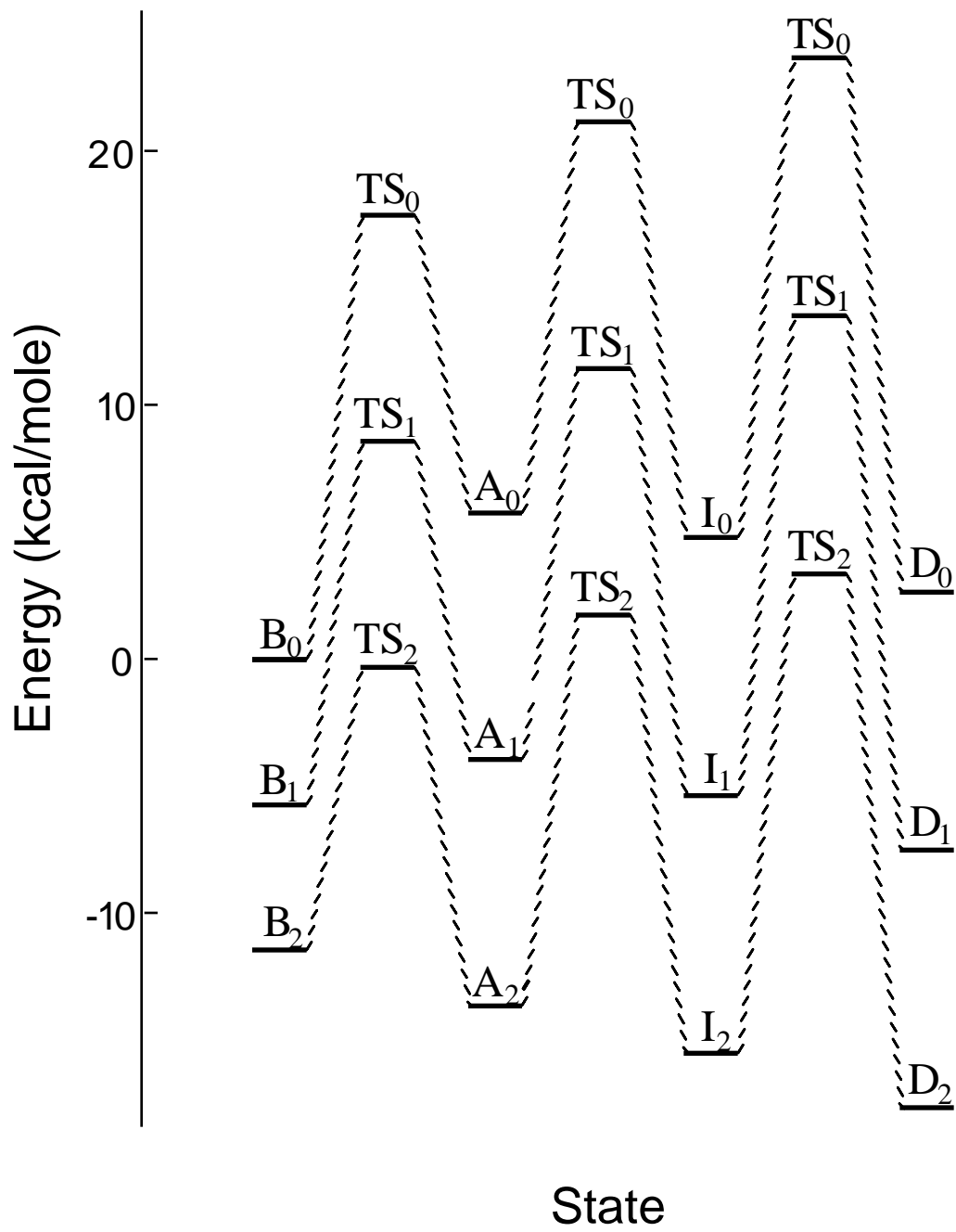


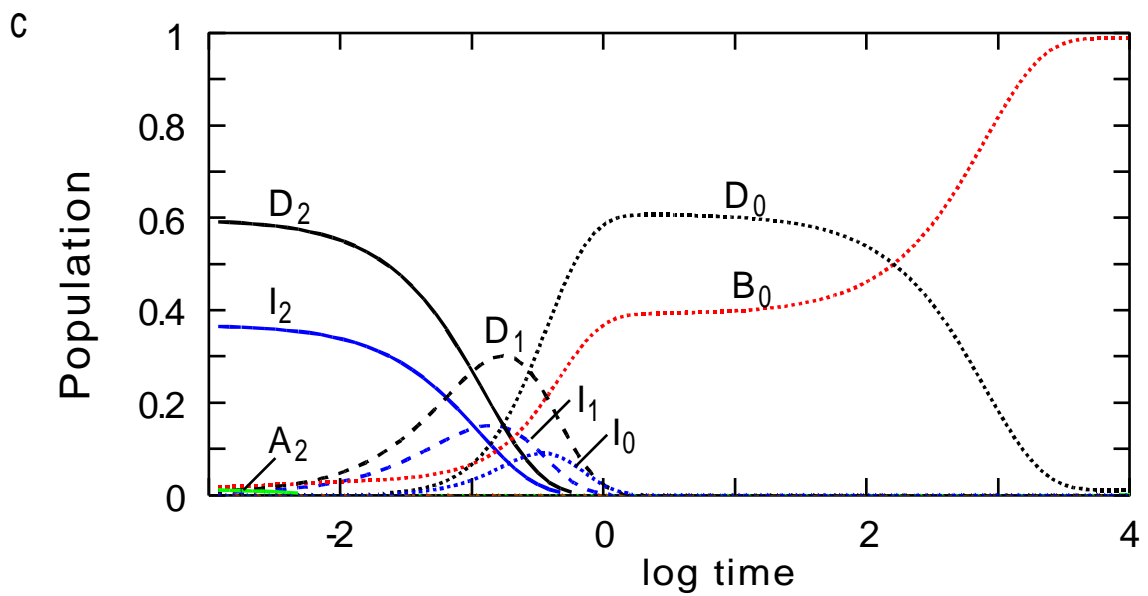
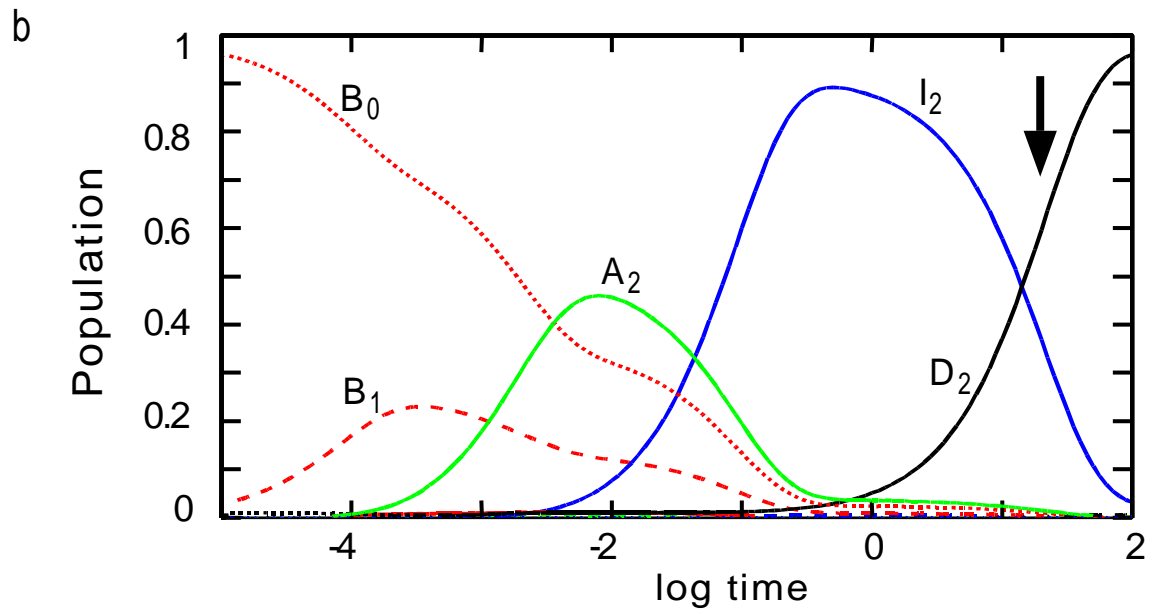
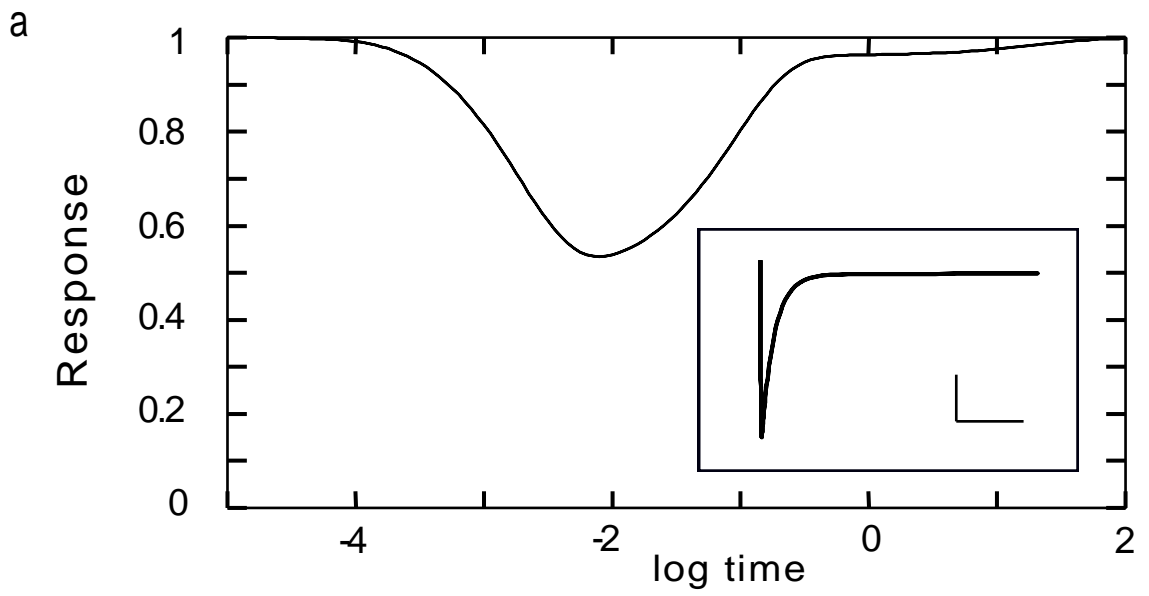


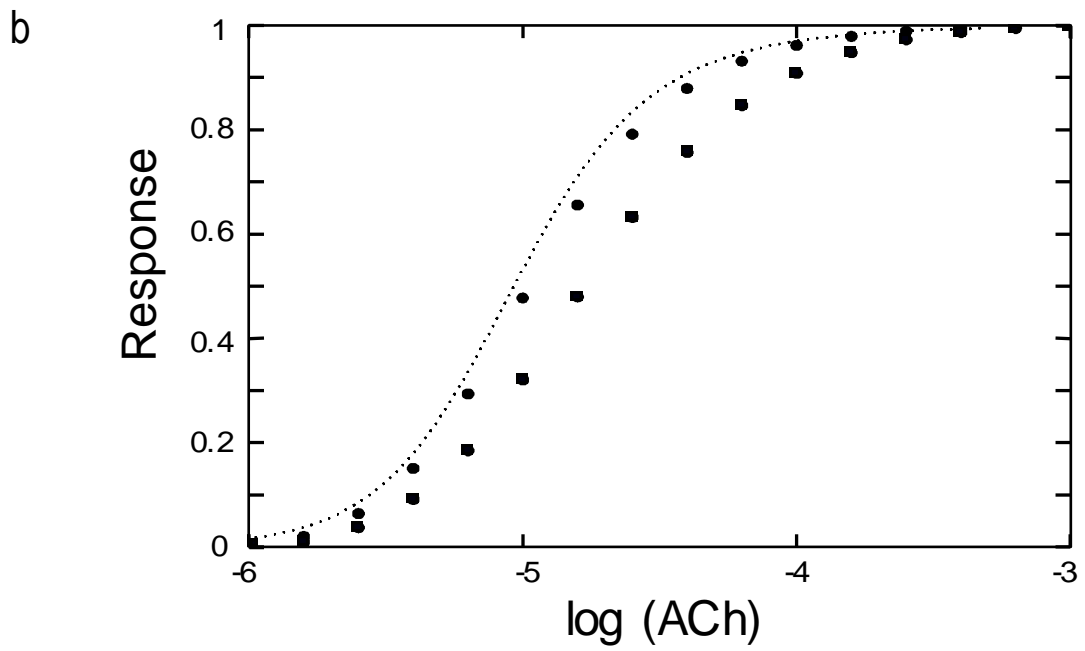
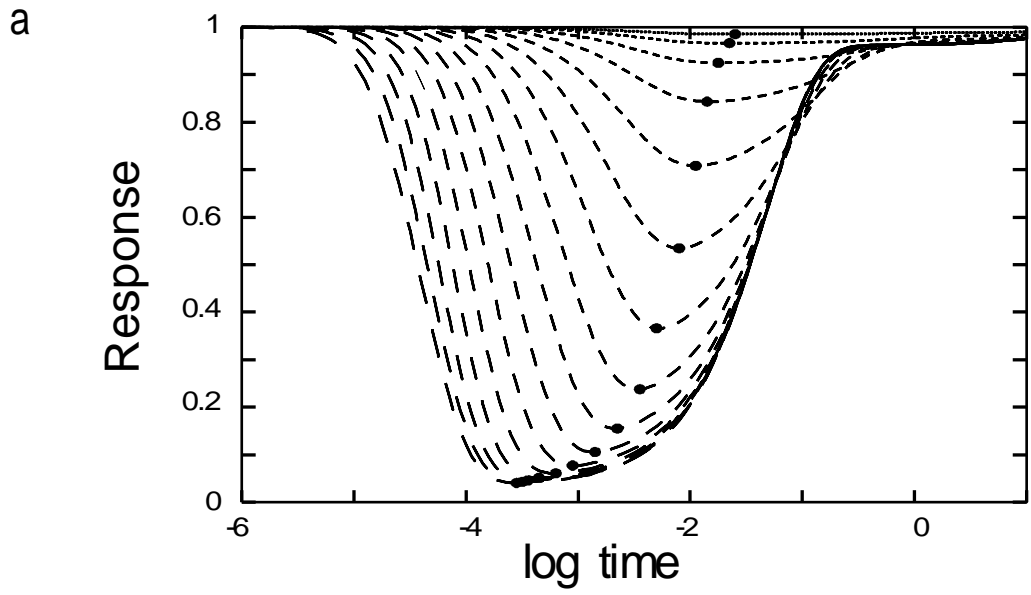


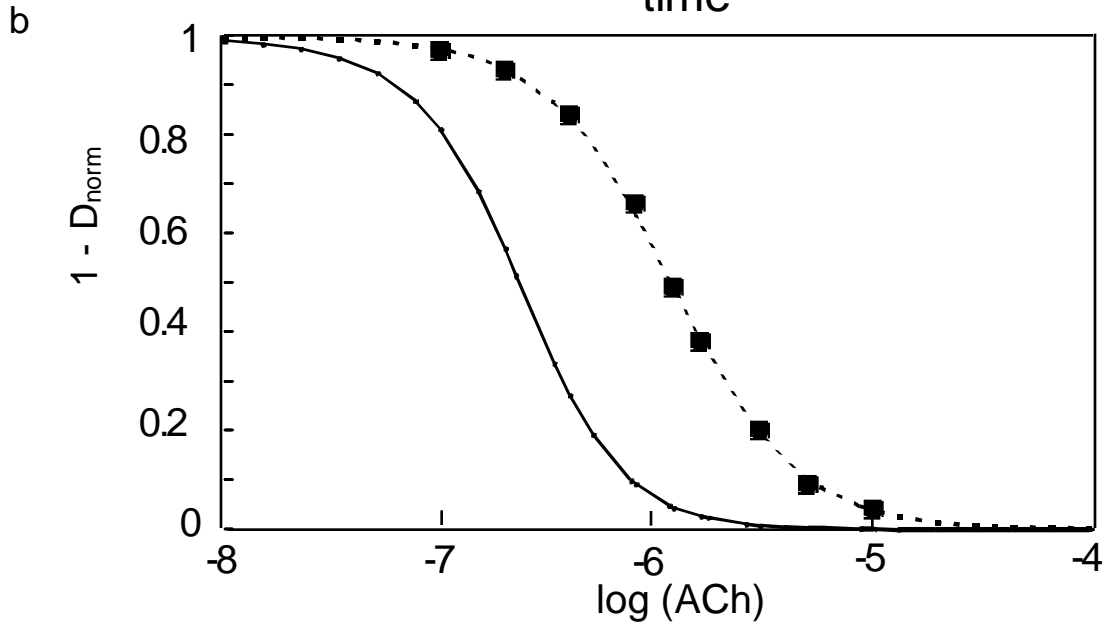
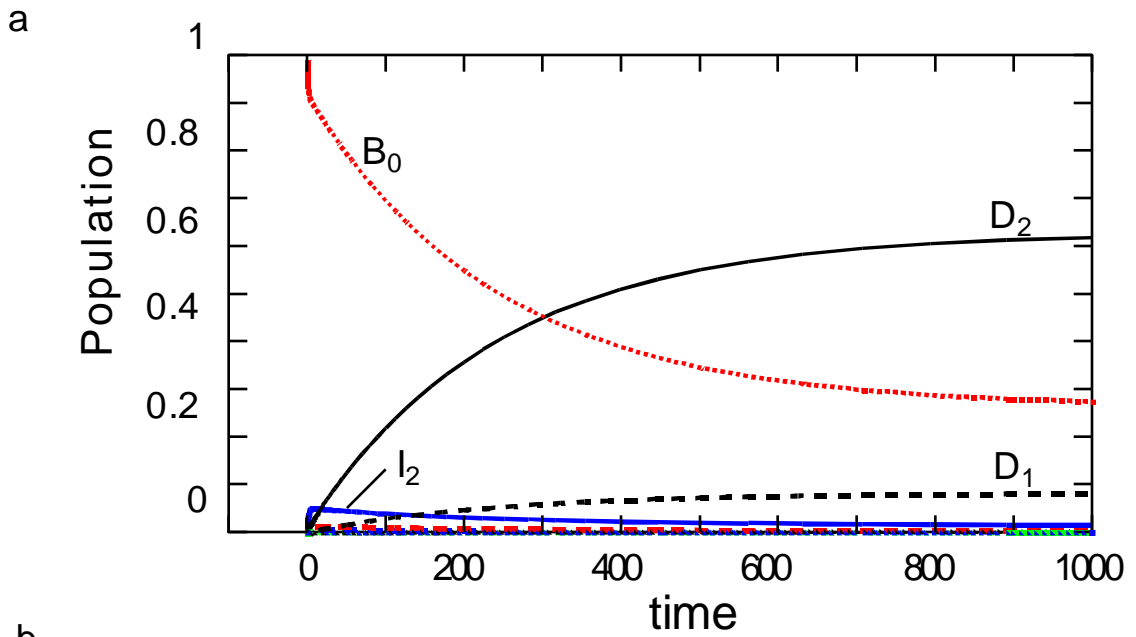


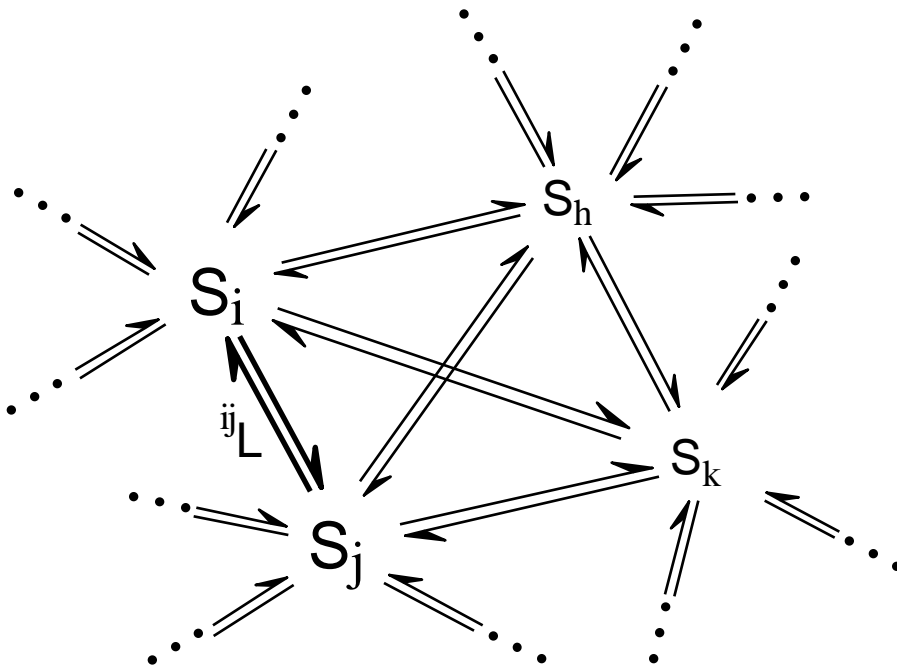






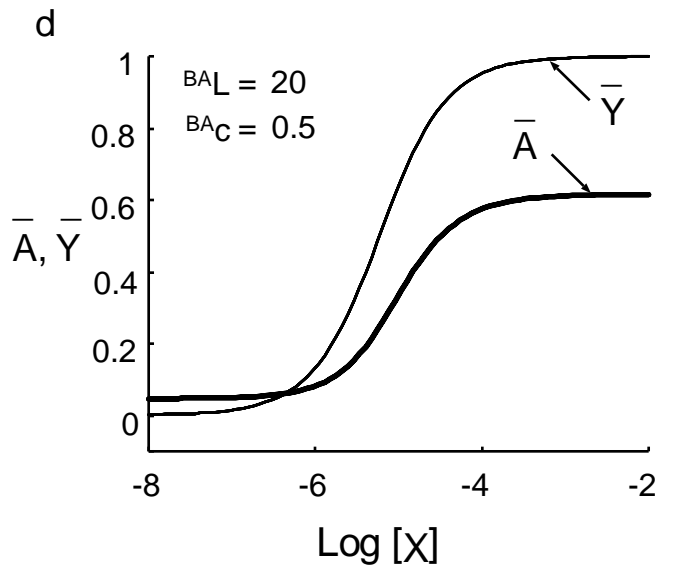
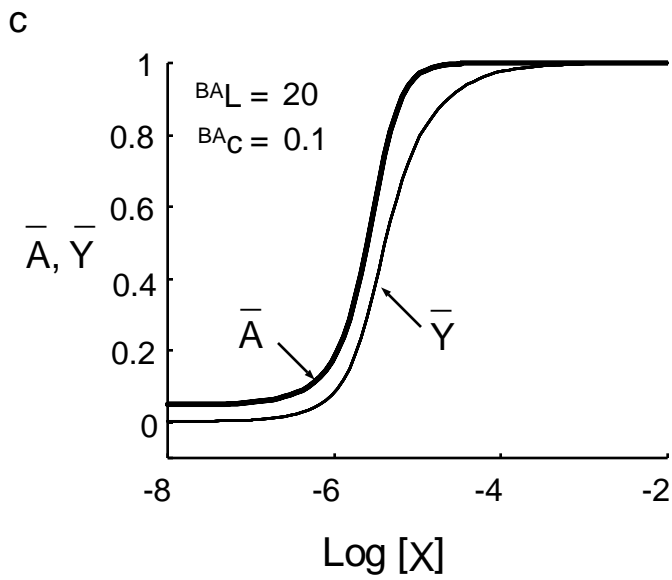
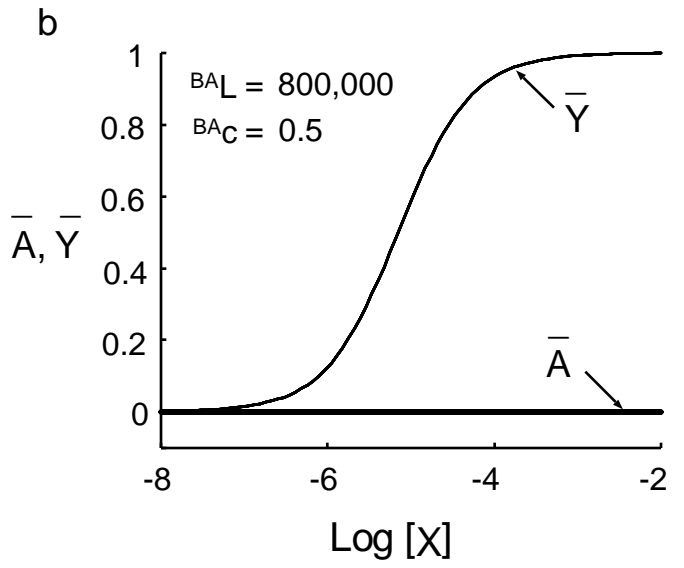
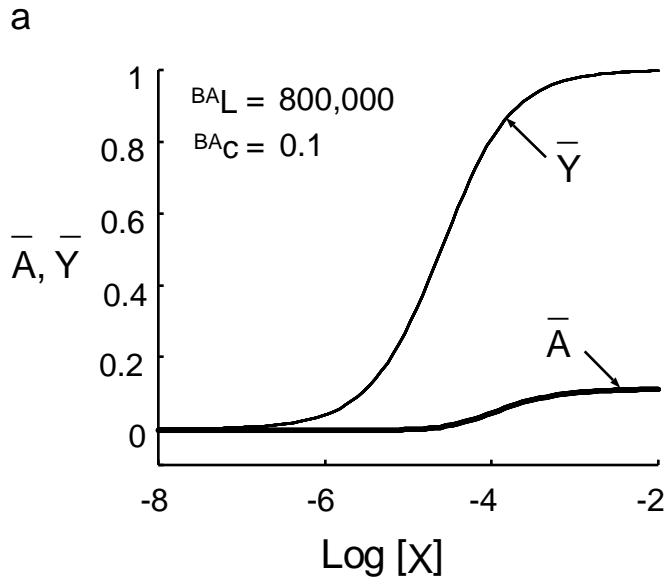


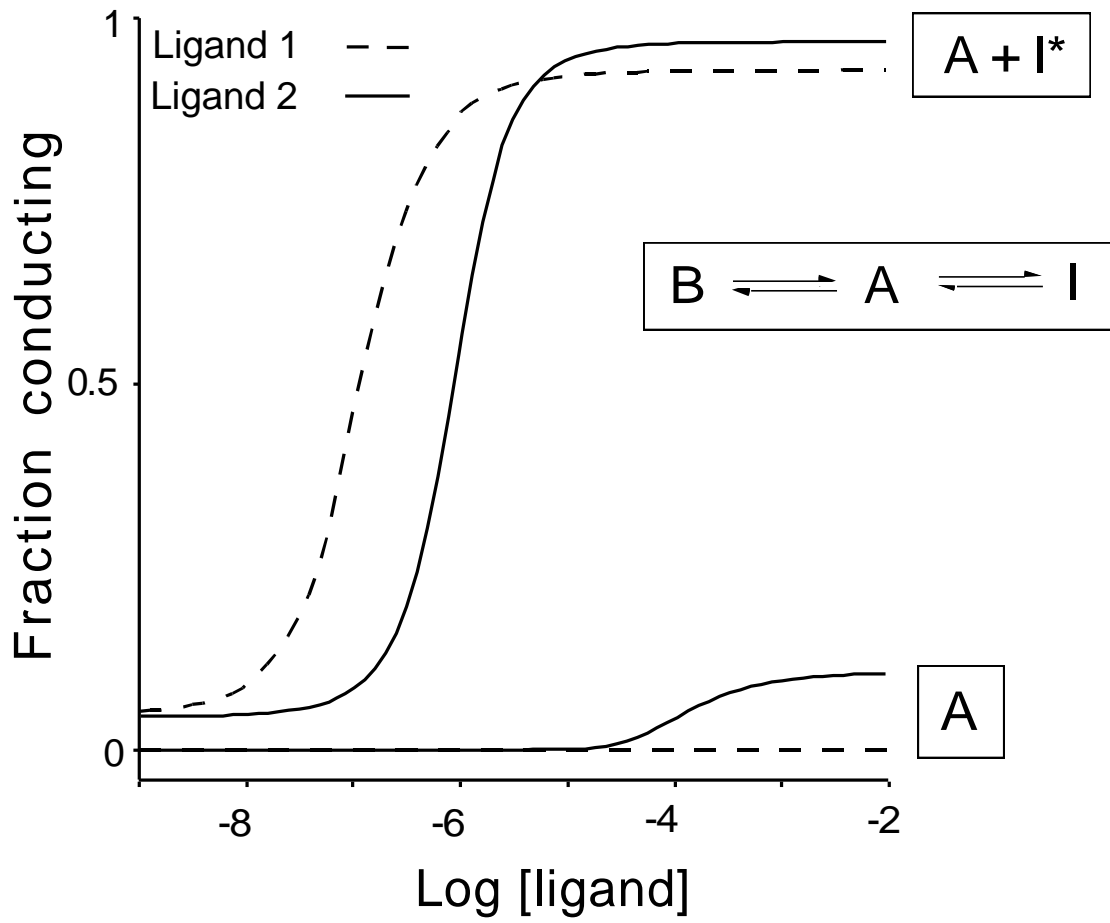


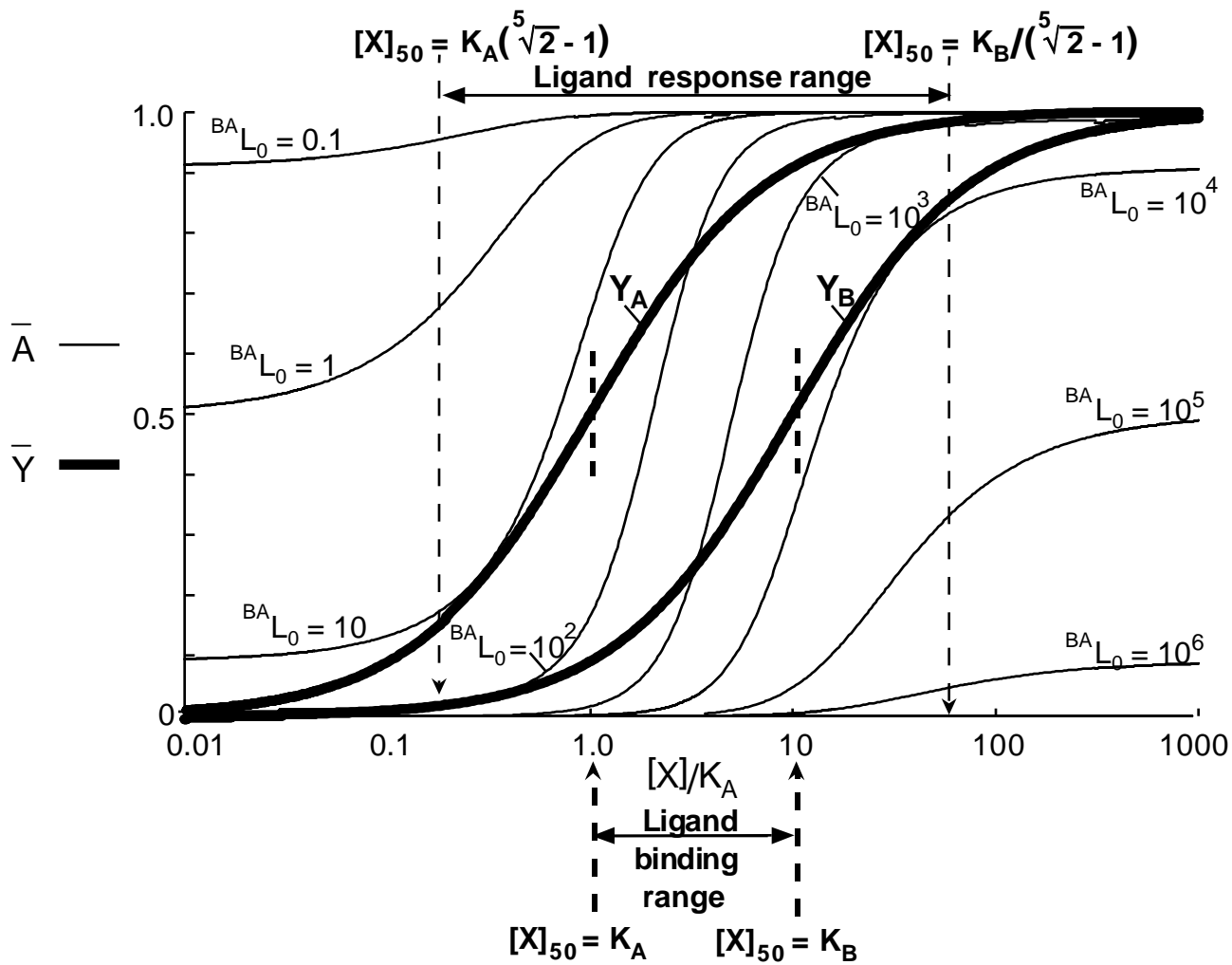


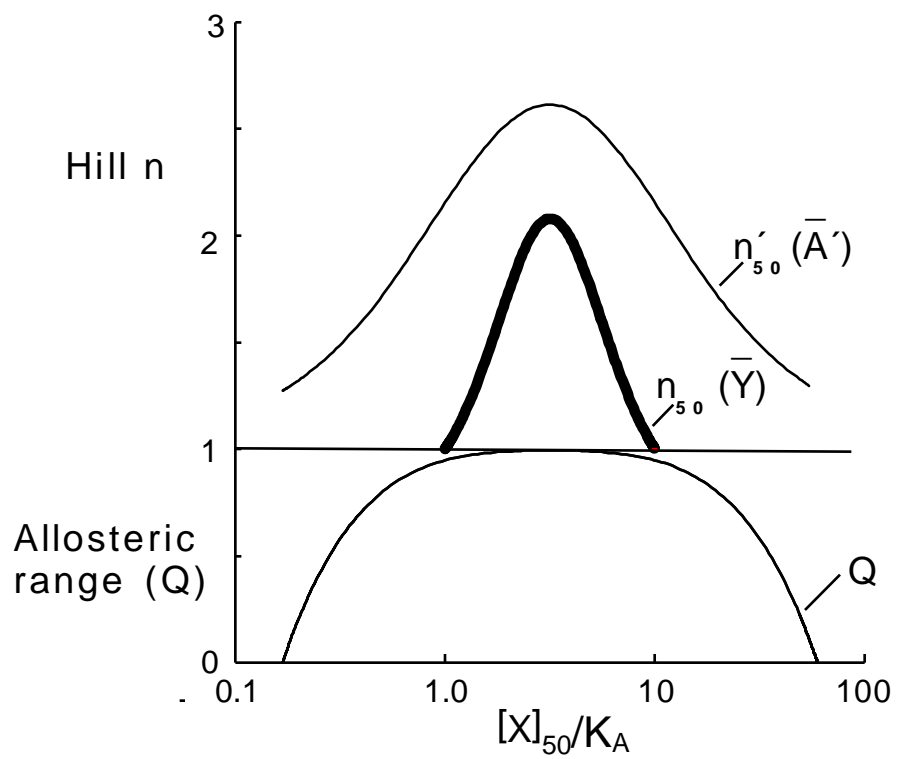
$\frac{S_i}{K_i}$	$\frac{S_j}{K_j}$
Σ_i	Σ_j
γ_i	γ_j

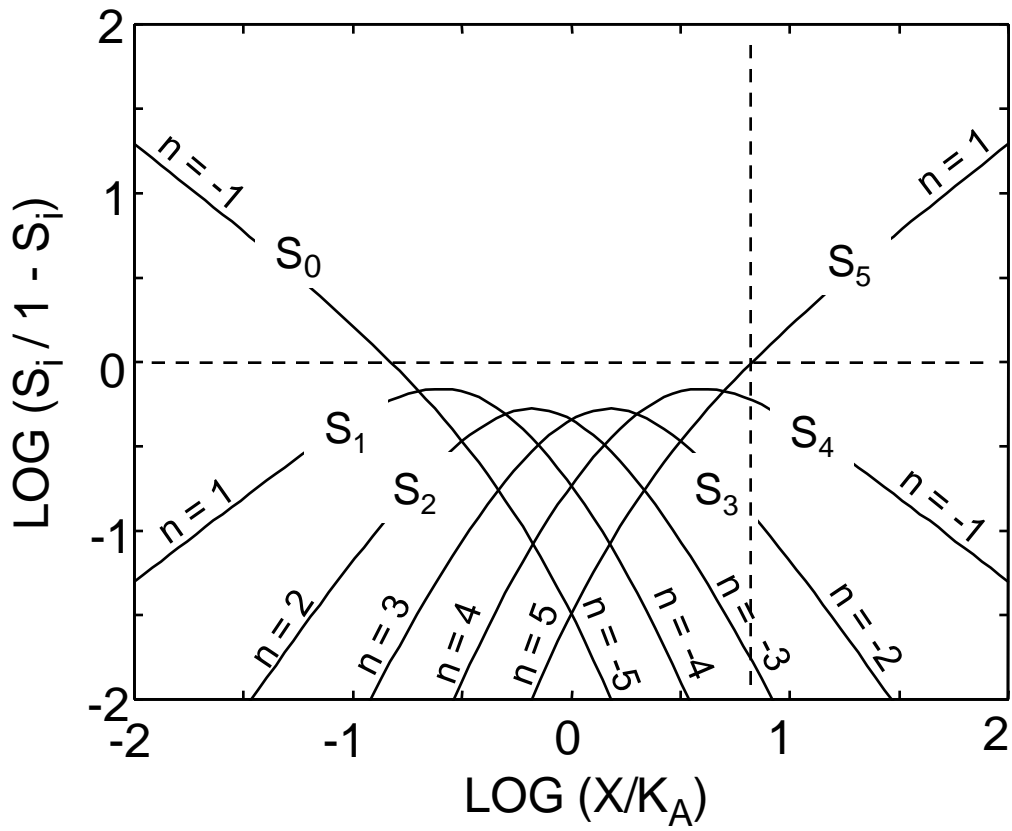
$$ij_L = [S_i] / [S_j]$$







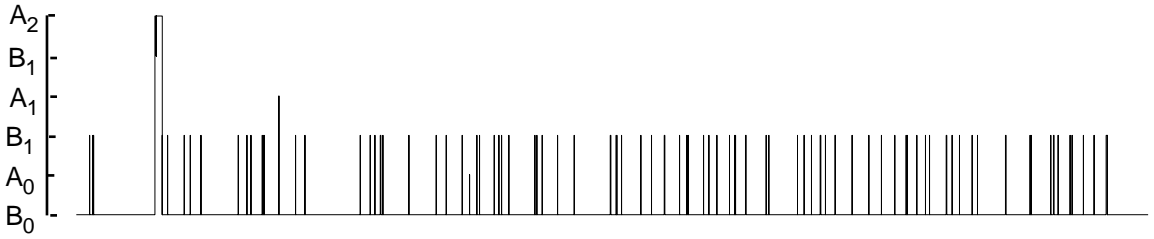




a

WILD TYPE

Molecular species:



Channel openings:

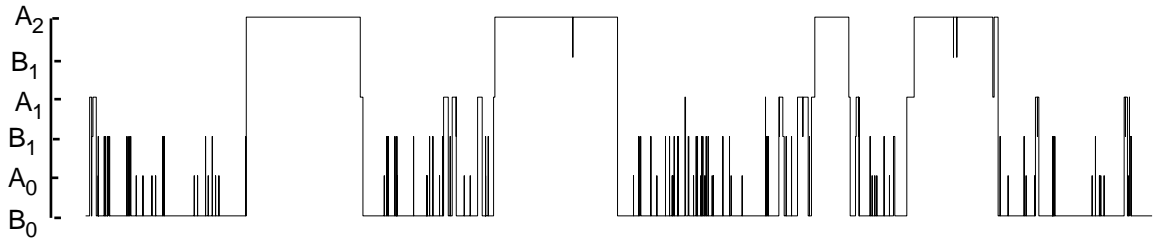


b

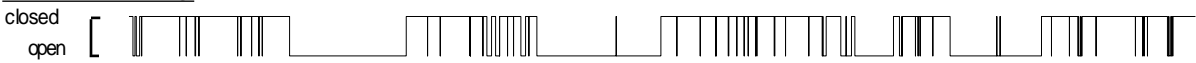
ϵ T264P

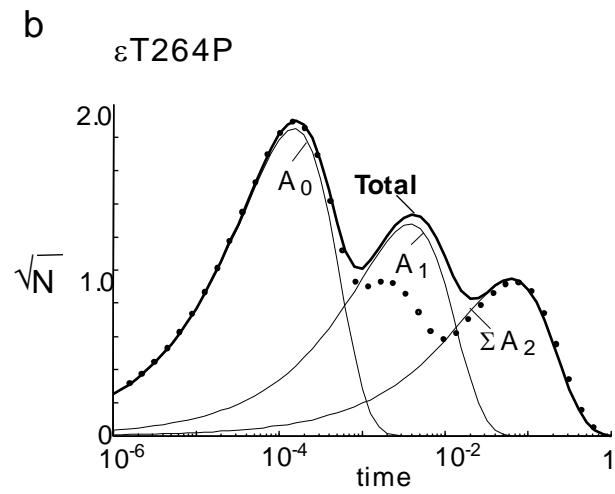
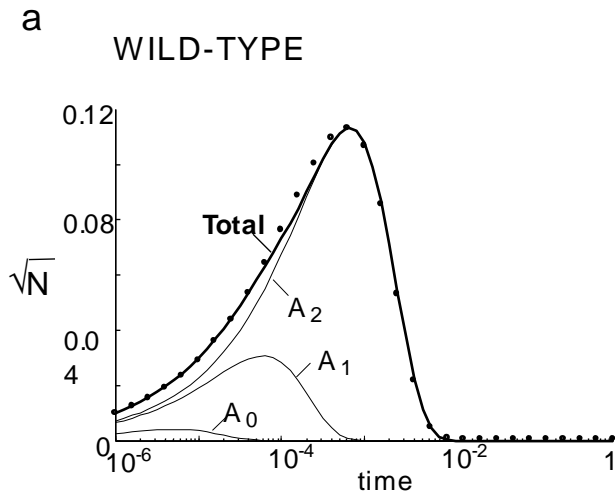
0.1 s

Molecular species:

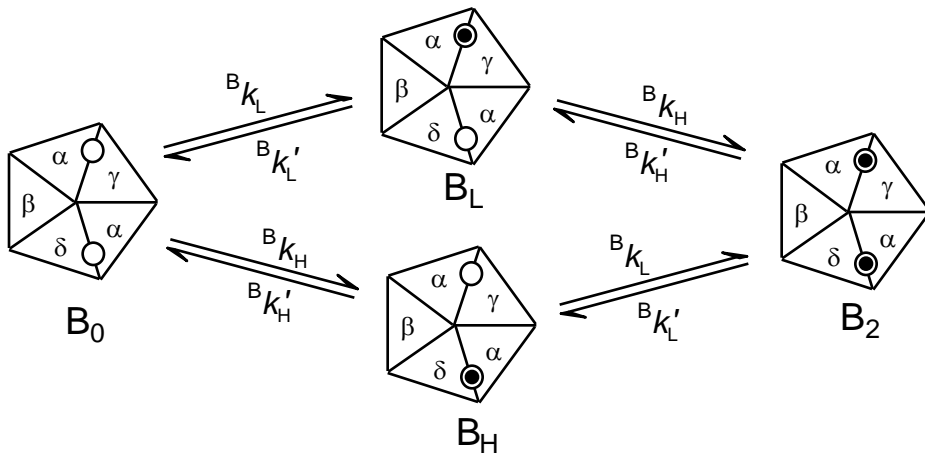


Channel openings:

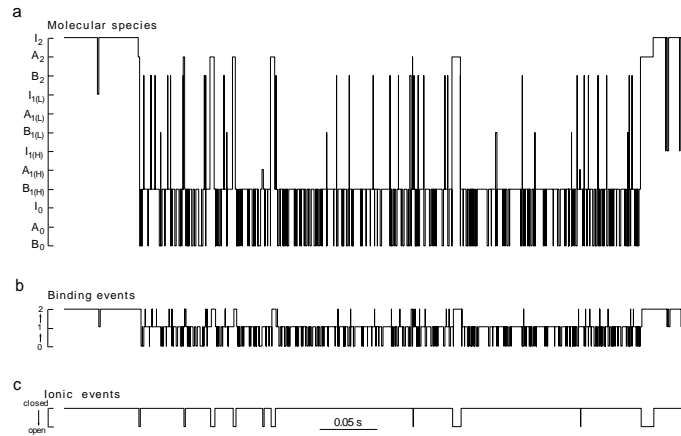




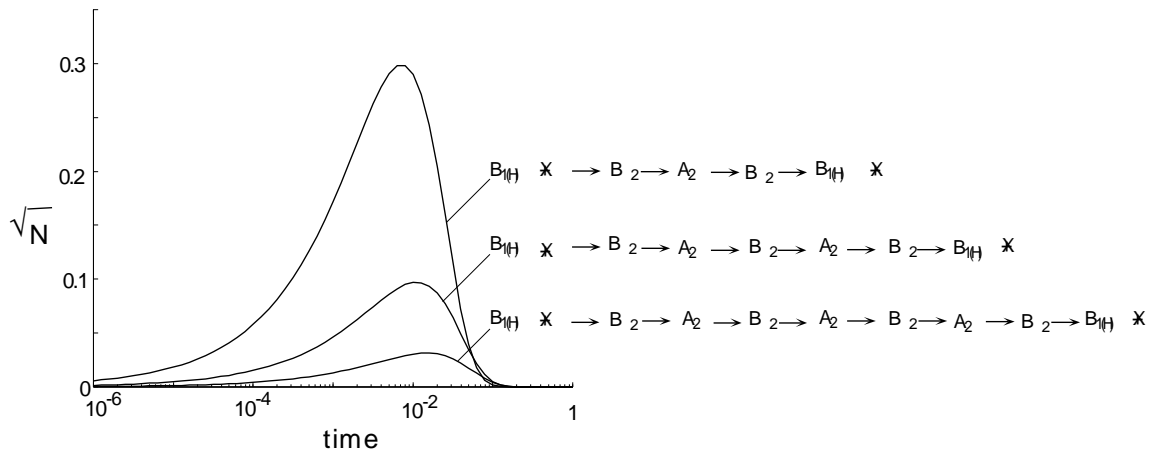
Edelstein & Changeux: Fig. 19



Edelstein & Changeux: Fig. 20



Edelstein & Changeux: Fig. 21



Edelstein & Changeux: Fig. 22

